Channel estimation forwireless relay networks using cooperative diversity techniques

Yi Zhang

▶ **To cite this version:**

Yi Zhang. Channel estimation forwireless relay networks using cooperative diversity techniques. Signal and Image processing. Ecole Centrale Marseille (ECM), 2012. English. NNT : . tel-02569081

HAL Id: tel-02569081
https://hal.science/tel-02569081

Submitted on 11 May 2020

HAL is a multi-disciplinary open access archive for the deposit and dissemination of scientific research documents, whether they are published or not. The documents may come from teaching and research institutions in France or abroad, or from public or private research centers.

L'archive ouverte pluridisciplinaire **HAL**, est destinée au dépôt et à la diffusion de documents scientifiques de niveau recherche, publiés ou non, émanant des établissements d'enseignement et de recherche français ou étrangers, des laboratoires publics ou privés.

ÉCOLE CENTRALE MARSEILLE

N° attribué par la bibliothèque
XXXX

TITRE :

ESTIMATION DU CANAL POUR LES RÉSEAUX DE CAPTEURS SANS-FIL UTILISANT LES TECHNIQUES DE DIVERSITÉ COOPÉRATIVE

THÈSE
pour obtenir le grade de DOCTEUR

délivré par L'ÉCOLE CENTRALE MARSEILLE

Discipline : Optique, Image et Signal

Effectuée à l'INSTITUT FRESNEL

Présentée et soutenue publiquement par :

Yi ZHANG

le 23 Novembre 2012

Directeur de thèse : Mr. Salah BOURENNANE
Co-Directeur de thèse : Mr. Mohammad-Ali KHALIGHI

École Doctorale : Physique et Sciences de la Matière

JURY :

Rapporteurs :	Mr. Kosai RAOOF	Université du Maine, Le Mans
	Mr. Yide WANG	Université de Nantes
Examinateur :	Mr. Zabih GHASSEMLOOY	Northumbria University, Royaume-Uni
Directeurs de thèse :	Mr. Salah BOURENNANE	École Centrale Marseille
	Mr. Mohammad-Ali KHALIGHI	École Centrale Marseille

ANNEE : 2012

ÉCOLE CENTRALE MARSEILLE

N° assigned by the library
XXXX

TITLE :

CHANNEL ESTIMATION FOR WIRELESS RELAY NETWORKS USING COOPERATIVE DIVERSITY TECHNIQUES

THESIS
to obtain the degree of Doctor of Philosophy

in ÉCOLE CENTRALE MARSEILLE

Major : Optics, Image, and Signal Processing

Prepared at INSTITUT FRESNEL, Marseille

Presented and publicly defended by :

Yi ZHANG

23 November 2012

Supervisor : Pr. Salah BOURENNANE
Co-supervisor : Dr. Mohammad-Ali KHALIGHI
Doctoral school : Physics and Materials Science

DOCTORAL COMMITTEE :

Reviewers :	Pr. Kosai RAOOF	Université du Maine (LAUM), Le Mans, France
	Pr. Yide WANG	Université de Nantes, France
Examiner :	Pr. Zabih GHASSEMLOOY	Northumbria University, UK
Supervisors :	Pr. Salah BOURENNANE	École Centrale Marseille, France
	Dr. Mohammad-Ali KHALIGHI	École Centrale Marseille, France

Table of contents

Abstract

RÉSUMÉ :
Cette thèse est consacrée à l'estimation du canal pour les réseaux de relais sans-fil utilisant le protocole *amplify-and-forward* lorsqu'un codage espace-temps distribué cohérent est effectué au niveau des relais pour permettre de bénéficier d'une diversité coopérative. Le réseau considéré est constitué de plusieurs relais distribués entre une source et une destination. Etant donné les contraintes pratiques pour acquérir l'état entier du canal de transmission, nous considérons le cas où nous disposons seulement d'un état partiel du canal. Dans ce cas, quand on effectue une estimation du canal basée uniquement sur des symboles pilotes, le récepteur aura des performances limitées puisque le nombre de ces pilotes doit être réduit au minimum pour des raisons d'efficacité énergétique du réseau. Pour pallier à ce problème, nous proposons d'utiliser une estimation semi-aveugle basée sur l'algorithme *expectation maximization* (EM). Dans un premier temps, nous considérons le codage espace-temps orthogonal au niveau des relais et une détection basée sur la minimisation de l'erreur quadratique moyenne. Après avoir étudié l'estimateur basé sur la formulation classique d'EM, nous proposons une version modifiée d'EM qui permet d'obtenir une estimation non-biaisée. Nous montrons l'intérêt de cette approche notamment pour les modulations d'ordre relativement élevé. Ensuite, dans un deuxième temps, nous considérons le cas de codage espace-temps non-orthogonal aux relais et proposons d'utiliser un récepteur itératif qui combine l'estimation semi-aveugle du canal et la détection basée sur l'annulation en parallèle des interférences entre-relais. Nous montrons l'avantage de cette technique par rapport à l'approche classique. Enfin, pour les conditions d'évanouissements rapides, au lieu d'utiliser une estimation semi-aveugle, nous proposons d'utiliser un schéma de détection amélioré qui prend en compte les erreurs d'estimation de canal et réduit l'impact de l'incertitude sur l'état du canal sur les performances du récepteur.

MOTS-CLÉS : Réseau de relais sans-fil, diversité coopérative, codage espace-temps distribué, connaissance partielle du canal, estimation semi-aveugle du canal, détection itérative.

ABSTRACT :
This thesis considers channel estimation in amplify-and-forward wireless relay networks when coherent distributed space-time block coding (DSTBC) is performed at the relays in the aim of benefiting from distributed diversity. The studied network consists in one source and one destination node, and several relay nodes distributed between them. Given the practical limitations to acquire full channel state information (CSI), we consider the case where only partial CSI is available at the destination node. Here, for the case of pilot-only-based channel estimation, we explain the limited receiver performance when pilot overhead should be kept to a minimum for the reasons of network energy efficiency. To overcome this problem, we firstly propose to use semi-blind (SB) channel estimation based on the expectation maximization (EM) algorithm. At a first step, we consider orthogonal DSTBC at the relays and minimum mean-square-error signal detection at the destination. In this case, starting by the classical formulation of EM for our system (that we call CB-EM for Classical Biased EM), we further propose a modified implementation of EM in view of obtaining an unbiased channel estimate at the receiver. We show the interest of the proposed scheme, called UL-EM (standing for Unbiased Linearly-combined EM), especially for relatively large signal constellations. At a second step, we consider non-orthogonal DSTBC at the relays, and propose to use an iterative CB-EM-based channel estimation and parallel interference cancelation for signal detection. This scheme allows an important performance improvement, as compared to the classical scheme. Finally, for the case

of relatively fast fading conditions, instead of using SB estimation, we propose to use an improved signal detection scheme that takes the channel estimation errors into account and reduces the impact of channel uncertainty on the receiver performance. We illustrate the interest of this scheme for relatively large signal constellations.

KEY WORDS : Wireless relay network (WRN), cooperative diversity, distributed space-time block coding (DSTBC), partial channel knowledge, semi-blind channel estimation, iterative signal detection.

Notations and Parameters

Notations

E{.}	expected value of random variable
$(.)^*$	Complex conjugate
$(.)^t$	Vector or matrix transpose
$(.)^\dagger$	Vector or matrix Hermitian transpose
||.||	Frobenius norm operator
diag{.}	Diagonal matrix
$\Re${.}	Real part operator
$\Im${.}	Imaginary part operator
Var{.}	Variance of random variable
$\prod$	Interleaving operator
$\otimes$	Kronecker product
$\boldsymbol{I}_R$	Identity matrix of dimension $R \times R$
$\mathbf{0}_R$	All-zero matrix of dimension $R \times R$
$K_i(.)$	Modified Bessel function of second kind and i-order
$\mathcal{N}(\mu, \sigma^2)$	Gaussian (normal) distribution with mean μ and variance σ^2
$\mathscr{CN}(\mu, \sigma^2)$	Complex circular Gaussian (normal) distribution with mean μ and variance σ^2

Parameters

T_i	Number of channel-uses in i-th hop
R	Number of relay nodes
q_1	Transmit power allocated to the source
q_2	Transmit power allocated to each relay
q	Total transmit power of the whole network during each channel-use
c	Weighting factor at each relay
N_d	Number of data symbol blocks per frame
N_p	Number of pilot blocks per frame
N_s	Total number of symbol blocks per frame
E_p	Pilot power
E_b	Averaged received energy per information bit
N_0	Noise unilateral power spectral density

List of Acronyms

ADC	Analog-to-Digital Convertor
AF	Amplify-and-Forward
APP	A Posteriori Probability
BICM	Bit-Interleaved Coded Modulation
BER	Bit-Error-Rate
CSI	Channel State Information
CB-EM	Classical Biased Expectation-Maximization
DemAF	Demodulate-And-Forward
DF	Decode-and-Forward
DSTBC	Distributed Space-Time Block Coding
EXIT	EXtrinsic Information Transfer
EM	Expectation Maximization
FER	Frame-Error-Rate
IRI	Inter-Relay Interference
IID	Independent Identically Distributed
LB	Lower Bound

LLR	Log-Likelihood Ratio
LS	Least Squares
LMMSE	Linear Minimum Mean-Square-Error
MAC	Media Access Control
MAP	Maximum A Posteriori
MI	Mutual Information
MIMO	Multiple-Input Multiple-Output
ML	Maximum Likelihood
NRNSC	Non-Recursive Non-Systematic Convolutional
OFDM	Orthogonal Frequency-Division Multiplexing
OFDMA	Orthogonal Frequency-Division Multiple Access
PIC	Parallel Interference Cancelation
PDF	Probability Density Function
PO	Pilot Only
QAM	Quadrature Amplitude Modulation
QoS	Quality of Service
QOSTBC	Quasi-Orthogonal Space-Time Block Coding
RV	Random Variable
SB	Semi-Blind
SISO	Single-Input Single-Output
SNR	Signal-to-Noise Ratio
SP	Set-Partition

TDMA Time-Division Multiple Access

TSw-Al Time-Switched Alamouti

UL-EM Unbiased Linearly-combined Expectation-Maximization

WRN Wireless Relay Network

WSN Wireless Sensor Network

List of Figures

Resumé étendu

Avec les progrès récents dans les domaines de communications sans-fil, microélectronique et micromécanique, on est aujourd'hui capable de déployer des capteurs multifonctionnels, de faible coût, de basse consommation et de petite taille. Ces capteurs qui peuvent communiquer entre eux sur de courtes distances, contiennent des composantes de capteur, de traitement du signal et de transmission. Un réseau de capteurs est constitué d'un grand nombre de capteurs, appelés souvent les nœuds du réseau, qui sont déployés massivement à l'intérieur ou autour d'un phénomène à observer. La plupart du temps, ces réseaux sont ad hoc, c'est à dire que l'on n'a pas besoin de déterminer ou de corriger la position des nœuds. Autrement dit, les capteurs sont distribués de manière aléatoire, parfois même dans les terrains inaccessibles ou sur les reliefs afin d'étudier les phénomènes météorologiques, par exemple. Ceci nécessite que le réseau de capteurs puisse s'organiser automatiquement pour récolter les informations et les transmettre vers les points de collecte.

Les applications potentielles pour les réseaux de capteurs sont nombreuses. Elles concernent par exemple, le domaine de la santé, les applications militaires, la surveillance ou monitoring du territoire ou de ressources, ou même des applications à domicile. Par exemple, dans le domaine de la santé, on peut évoquer la surveillance des patients ou encore l'assistance des patients invalides. Dans le domaine militaire, on peut parler des systèmes de surveillance, ciblage, reconnaissance, mais aussi les systèmes de collecte d'information pour les centres de commandement et de contrôle. On peut également parler des applications industrielles tel que le contrôle de qualité des produits, ou du monitoring des zones touchées par des catastrophes naturelles.

Les réseaux de capteurs constituent une des technologies clefs du siècle. Cependant, il reste encore de nombreux problèmes à résoudre, notamment en ce qui concerne la mise en place de ces réseaux. Les contraintes pratiques reviennent à des particularités de ces réseaux, et notamment les limitations sur les ressources spectrale, énergétique et calcul numérique au niveau de chaque nœud.

Comme dans la plupart des systèmes de communication sans-fil, les réseaux de capteurs sont soumis à des évanouissements (fading) du canal. Pour réduire l'effet du fading sur la qualité de transmission de données dans un réseau, il faut recourir à des techniques dites de diversité, qui permettent au récepteur de recevoir plusieurs copies du signal affectées différemment par l'effet

du canal sans-fil. Cependant, les techniques classiques de diversité ne peuvent pas être utilisées pour résoudre le problème considéré dans cette thèse en raison des contraintes fortes sur la taille des nœuds et leur coût. Par exemple, il n'est souvent pas pratique d'installer plusieurs antennes au niveau de chaque nœud. Pour remédier à ce problème, les techniques de diversité dites coopératives ou distribuées sont employées dans les réseaux de capteurs. Ainsi, les nœuds coopèrent entre eux pour apporter de la diversité spatiale. En d'autres termes, la diversité coopérative est un lien de communication multi-antennes virtuelles établi entre le nœud source et le nœud destinataire. Un cas simple des réseaux coopératifs sont les réseaux de relai. Ainsi, plusieurs nœuds ont la charge d'amplifier le signal reçu de la source et de le retransmettre vers le nœud destinataire. Nous nous intéressons dans cette thèse à ce type de réseau. Plus précisément, nous considérons un réseau de plusieurs relais distribués entre une source et une destination La transmission de données se fait en deux phases : premièrement, la source transmet les données vers les relais ; ensuite, dans une deuxième phase, les relais amplifient les signaux reçus et les transmettent vers la destination tandis que la source reste inactive. Ce fonctionnement correspond à la stratégie de coopération AF (pour Amplify-and-Forward) entre les relais. L'avantage de cette stratégie est que les relais n'ont pas besoin de connaitre l'état du canal, ce qui simplifie le protocole de transmission, réduit aussi les délais de transmission et la consommation d'énergie du réseau.

Afin d'apporter une diversité coopérative au niveau de la destination, outre l'amplification des signaux reçus par la source, les relais font souvent un traitement sur ces signaux qui consiste à effectuer un codage espace-temps en bloc distribué (DSTBC pour Distributed Space-Time Block Coding). Les schémas DSTBC qui sont souvent utilisés sont de type cohérent, c'est-à-dire que pour la détection du signal au récepteur, on a besoin de connaître l'état du canal de transmission. Ceci est classiquement fait à l'aide des séquences dites d'apprentissage (ou pilotes) qui sont envoyées fréquemment par la source. Le nœud destinataire peut alors mettre à jour l'état du canal en se basant sur ces séquences qui lui sont *a priori* connues. Cependant, l'état du canal ne peut pas être parfaitement connu et on n'est pas à l'abri des erreurs d'estimation du canal qui affectent les performances du récepteur. Une solution simple pour réduire ces erreurs est d'augmenter le nombre et la puissance des pilotes. Cette solution a évidemment pour conséquence de détériorer les efficacités énergétique et spectrale du réseau.

Nous nous intéressons justement dans cette thèse à l'étude de l'impact des erreurs d'estimation du canal sur les performances d'un réseau de relai décrit ci-dessus, et notamment à la proposition des solutions efficaces pour améliorer la qualité d'estimation du canal. Tout d'abord, dans le **Chapitre 2** nous présentons brièvement un état de l'art sur les réseaux de capteurs et nous nous intéressons plus particulièrement à l'efficacité énergétique d'un réseau de capteurs.

Ensuite, nous précisons dans le **Chapitre 3**, le cadre de notre étude et aussi les hypothèses générales sur lesquelles nous nous basons dans le reste de ce manuscrit. Nous expliquons en détail les aspects de coopération entre les nœuds et le codage DSTBC. Nous présentons également la formulation de notre système de transmission et décrivons les différentes approches de détection du signal et d'estimation du canal. De plus, une analyse détaillée des performances d'un réseau

de relais est présentée en étudiant les différentes méthodes de détection et d'estimation de canal. Même si ce chapitre peut paraître un peu long, les sujets abordés sont d'importance cruciale pour suivre les discussions dans les chapitres suivants. En effet, une bonne partie des résultats présentés telle que la comparaison détaillée des différents schémas de détection et d'estimation de canal, bien qu'introductifs, font partie des contributions de cette thèse.

Ensuite, dans le **Chapitre 4**, nous nous intéressons à l'aspect d'estimation du canal et proposons un schéma d'estimation semi-aveugle basé sur l'algorithme EM (Expectation Maximization) pour améliorer l'estimation du canal tout en gardant le nombre de symboles pilotes au minimum. Nous nous concentrons alors sur les schémas de codage DSTBC orthogonaux. Nous présentons d'abord un estimateur basé sur la formulation classique d'EM, que nous appelons CB-EM (pour Classical Biased EM) et l'implémentons dans un récepteur itératif avec le décodeur du canal. Nous montrons à l'aide des simulations de Monte Carlo l'amélioration des performances qu'on peut obtenir grâce à cette technique. Nous expliquons ensuite par une analyse plus détaillée que cet estimateur est biaisé et proposons une version modifiée de la formulation d'EM pour réduire le biais et obtenir de meilleures performances. L'approche proposée consiste à séparer les estimées du canal obtenues à base des symboles pilotes et de données, et à utiliser une combinaison linéaire des deux qui minimise la variance des erreurs d'estimation du canal. Nous montrons que le schéma d'estimation obtenu, appelé UL-EM (pour Unbiased Linearly-combined EM) permet une amélioration significative des performances du récepteur dans le cas des constellations du signal de taille relativement grande.

Nous traitons ensuite le cas du codage DSTBC non-orthogonaux dans le **Chapitre 5** où nous proposons d'utiliser un schéma de récepteur itératif qui effectue une annulation parallèle des interférences et la combine avec l'estimation du canal basée sur l'approche CB-EM. Nous montrons le gain en rapport signal-sur-bruit (RSB) en utilisant cette approche, par rapport à la détection simple MMSE (Minimum Mean-Square Error). Ce gain est surtout important pour les constellations de tailles relativement grandes. Nous analysons aussi la convergence du récepteur à l'aide des diagrammes EXIT (EXtrinsic Information Transfer).

Nous nous intéressons dans le **Chapitre 6** aux conditions d'évanouissements relativement rapides du canal. Dans ces conditions, il serait difficile d'implémenter en temps-réel les approches semi-aveugles d'estimation du canal. De plus, il est primordial dans ces condition de réduire au minimum le nombre des symboles pilotes et leur puissance. Ceci peut être le cas dans les réseaux ad-hoc mobiles telle que la téléphonie mobile. Dans ces conditions, pour réduire l'impact de l'incertitude sur l'état du canal sur les performances du système, nous proposons une méthode améliorée de détection du canal qui prend en compte les erreurs d'estimation de canal. Nous montrons que l'approche proposée conduit à une amélioration significative des performances du récepteur pour le cas des constellations du signal de grande taille. Aussi, le gain en RSB devient plus important pour les puissances faibles des pilotes.

Dans le **Chapitre 7** nous donnons nos conclusions relatives aux travaux réalisés au cours de

cette thèse ainsi que les principales perspectives que nous envisageons.

CHAPTER 1

General Introduction

1.1 Wireless sensor networks : merits and challenges

Wireless sensor networks (WSNs) are considered as one of the key technologies of the 21st century as they provide exceptional opportunities for monitoring and controlling homes, cities, and the environment [3, 4]. A WSN combines inexpensive, yet, smart devices that are usually deployed in large numbers. These devices, called "sensor nodes," include multiple onboard sensors and computation and communication units, and are networked through wireless links and probably the Internet. Thanks to the recent advances in microelectronics, micromechanics, and wireless communications, it is now possible to deploy multifunctional, low cost, low power consumption, and small size sensors. Potential applications of WSNs include environmental and structure monitoring, natural disaster prediction, homeland and physical security, healthcare, traffic surveillance, industrial and manufacturing automation, video surveillance, military sensing, home appliances and entertainment, etc.

The main advantages of wireless over wired sensor networks are the reduced deployment cost, ubiquity, and the property of self-reconfiguration. Instead of deploying a large quantity of wire routed through protective conduit, we simply need to place a small device at each sensing point [5], which drastically reduces the installation costs. Also, WSNs use low-cost embedded devices for a wide range of applications and do not rely on any pre-existing infrastructure [5]. This is in contrast to the existing cell phone, WiMAX or WiFi networks, which rely on the pre-deployment of extensive infrastructure support.

WSNs also have the ability to dynamically adapt to changing environment. As a matter of fact, sensor nodes are generally distributed randomly, and there is no need to determine or correct their position. Sometimes, they are deployed in inaccessible areas or on relief for studying the meteorological conditions, for example. This necessitates the automatic self-organization of the sensor nodes to collect information and to transmit it to the data fusion points [4, 1]. This is done thanks to the networking capability that fundamentally differentiates a WSN from a mere collection of sensors, by enabling cooperation, coordination, and collaboration among the nodes [3, 6]. In some WSNs, the nodes do not communicate with a nearby base station, but rather communicate with their local peers, which needs efficient algorithms for data aggregation, ad hoc routing,

and distributed signal processing [5, 7].

Due to size, cost, and energy limitations, WSNs are subject to tight communication and computation constraints. Especially, for battery-operated sensors, energy consumption is an important design parameter because in many applications, replacing batteries may be difficult or impossible. Therefore, the network lifetime should be extended through the design of efficient networking and communication and signal processing methods.

1.2 Thesis objective

This thesis focuses on a special kind of cooperative WSNs, i.e., wireless relay networks (WRNs). In such networks, some nodes are deployed in the environment and have the task of relaying the transmitted signals from a source node towards a destination node. We consider the case of coherent signalling where we need to identify the transmission channel parameters for efficient signal detection at the destination node. This is an important task in time-varying wireless channels subject to multipath fading. Considering the crucial need of network energy efficiency, we develop appropriate channel estimation methods that allow a reduction of the amount of training signals used for channel estimation, and try to make a trade-off between computational complexity and performance.

After a state-of-the-art on the WSNs, we consider the special WRN explained above, and describe the signal transmission by taking into account node cooperation. Meanwhile, we discuss the need to channel knowledge at the destination and explain how we can acquire this information in practice. We then focus on the channel estimation by proposing to use a special semi-blind (SB) estimation method, based on the expectation maximization (EM) algorithm, which consists of an iterative method to obtain the channel state based on the maximum likelihood criterion. Semi-blind estimation could be a solution to the problem of large pilot-overhead that helps avoid a reduction in the network energy efficiency due to the transmission of training sequences. A considerable part of the thesis concerns the adaptation of the EM-based estimation method to different cooperation schemes between the relay nodes. As an alternative to SB channel estimation, we next propose a detection scheme that takes into account the channel estimation errors and reduces their impact on the system performance.

1.3 Thesis overview

The dissertation is composed of the following chapters.

Chapter 2 presents a general state-of-the-art on WSNs including the main characteristics, limitations, and design challenges. We insist on the energy consumption issues in such networks and explain the relationship between energy consumption and the different protocol layers. We also describe the idea of cooperative communication and introduce the WRNs. Distributed space-

time coding at the relay nodes in view of exploiting some distributed diversity is then presented.

Chapter 3 is devoted to the description of signal transmission in a typical WRN. We start by describing the system model, and especially, specify the main assumptions that we make for later use in the following chapters regarding channel fading statistics. Power allocation over network nodes and DSTBC at the relay nodes are discussed in detail. Next, signal detection at the destination and the need to channel estimation are discussed. Meanwhile, we explain that in most cases, the destination can perform data detection based only on a partial channel state information (CSI). The performance of different detection methods under full or partial CSI knowledge, as well as different channel estimation techniques are then compared through the presentation of some simulation results.

Chapter 4 considers SB channel estimation in WRNs based on the EM algorithm in order to reduce considerably the amount of pilot overhead. Here, we focus on the case where orthogonal DSTBCs are performed at the relays. We start by the classical formulation of EM and show the considerable improvement that we achieve by this method when implemented in an iterative receiver at the destination. We next show that this classical formulation provides a biased estimate. To improve the quality of the channel estimate, we propose a modified EM formulation that provides an unbiased estimate. This modified method, called UL-EM (for Unbiased Linearly-combined EM) is shown to be advantageous, especially for relatively large signal constellations.

Chapter 5 studies SB channel estimation when a non-orthogonal DSTBC is employed at the relays. In this case, in order to reduce the impact of inter-relay interferences on the receiver performance, which originates from non-orthogonal DSTBC, we propose to perform parallel interference cancelation (PIC) together with EM channel estimation. Additionally, we analyze the convergence behavior of the iterative receiver by means of extrinsic information transfer (EXIT) charts.

Chapter 6 proposes an alternative to SB channel estimation to improve the receiver performance at the presence of estimation errors. For this purpose, we focus on maximum *a posteriori* (MAP) signal detection at the destination. We propose an improved detection rule that takes the channel uncertainties into account. Compared to the classical *mismatched* detector that uses the raw channel estimates in signal detection, the improved detector allows a significant performance improvement for the case of relatively large signal constellations. Again, the EXIT chart tool is used to investigate the receiver convergence behavior.

Finally, **Chapter 7** concludes the thesis and gives some perspectives for future work.

1.4 Thesis contributions

In summary, the key contributions of this thesis are :

– Comparative study of different signal detection methods and different CSI knowledge conditions at the destination.

– Developing an EM-based SB channel estimation method for the special WRN configuration

considered in this thesis.

- Modifying the classical EM formulation in the aim of obtaining an unbiased channel estimate and improved system performance.
- Adapting the SB estimator to the case of non-orthogonal DSTBC at the relays by performing iterative PIC detection.
- Proposing an improved detection rule to the case of WRN using MAP signal detection at the destination.

1.5 Author's publications

1.5.1 Journal papers

❶ Yi Zhang, M. A. Khalighi, and S. Bourennane, "Iterative channel estimation and data detection for Amplify-and-Forward relay networks," *IEEE Communications Letters*, vol. 16, no. 5, pp. 710-713, May 2012.

❷ Yi Zhang, M. A. Khalighi, and S. Bourennane, "EM-based Semi-blind Channel Estimation for Amplify-and-Forward Cooperative Relay Networks," *EURASIP Signal Processing*, under revision.

1.5.2 Conference papers

❶ Yi Zhang, M. A. Khalighi, and S. Bourennane, "EM-based channel estimation for cooperative relay networks," *IEEE International Conference on Telecommunications, (ConTEL)*, Graz, Austria, pp. 279-286, June 2011.

❷ Yi Zhang, M. A. Khalighi, M. S. Sadough, and S. Bourennane, "Signal Detection for Amplify-and-Forward Relay Networks With Imperfect Channel Estimation," *IEEE/IET International Symposium on Communication System Networks and Digital Signal Processing (CSNDSP)*, Poznań, Poland, pp. 1-5, July 2012.

CHAPTER 2

Wireless Sensor Networks, State-of-the-Art

2.1 Overview of wireless sensor networks

Recent advances in micro-sensor technology has enabled the development of wireless sensor networks (WSN) in a wide range of applications [1, 8, 9, 10]. For example, we can talk about monitoring patients or assisting disabled persons in the health area ; surveillance, targeting, and reconnaissance systems in military ; product quality control in industry ; and wildlife tracking and forest monitoring [11].

A WSN consists of a large number of sensor nodes that are deployed around or inside an environment [3, 4]. A typical sensor node is a battery-operated device, which is able to establish a relationship between the digital and the real world through a number of sensors. In order to monitor an environment, usually a large number of sensor nodes are required. These nodes exchange information or transmit the collected data to a sink or destination node through wireless links.

The general scheme of a WSN is depicted in Figure 2.1. A number of sensor nodes are distributed inside the field, and each node transmits the collected information to the destination node (user) while probably cooperating with other nodes. Sensor nodes usually have a relatively simple function and have a low energy capacity available. To establish a communication link between the sensor field and the user, one or several sink nodes are needed to be deployed, as can be seen in Figure 2.1. The collected information in the sensor field can be transmitted to the sink nodes via the communication links among nodes and according to a routing protocol. Then, sink nodes may retransmit the received information to the user through Internet or by means of a satellite link.

Depending on the mode of deployment, WSNs can be classified into two categories : structured and unstructured WSNs [11]. In a structured WSN, sensor nodes are deployed in a prearranged mode and on fixed positions. In this type of WSN, the number of sensor nodes is relatively small and the distribution of nodes needs to be carefully designed. Moreover, each node has usually expensive units for reliable communication [11, 12, 13]. Generally, due to the small number of nodes, the implementation complexity of a structured WSN is relatively low. On the other hand, in an unstructured (also called *ad hoc*) WSN, a large number of sensor nodes are randomly distributed in

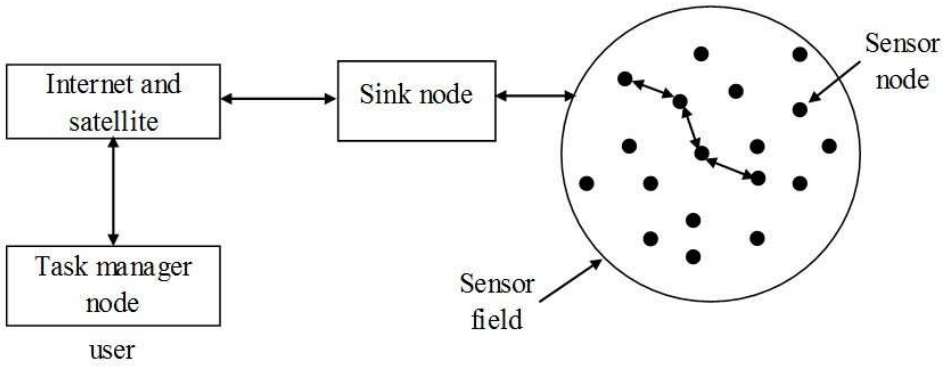

Figure 2.1 — General block diagram of a WSN.

the field [14, 15]. Compared with the structured case, an unstructured WSN can easily be deployed in remote geographic areas. Such a random deployment can be realized by dropping the sensor nodes from an airplane, for example. Sometimes, they are deployed in inaccessible areas or on relief for studying the meteorological conditions.

Due to this simple node deployment, unstructured networks have a wider application area than the structured ones. Meanwhile, their management is much more complex. In particular, such networks should have the possibility of automatic reconfigurability in the case of any change in the network topology due to a failure or run-out of the battery of some nodes [7]. In summary, some of the main practical limitations of WSNs are listed below.

- large number of sensor nodes ;
- dense deployment of sensor nodes that are prone to failure ;
- possibility of frequent change of network topology ;
- stringent constraints on the transmit power, computational capacity, and memory of sensor nodes ;
- absence of global identification of sensor nodes to avoid large amount of overload ;
- need to work in extreme weather conditions.

2.2 Sensor nodes

Usually, each node incorporates a transceiver and there are strict constraints on the weight and the size of each node, as well as on its computation, memory, and energy resources. Special attention should hence be devoted in the design of each node to the signal processing tasks and energy consumption.

2.2.1 Classification of sensor nodes

Depending on the application, sensor nodes can be classified into four categories : submote, mote, supermote, and gateway devices. A submote sensor node is a basic sensing device in its lo-

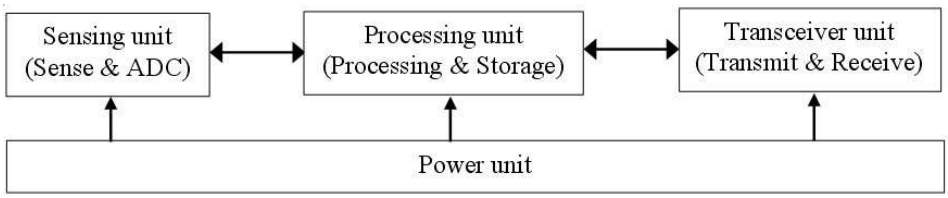

Figure 2.2 — General configuration of a sensor node.

west and simplest form and has a very limited energy capacity. Typically, it just transmits certain information in the case of sensing an event. A mote sensor node has a slightly more complex structure, compared with the submote case. This device is the essential part in multihop communication, which means that, in addition to sensing, the mote node can be used as relay for receiving information from other nodes and retransmitting it to another. However, due to its small structure, its energy capacity is very limited. A supermote, on the other hand, has a much larger capacity for data communication due to employing advanced signal processing equipments and a battery of larger capacity. The most powerful node of a network is the gateway node that is usually used as a sink node (see Figure 2.1). The gateway node firstly receives information from different paths by lower level sensor devices and then retransmits it to the user after some pre-processing.

2.2.2 Sensor configuration

Generally, except submote devices, the other three kinds of sensor nodes should include the four units of sensing, processing, transceiver, and power. Owing to the recent advances in microelectronics, micromechanics, and wireless communications, it is now possible to deploy multifunctional, low cost, low power consumption, and small size sensors. These sensor nodes are capable to communicate between them in a cooperative manner and over relatively short distances. A general configuration of such nodes is shown in Figure 2.2. We briefly describe these four units in the following.

- **The sensing unit** : This is the functional part by which we establish a relationship between analog and digital worlds. Generally, it consists of two functional modules : sensing and analog-to-digital convertor (ADC). The analog information obtained from the environment is passed to the processing unit after being converted to a digital signal by the ADC.
- **The processing unit** : The main functions of this unit are data storage and data processing. In order to optimize the node's power consumption, this unit usually works in one of four modes of off, sleep, idle, and active.
- **The transceiver unit** : To reduce the implementation complexity, this unit is usually subject to a half-duplex constraint. Moreover, considering the limitations on the node's size and power consumption, the transceiver unit is usually equipped to one single antenna for both transmitting and receiving. When the node works as a transmitter, the output of processing unit is transmitted to other nodes according to a routing protocol. On the other hand, when

it is used as a receiver, the unit stores the received data from other nodes. Again for the purposes of optimizing energy consumption, there are four operation modes for this unit : transmit, receive, idle, and sleep [7].

– **The power unit** : This is the most important part of the node that is generally made up of batteries of limited capacity. Obviously, the accomplishment of all of above-mentioned functions depends on this unit. Note that when nodes are deployed in an inaccessible region, recharging or replacing the battery is impractical. Consequently, energy efficient sensing, processing, and transceiver design are of critical importance in order to extend the network lifetime.

2.3 Energy consumption issues

Energy consumption is an important factor in the design of a WSN [16]. In fact, sensor nodes rely on the capacity of their battery, and recharging batteries can be quite difficult, especially in ad hoc networks. Therefore, maximizing the overall energy efficiency of a WSN is a critical challenge.

Depending on the rate of energy expenditure, energy consumption in a network can be classified into two factors : continuous and reporting energy consumption [3]. Continuous energy consumption refers to the minimum energy required for maintaining a network during its lifetime without any data transmission and reception. In general, it incorporates battery leakage and the energy expended in the phases of sleep, sensing, and signal processing. On the other hand, reporting energy consumption is the amount of energy used for data collection and transmission and depends on channel characteristics and network protocols. To reduce the reporting energy consumption, we should improve the efficiency of transmission and reception.

2.3.1 Network lifetime

The network lifetime is defined as the duration from the moment of network distribution to the moment it becomes out of work. Due to the network complexity, numerous possible events can result in the network paralysis. For instance, certain sensor nodes may exhaust their energy, or some nodes may be destroyed because of lightning, torrent, etc. The lifetime of a network is mainly related to the expected wasted energy and the expected reporting energy. The expected wasted energy is that consumed in a nonfunctional network, and the expected reporting energy is that consumed by all nodes in a randomly chosen data collection scenario [3].

2.3.2 Energy consumption and protocol layers

As Figure 2.3 shows, like in any other communication system, the sensor network protocol stack contains the following five layers : physical, data link, network, transport, and application [1, 8, 11]. The design of each layer and the interaction between them affect the network energy consumption.

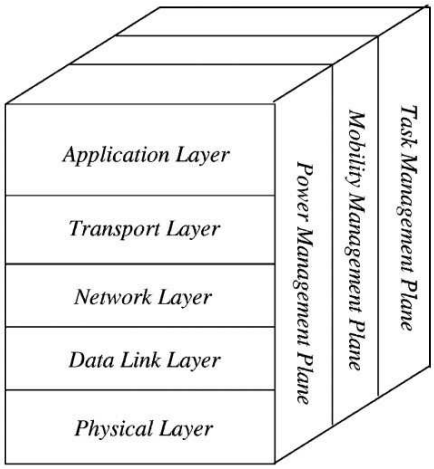

Figure 2.3 — The sensor network protocol stack (reproduced from [1]).

The first layer is known as the physical layer, which is used to design an adequate and robust modulation, as well as transmission and reception schemes, while taking power consumption issues into account. Notice that the transceiver power consumption also depends on the distance from the source to the destination node. In the case of long distances between these nodes, the physical layer should propose an energy efficient multihop strategy for saving energy.

The data link layer provides functional means to data transmission between nodes, and possibly the correction of the errors that may occur in the physical layer. A sublayer of data link layer is the medium access control (MAC) layer that provides addressing and channel access control mechanisms. Under the conditions of noisy environment and mobile nodes, the MAC layer should minimize the energy waste originating from packet collisions, overhearing, excessive retransmissions, control overheads, etc. [8, 11].

The network layer helps to design the data routing provided by the transport layer (see below). To maximize the network power efficiency, sensor nodes should employ an optimal transmission routing protocol [1]. In particular, when there are a large number of nodes located between the source and the destination nodes, there are lots of possible routes can be chosen for communication. Energy efficient routes should then be chosen depending on the available energy of the nodes and the required energy for data transmission over these routes.

The transport layer is responsible for maintaining the flow of data when the WSN application requires it. Generally, a WSN is capable of tolerating a certain degree of packet loss which results from packet collision, node failure, low quality communication link, etc. [11]. In order to preserve the quality of service (QoS), data retransmission should be done for the lost packets. This, in turn, requires more energy expenditure. So, the use of an efficient transport layer protocol is important for energy saving.

Lastly, the application layer concerns the different applications that are set up according to the sensing tasks.

We notice from Figure 2.3 that in addition to the power management plane, the design of the different protocol layers should take into consideration the mobility and task management. In other words, we should reduce the overall network power consumption while satisfying the mobility and task requirements.

2.4 Design challenges of WSNs

There remain still many challenges ahead for WSNs, especially concerning the implementation aspects. A WSN should satisfy different design criteria depending on the specific application. However, there are some design challenges that concern most of the WSNs [10]. We briefly introduce two examples in the following.

2.4.1 Trade-off between communication and computation

Prior to data transmission, we could perform some pre-processing to reduce the volume of collected data, e.g. by compressing the measurement information. In a larger scale, a so-called cluster node could be in charge of the compression of data collected from different nodes in a cluster, before transferring it to the sink node. This can reduce considerably the energy expended for data transmission. However, some energy is required for performing the pre-processing and data compression. The larger the number of nodes in a cluster is, the more considerable will be the required energy for pre-processing. Therefore, to optimize power consumption, a tradeoff should be considered between data transmission and pre-processing.

2.4.2 Connectivity and coverage in hostile environments

In some applications, the battery of some nodes may end up when they are deployed in certain wireless-unfriendly locations. Also, some nodes could experience temporary or permanent hardware failure when the environmental conditions are changed, e.g. due to torrential rains, fire hazards, etc. In order to eliminate the influence of such failures on the entire WSN function, it is necessary to dimension the number of nodes and their communication ranges, and also to employ an efficient routing protocol to ensure node connectivity and the coverage of the entire region.

2.5 Cooperative communication

2.5.1 Multipath fading

Like in most wireless communication systems, a sink node in a WSN receives signals arriving from different propagation paths due to the existing scatterers/reflectors in the environment. The received signals may add up constructively or destructively at the destination, which causes signal fading. Multipath fading can considerably deteriorate the quality of data transmission. Depending

on the channel coherence interval and the transmission rate, slow or fast fading conditions may hold. In particular, quasi-static fading conditions hold when the channel coherence time is larger than the frame size.

2.5.2 Cooperative diversity in WSNs

Fading has an important impact on the quality of data transmission and efficient diversity techniques should be employed to reduce its destructive effect. By exploiting some kind of diversity, e.g. in time, frequency, space, or polarization, a significant improvement in the system performance can be obtained conditioned to the independence of the fading on the different signal copies. Usually, the most efficient solution is to use multiple antennas at the transmitter and/or at the receiver to average over channel fading [17, 18]. However, the classical diversity techniques cannot be employed in a WSN due to the stringent constraints on the nodes' size and cost. In particular, it is impractical to use multiple antennas at each sensor node. As a result, *cooperative* or *distributed* diversity techniques are mostly employed in WSNs where nodes cooperate among each other to exploit some amount of diversity [19, 20, 21, 22]. In other words, by cooperative diversity, a virtual multi-antenna communication link is established between the source and the destination nodes. Several cooperating schemes have been proposed in the literature so far. In [23], repetition-coding is proposed that has a low implementation complexity at the expense of spectral efficiency. A better spectral efficiency is obtained through the use of channel coding to obtain cooperation diversity as proposed in [19, 24]. Most of the proposed techniques, however, consider the use of some relay nodes to provide cooperative diversity. In these so-called wireless relay networks, the relays cooperate among them in order to provide some distributed spatial diversity, as it is explained in the following section.

2.6 Wireless relay networks

A simple form of cooperative diversity networks is a wireless relay network (WRN) where some nodes have the role of relaying the signal transmitted from a source node towards a destination node [25, 26, 27, 28, 29]. In such networks, data transmission usually takes place in a multi-hop manner. When more than one relay node participates in signal transmission, the relay nodes cooperate with each other through the use of some kind of space-time coding in order to benefit from distributed diversity. This is called distributed space-time coding.

Figure 2.4 shows the general scheme of a WRN [2]. It includes four kinds of sensor nodes, i.e., source nodes, cluster nodes, relay (cooperative) nodes, and a sink node. The sensor field is segmented into several clusters, where each of them includes one cluster head node and a number of source and relay nodes. Assume that the event happens in the field of the first cluster. At the beginning, the source nodes firstly report the information to their cluster head node. Then, the cluster head node transmits the information to the next cluster head node while using the relay nodes

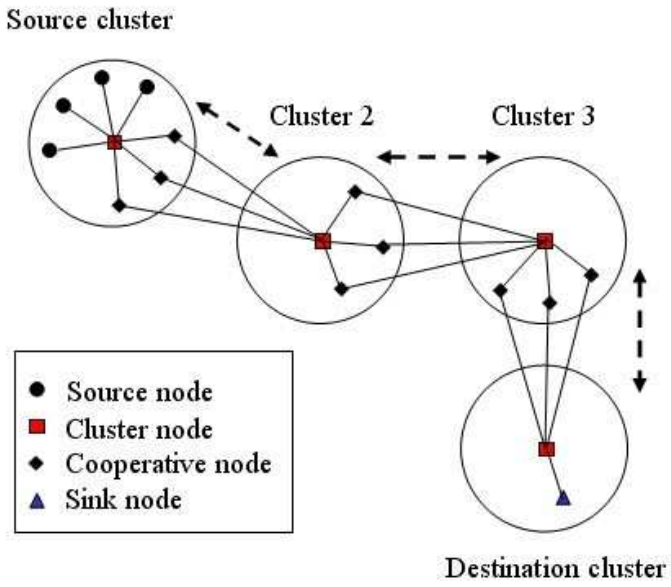

Figure 2.4 — General scheme of a WRN [2].

to exploit some cooperative diversity. After multiple hops between the clusters, the information is received at the last cluster head node which is able to communicate it to the sink node.

As we will see, a much simpler network is considered in this thesis, comprised of one source node, one destination node, and a number of relay nodes. For such a network, we consider dual-hop data transmission, where in a first hop, data is transmitted from the source to the relays, and then, in a second hop, the received signals are processed at the relays and retransmitted to the destination. We will focus on this simple network configuration in the sequel.

2.6.1 Cooperation strategies

There are three main cooperation strategies regarding the data processing done at the relays in the second hop : amplify-and-forward (AF) [30, 31, 32, 33], decode-and-forward (DF) [20, 21, 34, 35] and demodulate-and-forward (DemAF) [36, 37].

By the AF mode, the relay nodes just amplify the (noisy) received signal from the source node (or a superior level cluster head) and then simply convey it to the destination node (or to a lower level cluster head) [22, 30, 38]. The destination node firstly combines the received signal transmitted from the relays and then makes a final decision on the transmitted data. Although noise is amplified at the relays, the destination also receives several independently faded versions of the signal and can make more reliable decisions on them. The advantage of the AF strategy is that the relays have no requirement to the channel state information (CSI). So, this scheme is interesting regarding power consumption and transmission delay considerations.

On the other hand, by the DF mode, the relay nodes firstly decode the received signal and

then re-encode and forward it to the destination. This way, the noise can be greatly reduced at the expense of complexity and power consumption at the relays. By the DF scheme, CSI is required for signal detection at the relays, which increases their complexity and energy consumption, as compared with the AF scheme. Also, we may suffer from erroneous data transmission from the relays. It is shown in [39, 40] that the performance of AF outperforms that of DF when a direct communication link between the source and the destination can be supported.

The so-called demodulate-and-forward (DemAF) is the another cooperation strategy which has been proposed in [37, 38, 41]. By DemAF, the received signals at the relays are first demodulated, and then remodulated to reconstruct the transmitted symbols before being sent to the destination. This way, we can effectively eliminate the influence of noise amplification at the relays. However, this comes at the expense of increased network's energy consumption.

Throughout this thesis, we consider the amplify-and-forward cooperation strategy at the relays.

2.6.2 Distributed space-time coding

For the purpose of node cooperation, the use of distributed space time block coding (DSTBC) has extensively been studied in the literature (see for example [22, 27, 42, 43, 44, 45]). Depending on whether the destination knows the CSI or not, there are three main types of DSTBC that can be employed : non-coherent DSTBCs, differential DSTBCs, and coherent DSTBCs. For non-coherent schemes, the destination does not know the CSI but knows the channel statistics [46, 47]. For coherent DSTBCs, the destination needs the CSI for signal detection that can be estimated through using some training (pilot) symbols, for instance [28, 48]. Since coherent DSTBCs have less complexity than their non-coherent counterparts, they are more widely used in WRNs [42, 48, 49]. When the destination has no knowledge of the channel from source to relays but knows the CSI of the channel from the relays to the destination, a so-called partial coherent DSTBC is also proposed in [50, 51]. The other choice is to use a differential DSTBC which requires neither the CSI nor the channel statistics [27, 52, 53]. Although this latter solution simplifies the receiver (at the destination) due to the linear decoding complexity, the code design is more difficult than coherent DSTBCs [53]. Also, differential schemes suffer from a 3 dB loss in the detection signal-to-noise ratio (SNR) compared to the coherent schemes.

2.7 Chapter summary

We provided a brief state-of-the-art on WSNs and the related potential problems and challenges. We explained the different applications of these networks and the classification of structured and ad hoc networks. Special attention was devoted to energy consumption in WSNs and the different factors that can play an important role in minimizing it. We then discussed the problem of multipath fading and the techniques of cooperative diversity to mitigate the fading effect. A spe-

cial and important type of cooperative networks, i.e., WRN, was then introduced and described.

In the following chapters, we will focus on a relatively simple configuration of AF WRNs where a source node communicates with a destination node while benefiting from the cooperation of a number of relay nodes. The general formulation of the transmission link, DSTBC signaling at the relays, and signal transmission and detection will be considered in the next chapter.

CHAPTER 3

Signal Transmission in a WRN Case Study

3.1 Introduction

After the general state-of-the-art on WSNs presented in Chapter 2, we specify in this chapter the framework of this thesis on which the succeeding chapters are based on. We consider a simple case of WRNs where two or more relay nodes are inserted between the source and the destination. The source node can be of submote or mote sensor type, and the relays and the destination node can be of supermote or gateway type (see Chapter 2). Nodes are considered to be subject to a half-duplex constraint due to hardware implementation limitations, and so, dual-hop data transmission is performed. It means that the process of data transmission is divided into two steps. In the first hop, data is transmitted from the source to the relays. Next, in the second hop, the received signals are processed at the relays and retransmitted to the destination while the source node remains idle. This transmission protocol is also called "listen-and-transmit" [42]. We describe the signal transmission aspects in such a network by firstly explaining our main assumptions and the formulation of signal transmission in Section 3.2. Signal detection at the destination is described in Section 3.3 where we discuss the need to the *partial* CSI at the destination. Estimating this CSI is considered in Section 3.6. Lastly, we provide some simulation results in Section 3.7 to study the performances of different signal detection and channel estimation schemes.

3.2 Assumptions and system model

The block diagram of Figure 3.1 shows how data transmission takes place between the different network nodes. We suppose that there is no direct transmission link between the source and the destination and assume perfect time-synchronization among all nodes. Working in AF signaling mode, the relays perform DSTBC coding on the received signals from the source before amplifying and retransmitting them to the destination, while the source node remains idle. Remember from Chapter 2 that the AF mode has the advantages of reduced transmission delay, complexity, and power consumption at the relays [34, 43, 54]. We consider the bit-interleaved code modula-

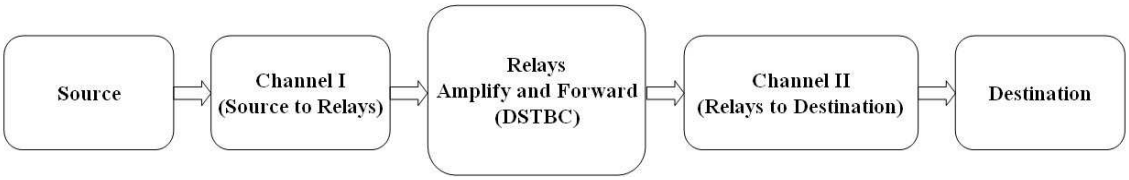

Figure 3.1 — Data transmission block diagram in a typical AF WRN.

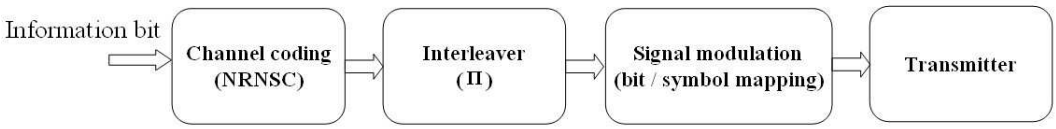

Figure 3.2 — Block diagram of the BICM scheme at the source node.

tion (BICM) scheme [55] at the source node as depicted in Figure 3.2. This way, the information bits are firstly encoded using a non-recursive non-systematic convolutional (NRNSC) code, and then interleaved pseudo-randomly before bit-symbol mapping according to a signal modulation scheme. We consider mostly the quadrature amplitude modulations (QAM) here. We denote the modulation scheme by M-QAM, where M denotes the number of signal constellation points.

3.2.1 Network structure and definitions

Consider the WRN shown in Figure 3.3, which is composed of one source node, R relay nodes, and one destination node. Let $\boldsymbol{s} = [s_1 \;\; s_2 \cdots s_{T_1}]^t$ be a transmitted block of symbols from the source, where $(.)^t$ denotes transposition and T_1 corresponds in fact to the number of channel-uses in the first hop. We consider power-normalized transmitted symbols and impose $\mathrm{E}\{\boldsymbol{s}^\dagger \boldsymbol{s}\} = T_1$, where $(\cdot)^\dagger$ stands for the Hermitian operator and $\mathrm{E}\{.\}$ denotes the expected value. Upon the reception of these signals, the relays amplify and retransmit them according to a DSTBC scheme, by which

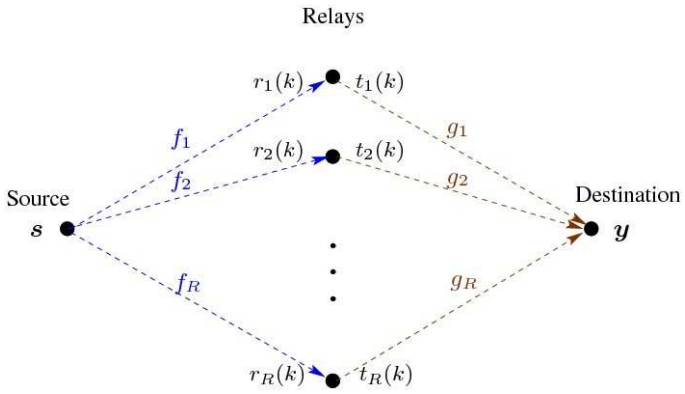

Figure 3.3 — General scheme of the studied WRN : f_i and g_i represent fading coefficients corresponding to the source-relays and relays-destination sub-channels, respectively.

the received block of T_1 signals is mapped to a block of T_2 signals; with T_2 denoting the number of channel-uses during the second hop. To have the same data rate in the source-to-relays and relays-to-destination transmission steps, we set $T_1 = T_2 = T$.

Let $\boldsymbol{r}_i(k)$ and $\boldsymbol{t}_i(k)$ represent the received and the retransmitted signals at the i-th relay and corresponding to the k-th block, respectively. The corresponding received block at the destination is denoted by $\boldsymbol{y} = [y_1 \;\; y_2 \cdots y_T]^t$. Each symbol frame corresponds to N_s blocks of T symbols each. We further denote the channel fading coefficient from the source to the i-th relay by f_i, and that from the i-th relay to the destination by g_i, $i = 1, ..., R$. Without loss of generality, we consider Rayleigh, frequency non-selective and independent identically-distributed (IID) fading for f_i and g_i and model them by $\sim \mathcal{CN}(0,1)$, where $\mathcal{CN}(\mu, \sigma^2)$ represents a complex circular Gaussian distribution of mean μ and variance σ^2.

3.2.2 Power distribution over network nodes

Let q be the total transmit power of the whole network during each channel-use. Also, let q_1 and q_2 be the transmit power allocated to the source and to each relay, respectively. Optimal power distribution among the source and the relays for minimizing the pairwise error probability is considered in [42, 44] where it is shown that the optimal solution is given by (3.1) for the case of $T_1 < T_2$:

$$\begin{cases} q_1 = \dfrac{\sqrt{(q + T_2/T_1)(q+1)T_2/T_1} - (q + T_2 \;/\; T_1)}{T_2/T_1 - 1} \\ q_2 = \dfrac{(q - q_1)T_1}{R\; T_2} \end{cases} \tag{3.1}$$

For $T_1 = T_2$ which is the case we consider in this manuscript, the optimal power distribution solution becomes [42, 44] :

$$q_1 = \frac{q}{2} \quad , \quad q_2 = \frac{q}{2R}. \tag{3.2}$$

Note that this solution also results in maximizing the expected value of the received SNR [42]. Also, note that by using this solution, we assume that we have equal power available at all the relay nodes. Our formulation can be generalized to the case of different available powers at different relays, however [56].

Considering the solution of (3.2), the transmitted symbols from the source and the relays should be weighted accordingly. To do this, the transmitted symbols from the source are weighted by $\sqrt{q_1}$ and those at the relays are weighted by a scalar c given below :

$$c = \sqrt{\frac{q_2}{q_1 + \sigma_{nr}^2}}, \tag{3.3}$$

where σ_{nr}^2 is the variance of the additive noise at the relay nodes, assumed to be Gaussian-distributed. Denoting the noise at i-th relay by n_{r_i}, we consider $n_{r_i} \sim \mathcal{CN}(0,\, \sigma_{nr}^2)$.

3.3 Data transmission formulation

Remember the dual-hop transmission protocol from Section 3.2. Each frame of *data* symbols (i.e., excluding pilots) is divided into N_d blocks of T symbols. After the first hop, upon the transmission of a block of symbols, the received signal vector at the i-th relay, corresponding to the k-th block, is :

$$\boldsymbol{r}_i(k) = \sqrt{q_1} f_i \, \boldsymbol{s}(k) + \boldsymbol{n}_{r_i}(k) \quad , \quad i = 1,2,...R, \quad k = 1,...,N_d, \tag{3.4}$$

where the vectors are of size $(T \times 1)$. For the sake of notation simplicity, hereafter we will mostly not indicate the block reference k. Next, in the second hop, at the relays, we perform DSTBC on the received signals. Let $\boldsymbol{C}_i$ of dimension $(T \times T)$ be the precoding matrix at the i-th relay. The retransmitted $(T \times 1)$ vector $\boldsymbol{t}_i$ from this relay is :

$$\boldsymbol{t}_i = c \, \boldsymbol{C}_i \, \boldsymbol{r}_i^{(*)}, \tag{3.5}$$

where $\boldsymbol{r_i}^{(*)} = \boldsymbol{r_i}^*$ if complex conjugation needs to be done on $\boldsymbol{r_i}$ according to the DSTBC scheme, and $\boldsymbol{r_i}^{(*)} = \boldsymbol{r_i}$ otherwise. Note that if we do not want to use such a notation, to provide a general formulation for the received signal, we should separate the real and imaginary parts of the parameters, like in [42, 57, 58]. For the sake of notation simplicity, we do not adopt this approach in this chapter. As we will see, in our study, we consider some classical DSTBCs ; we will simply specify the receiver formulation for them. Finally, the vector of received signals at the destination is described as :

$$\boldsymbol{y} = \sum_{i=1}^{R} g_i \, \boldsymbol{t}_i + \boldsymbol{n}_d, \tag{3.6}$$

where $\boldsymbol{n}_d$ denotes the vector of the received noise. We denote the variance of its entries by σ_d^2. Using equations (3.4), (3.5), and (3.6), we have :

$$\boldsymbol{y} = \sum_{i=1}^{R} c \sqrt{q_1} \underbrace{f_i^{(*)} g_i}_{h_i} \underbrace{\boldsymbol{C}_i \, \boldsymbol{s}^{(*)}}_{\boldsymbol{p}_i} + \underbrace{\sum_{i=1}^{R} c \, \boldsymbol{C}_i \, g_i \, \boldsymbol{n}_{ri}^{(*)} + \boldsymbol{n}_d}_{\boldsymbol{z}}. \tag{3.7}$$

Here, we defined the $(T \times 1)$ vector $\boldsymbol{p}_i = \boldsymbol{C}_i \, \boldsymbol{s}^{(*)}$, the $(T \times 1)$ vector $\boldsymbol{z}$ as the vector of the total received noise at the destination, and $h_i = f_i^{(*)} g_i$. For simplicity, we assume that we have the same noise variance at the relays and at the destination and set $\sigma_{nr}^2 = \sigma_d^2 = \sigma^2$. To write $\boldsymbol{y}$ in a vector multiplication form, we also define the $(R \times 1)$ vector $\boldsymbol{h}$ and the $(T \times R)$ matrix $\boldsymbol{P}$ as follows.

$$\boldsymbol{h} = \left[f_1^{(*)} g_1 \, , \, f_2^{(*)} g_2 \, , \ldots , f_R^{(*)} g_R \right]^t \tag{3.8}$$

$$\boldsymbol{P} = \left[\boldsymbol{C}_1 \boldsymbol{s}^{(*)} \, , \, \boldsymbol{C}_2 \boldsymbol{s}^{(*)} , \ldots , \boldsymbol{C}_R \boldsymbol{s}^{(*)} \right] \tag{3.9}$$

Then,

$$\boldsymbol{y} = c \sqrt{q_1} \, \boldsymbol{P} \, \boldsymbol{h} + \boldsymbol{z}. \tag{3.10}$$

3.4 Node cooperation and DSTBC at the relays

In order to perform node cooperation, we consider the use of coherent DSTBC at the relays that allows a simpler implementation and a better system performance (see Subsection 2.6.2). As we will explain later in Section 3.6, for the case of performing coherent DSTBC at the relays, in practice, we have to estimate the CSI at the destination by using some pilot (training) sequences. In this manuscript, we focus on the cases of two and four relay nodes. The corresponding DSTBCs are presented in the following.

3.4.1 Case of two relay nodes

For $R = 2$, the appropriate DSTBC at the relays is the famous Alamouti scheme [59]. For this scheme, a received vector $\boldsymbol{s} = [s_1, s_2]^t$ at the relays is mapped to the following transmission matrix :

$$\boldsymbol{P} = \begin{bmatrix} s_1 & -s_2^* \\ s_2 & s_1^* \end{bmatrix}. \tag{3.11}$$

Note that for this scheme, which provides full rate and full diversity, we have $T = 2$. Matrix $\boldsymbol{P}$ can also be written in the following form :

$$\boldsymbol{P} = \left[\boldsymbol{C}_1 \boldsymbol{s}, \boldsymbol{C}_2 \boldsymbol{s}^* \right] \text{ with } \boldsymbol{C}_1 = \begin{bmatrix} 1 & 0 \\ 0 & 1 \end{bmatrix}, \ \boldsymbol{C}_2 = \begin{bmatrix} 0 & -1 \\ 1 & 0 \end{bmatrix} \tag{3.12}$$

Using the formulation of (3.10), vector $\boldsymbol{h}$ is given by :

$$\boldsymbol{h} = \begin{bmatrix} f_1 g_1 \\ f_2^* g_2 \end{bmatrix}. \tag{3.13}$$

3.4.2 Case of four relay nodes

For $R = 4$, there is no orthogonal DSTBC scheme which can satisfy the conditions of full rate and full diversity at the same time for the case of complex constellations [60]. Here, as an orthogonal scheme, we use the full-rate time-switched Alamouti scheme [58] that we denote by TSw-Al with $T = R = 4$. By this scheme, the received vector $\boldsymbol{s} = \left[s_1, s_2, s_3, s_4 \right]^t$ at the relays is mapped to the following transmission matrix.

$$\boldsymbol{P} = \sqrt{2} \begin{bmatrix} s_1 & -s_2^* & 0 & 0 \\ s_2 & s_1^* & 0 & 0 \\ 0 & 0 & s_3 & -s_4^* \\ 0 & 0 & s_4 & s_3^* \end{bmatrix} \tag{3.14}$$

Here, the factor $\sqrt{2}$ ensures the normalized transmit power from the relays. Performing TSw-Al on the received signals at the relays turns to do Alamouti DSTBC alternatively on one pair of the relay nodes, while turning the other pair off. Matrix $\boldsymbol{P}$ in this case can be written in the following form.

$$\boldsymbol{P} = \left[\boldsymbol{C}_1 \boldsymbol{s}, \boldsymbol{C}_2 \boldsymbol{s}^*, \boldsymbol{C}_3 \boldsymbol{s}, \boldsymbol{C}_4 \boldsymbol{s}^* \right], \tag{3.15}$$

where

$$\boldsymbol{C}_1 = \sqrt{2}\begin{bmatrix} 1 & 0 & 0 & 0 \\ 0 & 1 & 0 & 0 \\ 0 & 0 & 0 & 0 \\ 0 & 0 & 0 & 0 \end{bmatrix},\ \boldsymbol{C}_2 = \sqrt{2}\begin{bmatrix} 0 & -1 & 0 & 0 \\ 1 & 0 & 0 & 0 \\ 0 & 0 & 0 & 0 \\ 0 & 0 & 0 & 0 \end{bmatrix},\ \boldsymbol{C}_3 = \sqrt{2}\begin{bmatrix} 0 & 0 & 0 & 0 \\ 0 & 0 & 0 & 0 \\ 0 & 0 & 1 & 0 \\ 0 & 0 & 0 & 1 \end{bmatrix},\ \boldsymbol{C}_4 = \sqrt{2}\begin{bmatrix} 0 & 0 & 0 & 0 \\ 0 & 0 & 0 & 0 \\ 0 & 0 & 0 & -1 \\ 0 & 0 & 1 & 0 \end{bmatrix}.$$

Also, according to the formulation of (3.10), we have :

$$\boldsymbol{h} = \left[f_1 g_1,\ f_2^* g_2,\ f_3 g_3,\ f_4^* g_4 \right]^t. \tag{3.16}$$

Note that the precoding matrices $\boldsymbol{C}_i$ are orthonormal but not unitary. The interest of the TSw-Al scheme is that the complexity of the optimal detector at the receiver grows linearly with R.

On the other hand, if we want to use a unitary DSTBC matrix for the case of four relays in order to be equitable between different relays and among different channel-uses, a good choice is the full-rate quasi-orthogonal scheme with $T = R = 4$, proposed by Jafarkhani in [61]. For this scheme, the vector $\boldsymbol{s}$ is mapped to the following transmission matrix.

$$\boldsymbol{P} = \begin{bmatrix} s_1 & -s_2^* & -s_3^* & s_4 \\ s_2 & s_1^* & -s_4^* & -s_3 \\ s_3 & -s_4^* & s_1^* & -s_2 \\ s_4 & s_3^* & s_2^* & s_1 \end{bmatrix} \tag{3.17}$$

It can equivalently be written in the following form :

$$\boldsymbol{P} = \left[\boldsymbol{C}_1 \boldsymbol{s}, \boldsymbol{C}_2 \boldsymbol{s}^*, \boldsymbol{C}_3 \boldsymbol{s}^*, \boldsymbol{C}_4 \boldsymbol{s} \right],\ \ \boldsymbol{s} = \left[s_1,\ s_2,\ s_3,\ s_4 \right]^t, \tag{3.18}$$

where

$$\boldsymbol{C}_1 = \boldsymbol{I}_4,\ \boldsymbol{C}_2 = \begin{bmatrix} 0 & -1 & 0 & 0 \\ 1 & 0 & 0 & 0 \\ 0 & 0 & 0 & -1 \\ 0 & 0 & 1 & 0 \end{bmatrix},\ \boldsymbol{C}_3 = \begin{bmatrix} 0 & 0 & -1 & 0 \\ 0 & 0 & 0 & -1 \\ 1 & 0 & 0 & 0 \\ 0 & 1 & 0 & 0 \end{bmatrix},\ \boldsymbol{C}_4 = \begin{bmatrix} 0 & 0 & 0 & 1 \\ 0 & 0 & -1 & 0 \\ 0 & -1 & 0 & 0 \\ 1 & 0 & 0 & 0 \end{bmatrix}.$$

Here, $\boldsymbol{I}_4$ denotes as the identity matrix of dimension (4×4). Also,

$$\boldsymbol{h} = \left[f_1 g_1,\ f_2^* g_2,\ f_3^* g_3,\ f_4 g_4 \right]^t. \tag{3.19}$$

We will denote this scheme by QOSTBC (QO standing for Quasi-Orthogonal), which exhibits partial orthogonality (between rows 1 and 2, 1 and 3, 2 and 4, and 3 and 4). Note that optimal signal detection at the destination is more computationally complex for this scheme than for TSw-Al.

3.5 Signal detection at the destination

Taking into account the BICM scheme used at the source, we perform soft signal demodulation followed by soft channel decoding, which is a rather classical approach. The block diagram of

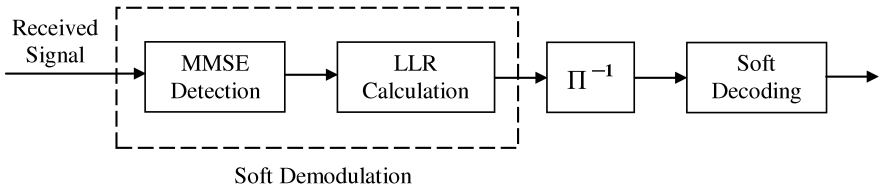

Figure 3.4 — Signal detection and channel decoding at the destination.

the receiver at the destination is shown in Figure 3.4. For space-time decoding and signal demodulation, we first perform minimum mean-square-error (MMSE) detection and then convert the detected symbols to log-likelihood ratios (LLRs) [62]. These LLRs are next passed to the Max-Log-MAP channel decoder [63] after being de-interleaved (the Π^{-1} block). We will briefly provide in the following details on the main blocks of the demodulator. For MMSE signal detection, we consider two cases where *full* or *partial* CSI is available at the destination.

3.5.1 MMSE detection under full CSI

Consider the simple case of $R = 2$ and Alamouti DSTBC. Corresponding to each block of $T = 2$ symbols $\boldsymbol{s} = [s_1, s_2]^t$, MMSE detection results in the following equations :

$$\begin{cases} \hat{s_1} &= c\sqrt{q_1}\left(h_1^* y_1 + h_2 y_2^*\right) / \left(c^2 q_1 \boldsymbol{h}^\dagger \boldsymbol{h} + \sigma_{\boldsymbol{z}}^2\right) \\ \hat{s_2} &= c\sqrt{q_1}\left(h_1^* y_2 - h_2 y_1^*\right) / \left(c^2 q_1 \boldsymbol{h}^\dagger \boldsymbol{h} + \sigma_{\boldsymbol{z}}^2\right) \end{cases} \tag{3.20}$$

where, for instance, $\hat{s_1}$ stands for the detected signal corresponding to s_1 and h_1 is the first entry of $\boldsymbol{h}$. Also, the variance of the total received noise is defined as $\sigma_{\boldsymbol{z}}^2 = \mathrm{E}\{\boldsymbol{z}^\dagger \boldsymbol{z}\}$. Note that the MMSE formulation does not make any assumption on the distribution of $\boldsymbol{z}$ [64]. To give a simple expression for the detector, we propose to define the vectors $\boldsymbol{y}' = [y_1\,,\, y_2^*]^t$ and $\boldsymbol{s}' = [s_1\,,\, s_2^*]^t$, and the matrix $\boldsymbol{H}$ as follows [65].

$$\boldsymbol{H} = c\sqrt{q_1}\begin{bmatrix} h_1 & -h_2 \\ h_2^* & h_1^* \end{bmatrix} \tag{3.21}$$

Then, MMSE detection for $\boldsymbol{s}'$ gives :

$$\hat{\boldsymbol{s}'} = \left(\boldsymbol{H}^\dagger \boldsymbol{H} + \sigma_{\boldsymbol{z}}^2 \boldsymbol{I}_R\right)^{-1} \boldsymbol{H}^\dagger \boldsymbol{y}'. \tag{3.22}$$

Obviously, having calculated $\hat{\boldsymbol{s}'}$, we can obtain $\hat{\mathbf{s}}$, the estimate of $\boldsymbol{s}$. Similarly, for the case of $R = 4$ with TSw-Al DSTBC, we propose to define the vectors $\boldsymbol{y}' = [y_1\,,\, y_2^*\,,\, y_3^*\,,\, y_4]^t$ and $\boldsymbol{s}' = [s_1\,,\, s_2^*\,,\, s_3^*\,,\, s_4]^t$, and the matrix $\boldsymbol{H}$ as follows.

$$\boldsymbol{H} = c\sqrt{2q_1}\begin{bmatrix} h_1 & -h_2 & 0 & 0 \\ h_2^* & h_1^* & 0 & 0 \\ 0 & 0 & h_3^* & -h_4^* \\ 0 & 0 & h_4 & h_3 \end{bmatrix} \tag{3.23}$$

Then, the MMSE detector for $\boldsymbol{s}'$ is given by (3.22). For the case of $R = 4$ with QOSTBC at the relays, we can still formulate the MMSE detector as in (3.22) using the following definition for $\boldsymbol{H}$:

$$\boldsymbol{H} = c\sqrt{q_1}\begin{bmatrix} h_1 & -h_2 & -h_3 & h_4 \\ h_2^* & h_1^* & -h_4^* & -h_3^* \\ h_3^* & -h_4^* & h_1^* & -h_2^* \\ h_4 & h_3 & h_2 & h_1 \end{bmatrix} \tag{3.24}$$

The same definitions of $\boldsymbol{y}'$ and $\boldsymbol{s}'$ as for TSw-Al apply to this case and $\hat{\boldsymbol{s}}'$ is given by (3.22). Note that MMSE detection is not optimal for this last scheme. Assuming that g_i are known at the destination, which is true if we have *full* CSI (i.e., known f_i and g_i), from (3.7) we have :

$$\sigma_{\boldsymbol{z}}^2 = T\sigma^2\left(1 + c^2\sum_{i=1}^{R}|g_i|^2\right) \tag{3.25}$$

Under available *full* CSI, $\boldsymbol{z}$ in (3.7) is Gaussian distributed. Under these conditions, the MMSE detector for the Alamouti ($R = 2$) and TSw-Al ($R = 4$) schemes is equivalent to the optimal maximum likelihood (ML) detector.

3.5.2 MMSE detection under partial CSI

In order that the destination can estimate g_i, the relays should send some pilots independently from the source. Alternatively, they could estimate f_i and transmit them to the destination. Both solutions increase the transmission protocol complexity, energy consumption at the relays, and the overall data-rate loss. As we will explain in Section 3.6, we can obtain an estimation of the vector $\boldsymbol{h}$ at the destination ; what we will refer to as *partial* CSI. Meanwhile, we cannot obtain $\sigma_{\boldsymbol{z}}^2$ from (3.25) as g_i are unknown. Also, $\boldsymbol{z}$ cannot be modeled by a Gaussian random process. Assuming Rayleigh fading conditions, g_i are Gaussian and hence in (3.7), we have the product of two Gaussian random variables (RVs) which is not Gaussian distributed. To calculate $\sigma_{\boldsymbol{z}}^2$, similar to what is proposed by [66] for the case of ML detection, we approximate z_i with a Gaussian RV $\hat{z}_i$ verifying the following conditions :

$$\mathrm{E}\{\hat{z}_i\} = \mathrm{E}\{z_i\} = 0 \text{ and } \mathrm{Var}\{\hat{z}_i\} = \mathrm{Var}\{z_i\}, \tag{3.26}$$

where Var{.} denotes variance. We will refer to this method as "Gaussian approximation." Then, the variance $\sigma_{\boldsymbol{z}}^2$ is replaced by :

$$\sigma_{\hat{\boldsymbol{z}}}^2 = T\sigma^2\left(1 + c^2\sum_{i=1}^{R}\sigma_{g_i}^2\right) = T\sigma^2(1 + c^2R), \tag{3.27}$$

where the second equality holds because we assumed normalized channel coefficients.
A so-called "enhanced Gaussian approximation" has also been proposed [67] by which z_i is approximated by a Gaussian RV $\tilde{z}_i$ satisfying the following conditions :

$$\mathrm{E}\{\tilde{z}_i\} = \mathrm{E}\{z_i\} = 0 \text{ and } \mathrm{Var}\{\tilde{z}_i\} = \mathrm{Var}\{z_i|\hat{\boldsymbol{h}}\}. \tag{3.28}$$

Consequently, the variance $\sigma_{\boldsymbol{z}}^2$ is replaced by :

$$\sigma_{\hat{\boldsymbol{z}}}^2 = T\sigma^2\left(1 + c^2\sum_{i=1}^{R} G(\hat{h}_i)\right),\ \ G(\hat{h}_i) = \frac{\|\hat{h}_i\| K_1(2\|\hat{h}_i\|)}{K_0(2\|\hat{h}_i\|)}. \tag{3.29}$$

Here, $\|.\|$ is the Frobenius norm, and $K_0(.)$ and $K_1(.)$ denote the modified Bessel functions of the second kind and zero- and first-order, respectively.

3.5.3 LLR calculation

LLR calculation on the detected symbols $\hat{\boldsymbol{s}}$ is again done assuming Gaussian $\boldsymbol{z}$. Consider the example of QPSK modulation and $R = 2$ with Alamouti DSTBC for instance. Having obtained $\hat{s}_1$ by MMSE detection, the expression of LLR on the bit b_1 corresponding to the real part of s_1 is given by [58] :

$$\mathrm{LLR}_1 = \log\frac{\exp\left(-\frac{(\hat{s}_{1\Re} - \alpha\sqrt{2}/2)^2}{\sigma_\zeta^2}\right)}{\exp\left(-\frac{(\hat{s}_{1\Re} + \alpha\sqrt{2}/2)^2}{\sigma_\zeta^2}\right)} = \frac{2\,\alpha\sqrt{2}\,\hat{s}_{1\Re}}{\sigma_\zeta^2} \tag{3.30}$$

where $\hat{s}_{1\Re}$ denotes the real part of $\hat{s}_1$, and

$$\alpha = \frac{c^2 q_1 \|\boldsymbol{h}\|^2}{c^2 q_1 \|\boldsymbol{h}\|^2 + \sigma_{\boldsymbol{z}}^2}\ ,\ \sigma_\zeta^2 = \frac{c^2 q_1 \|\boldsymbol{h}\|^2}{\left(c^2 q_1 \|\boldsymbol{h}\|^2 + \sigma_{\boldsymbol{z}}^2\right)^2} \tag{3.31}$$

After simplification, we obtain :

$$\mathrm{LLR}_1 = 2\sqrt{2}\,\hat{s}_{1\Re}\,(c^2 q_1 \|\boldsymbol{h}\|^2 + \sigma_{\boldsymbol{z}}^2), \tag{3.32}$$

and $\sigma_{\boldsymbol{z}}^2$ is replaced by $\sigma_{\hat{\boldsymbol{z}}}^2$ or $\sigma_{\tilde{\boldsymbol{z}}}^2$, calculated from (3.27) or (3.29), respectively.

3.5.4 ML signal detection

The interest of MMSE detection is that it is a relatively low complexity scheme. In order to see the practical interest of this detector in our context, we also consider the optimal maximum likelihood (ML) detector, adapted to the block diagram of Fig. 3.4. In other words, we use the ML criterion to detect the transmitted symbols $\hat{\boldsymbol{s}}$, and then, convert it to the LLRs on its constituting bits. [1] We intend to compare the performances of the two detection methods for different DSTBC schemes and see the interest of MMSE detection. (This is done later in Section 3.7.)

According to the ML algorithm, we should maximize the likelihood function $p(\boldsymbol{y}|\boldsymbol{h},\boldsymbol{s})$ to obtain the ML-detected symbol vector $\hat{\boldsymbol{s}}_{\mathrm{ML}}$. Equivalently, we consider the likelihood $p(\boldsymbol{y}'|\boldsymbol{h},\boldsymbol{s}')$ and obtain $\hat{\boldsymbol{s}}'_{\mathrm{ML}}$, where $\boldsymbol{y}'$ and $\boldsymbol{s}'$ were defined previously in Subsection 3.5.1. Assuming perfect *full* CSI and Gaussian noise at the receiver, $\hat{\boldsymbol{s}}'_{\mathrm{ML}}$ can be calculated as follows [68] :

$$\hat{\boldsymbol{s}}'_{\mathrm{ML}} = \arg\min_{\boldsymbol{s}'}\left\{D_{\mathrm{ML}}(\boldsymbol{s}', \boldsymbol{y}', \boldsymbol{h})\right\}, \tag{3.33}$$

1. The general formulation of the ML soft demodulator will be later given in Chapter 6.

where the metric D_{ML} is calculated from the likelihood function $p(\boldsymbol{y}'|\boldsymbol{h},\boldsymbol{s}')$:

$$D_{\mathrm{ML}}(\boldsymbol{s}',\boldsymbol{y}',\boldsymbol{h}) = -\log p(\boldsymbol{y}'|\boldsymbol{h},\boldsymbol{s}'). \tag{3.34}$$

Assuming Gaussian noise at the receiver, we can show that D_{ML} is related to the Euclidean distance between $\boldsymbol{y}'$ and $\boldsymbol{H}\boldsymbol{s}'$:

$$D_{\mathrm{ML}}(\boldsymbol{s}',\boldsymbol{y}',\boldsymbol{h}) = T\log(\pi\sigma_z^2) + \frac{\|\boldsymbol{y}' - \boldsymbol{H}\,\boldsymbol{s}'\|^2}{\sigma_z^2}. \tag{3.35}$$

Note that for ML detection under full CSI, we use (3.35), where we calculate the parameter σ_z^2 from (3.25). Under partial CSI knowledge, we calculate it using (3.27) or (3.29) based on the approximation method that we consider.

3.6 Channel estimation

As we noticed from the previous section, since we use coherent DSTBC at the relays, we need to estimate the CSI at the destination based on some pilot symbols, before proceeding to data detection. Two protocols can be used for pilot transmission in AF cooperative relay networks. In the first protocol, firstly, the source transmits the pilot signals to the relays. Then, during a second phase, the relays retransmit the corresponding received signals to the destination one by one in a time-division multiple access (TDMA) mode [48]. In the second protocol, that we consider in this manuscript, DSTBC is performed on the pilots in the same way as on the data symbols in order to benefit from distributed space diversity [56]. To obtain the same channel estimation quality, the TDMA protocol needs more channel-uses to be devoted to pilot transmission, especially for increased number of relays. In other words, by performing DSTBC on the pilots, we obtain a better channel estimate or, equivalently, we suffer from less data-rate loss for the same quality of channel estimate. Note that for both methods, as we will see later, we do not obtain *full* CSI but a *partial* CSI estimate (see Subsection 3.5.2). We explain in the following two methods for channel estimation based only on pilot symbols : the least squares (LS) and the linear MMSE (LMMSE) estimators.

3.6.1 LS channel estimation

We consider equal power allocation among pilot and data symbols in the two transmission hops. Our study can be generalized to the case of optimal power allocation, however [69]. Consider the $(T \times 1)$ vector $\boldsymbol{s_0}$ of BPSK-modulated pilot symbols transmitted from the source. Denoting the corresponding received vector at the destination by $\boldsymbol{y}_0$, from (3.10) we have :

$$\boldsymbol{y}_0 = c\sqrt{q_1}\boldsymbol{P}_0\,\boldsymbol{h} + \boldsymbol{z}_0, \tag{3.36}$$

where $\boldsymbol{z}_0$ is the received noise vector, and the $(T \times R)$ matrix $\boldsymbol{P}_0$ corresponds to distributed space-time processing on $\boldsymbol{s}_0$ at the relays :

$$\boldsymbol{P}_0 = \left[\boldsymbol{C}_1\,\boldsymbol{s}_0^{(*)},\ \boldsymbol{C}_2\,\boldsymbol{s}_0^{(*)},\ldots,\boldsymbol{C}_R\,\boldsymbol{s}_0^{(*)}\right]. \tag{3.37}$$

If we consider N_p (identical) blocks of T pilot symbols, the LS channel estimate solution gives [70] :

$$\hat{\boldsymbol{h}}_{\mathrm{LS}}^{p} = \frac{1}{c\sqrt{q_1}N_p}\left(\boldsymbol{P}_0^{\dagger}\boldsymbol{P}_0\right)^{-1}\sum_{k=1}^{N_p}\boldsymbol{P}_0^{\dagger}\,\boldsymbol{y}_0(k)\,. \tag{3.38}$$

The optimal solution (in the sense of minimizing the variance of estimation errors) is obtained for diagonal $\boldsymbol{P}_0^{\dagger}\boldsymbol{P}_0$. This is the case when orthogonal DSTBC is done at the relays, whatever $\boldsymbol{s}_0$. For $R=2$ with Alamouti and $R=4$ with TSw-Al, we just set $\boldsymbol{s}_0=[1\ \ 1]^t$ and $\boldsymbol{s}_0=[1\ \ 1\ \ 1\ \ 1]^t$, respectively. For $R=4$ and QOSTBC at the relays, we can still use $\boldsymbol{s}_0=[1\ \ 1\ \ 1\ \ 1]^t$ that results in diagonal $\boldsymbol{P}_0^{\dagger}\boldsymbol{P}_0$. Notice that (3.38) does not coincide with the ML estimate as $\boldsymbol{z}_0$ is not Gaussian. (We do not consider ML estimation here due to its high computational complexity in our case.)

3.6.2 LMMSE channel estimation

Let us also consider the MMSE estimation solution. In contrast to the LS solution that assumes a given realization of $\boldsymbol{h}$ (that is, considers $\boldsymbol{h}$ as deterministic), the MMSE solution minimizes the variance of estimation errors by considering the random channel and by taking its statistics into account. Instead of MMSE, we consider here the LMMSE solution that is simpler to implement, given the non-Gaussian noise $\boldsymbol{z}_0$ in our case. Note that the LMMSE solution is equivalent to MMSE for Gaussian noise [64]. It can be shown that :

$$\hat{\boldsymbol{h}}_{\mathrm{LMMSE}}^{p} = \frac{1}{c\sqrt{q_1}N_p}\left(\boldsymbol{P}_0^{\dagger}\boldsymbol{C}_{z_0}^{-1}\boldsymbol{P}_0+\boldsymbol{C}_{\boldsymbol{h}}^{-1}\right)^{-1}\sum_{k=1}^{N_p}\boldsymbol{P}_0^{\dagger}\,\boldsymbol{C}_{z_0}^{-1}\boldsymbol{y}_0(k)\,, \tag{3.39}$$

where $\boldsymbol{C}_{\boldsymbol{h}}$ of dimension $(R\times R)$ and $\boldsymbol{C}_{\boldsymbol{z}_0}$ of dimension $(T\times T)$ are the covariance matrices of the channel and $\boldsymbol{z}_0$, respectively. Given that $\boldsymbol{z}_0$ is white, and considering an IID and normalized channel for our WRN, i.e., taking $\boldsymbol{C}_{\boldsymbol{h}}=\boldsymbol{I}_R$, we can simplify (3.39) as follows.

$$\hat{\boldsymbol{h}}_{\mathrm{LMMSE}}^{p} = \frac{1}{c\sqrt{q_1}N_p}\left(\boldsymbol{P}_0^{\dagger}\boldsymbol{P}_0+\sigma_z^2\boldsymbol{I}_R\right)^{-1}\sum_{k=1}^{N_p}\boldsymbol{P}_0^{\dagger}\,\boldsymbol{y}_0(k) \tag{3.40}$$

3.7 Performance study through numerical results

In this section, we present some simulation results to evaluate the performance of the considered WRN case studies for different data detection and channel estimation methods described before. Performance evaluation is done in terms of the average bit-error-rate (BER) versus SNR that is considered in the form of E_b/N_0. Here, E_b is the average received energy per information bit at the destination, and N_0 is the unilateral power spectral density of the noise.

3.7.1 Simulation parameters

Regarding the BICM scheme used at the source, we consider the use of the rate 1/2 NRNSC channel code of constraint length 3 defined in octal form by $(5,7)_8$, as well as pseudo-random

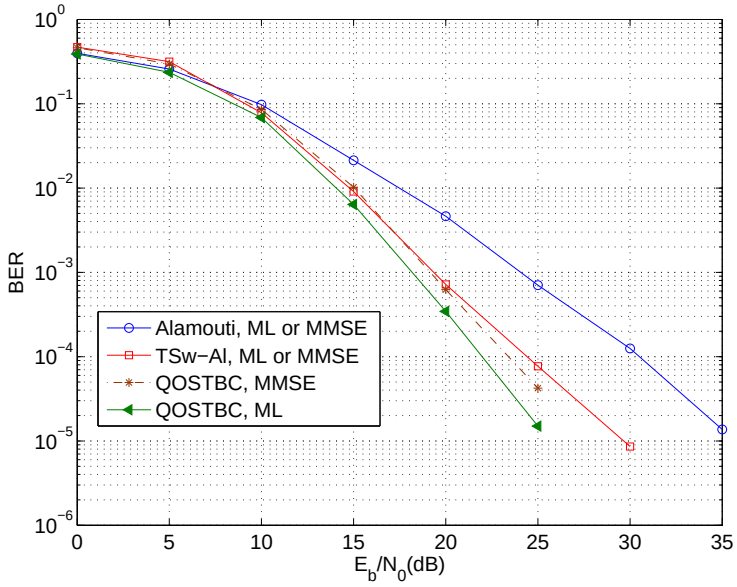

Figure 3.5 — Performance comparisons between ML and MMSE detection under perfect full CSI, $N_p = 1$, QPSK modulation and $(5,7)_8$ channel code.

bit interleaving. The interleaver size, which is also the number of encoded bits per frame, is set to $N_b = 128$. Gray mapped QPSK and 16-QAM modulations are considered for data symbols. Also, normalized channel coefficients are considered according to the Rayleigh IID quasi-static fading model. By the quasi-static fading model, the channel coefficients remain constant during the transmission of N_s blocks of symbols, and they change to new independent values form one frame to next.

3.7.2 ML versus MMSE detection under full CSI

Firstly, let us compare ML and MMSE signal detection methods under the assumption of perfect available full CSI at the receiver. We have presented the BER performance curves in Figure 3.5. Note that for the case of orthogonal DSTBC, ML is equivalent to MMSE detection. The difference of the two detectors is for the case of non-orthogonal QOSTBC for $R = 4$, where ML detection provides an interesting performance improvement, compared with the MMSE method. For instance, at a target BER of 10^{-4}, the SNR improvement is about 1.4 dB. In fact, here, ML takes its advantage over MMSE detection because of treating the inter-relay interference (IRI) due to the non-orthogonal DSTBC structure.
In the following, however, we will focus on the MMSE detection, even for the case of $R = 4$ with QOSTBC. The reason is the lower computational complexity of the MMSE detector, especially for increased signal constellation size.

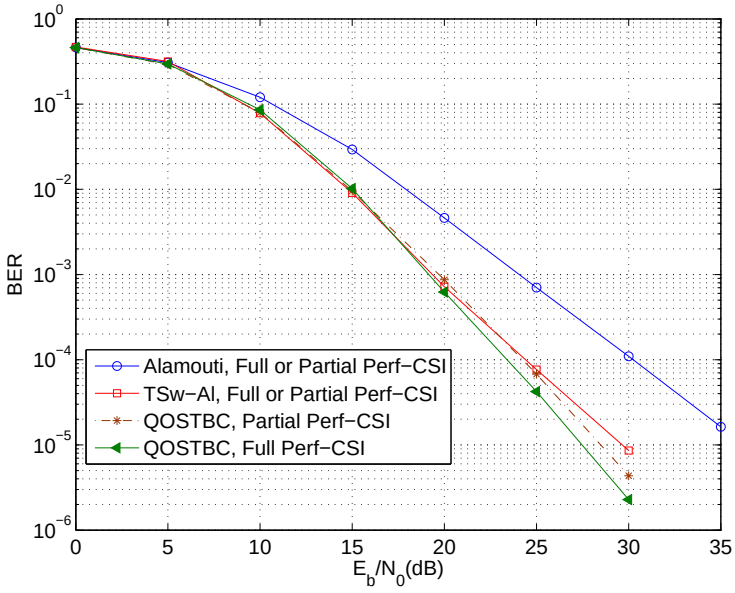

Figure 3.6 — Performance comparisons between full and partial CSI obtained at the destination, MMSE signal detection, $N_p = 1$, QPSK modulation and $(5,7)_8$ channel code.

3.7.3 Performance comparison under perfect full or partial CSI

Considering MMSE detection at the receiver, let us compare the BER performance under perfect full and partial channel knowledge for the three case studies. Results are shown in Figure 3.6. In fact, we have the same performance for Alamouti and TSw-Al DSTBCs for $R = 2$ and 4. In fact for these orthogonal schemes, σ_z^2 does not depend on $\boldsymbol{h}$, and hence, we have the same performance for full and partial CSI. For instance, for the Alamouti scheme, this can be seen from (3.20) and (3.32) ; the term $(c^2 q_1 \boldsymbol{h}^\dagger \boldsymbol{h} + \sigma_z^2)$ cancels out in the calculated LLRs and thus, they do not depend on σ_z^2. This is not the case for $R = 4$ with QOSTBC, however. For this case, we notice from Figure 3.6 an improvement of about 1 dB in E_b/N_0 at BER = 10^{-5} when full CSI is available at the destination.

3.7.4 Gaussian versus enhanced Gaussian approximation under perfect partial CSI

Let us now consider the comparison between Gaussian and enhanced Gaussian approximations for the received noise at the destination (see Subsection 3.5.2). The corresponding BER performances are presented in Figures 3.7 and 3.8 for the cases of QPSK and 16-QAM modulations, respectively. From the discussions of the previous subsection, it can be deduced that this approximation does not have any impact on the performance for the case of orthogonal DSTBCs. For QOSTBC, we have a negligible improvement by using the enhanced Gaussian approximation for the case of QPSK modulation. The improvement is a little more important for 16-QAM modula-

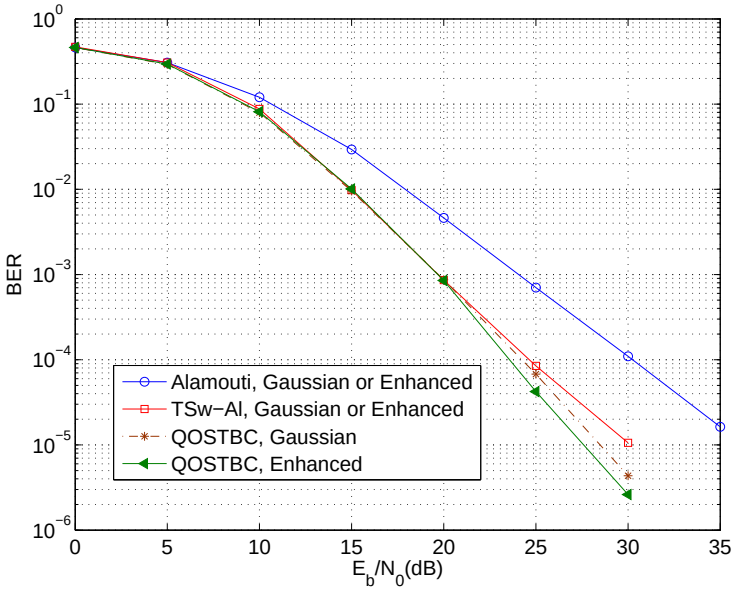

Figure 3.7 — Performance comparisons between Gaussian and enhanced Gaussian approximation, MMSE detection under perfect partial CSI, QPSK modulation and $(5,7)_8$ channel code.

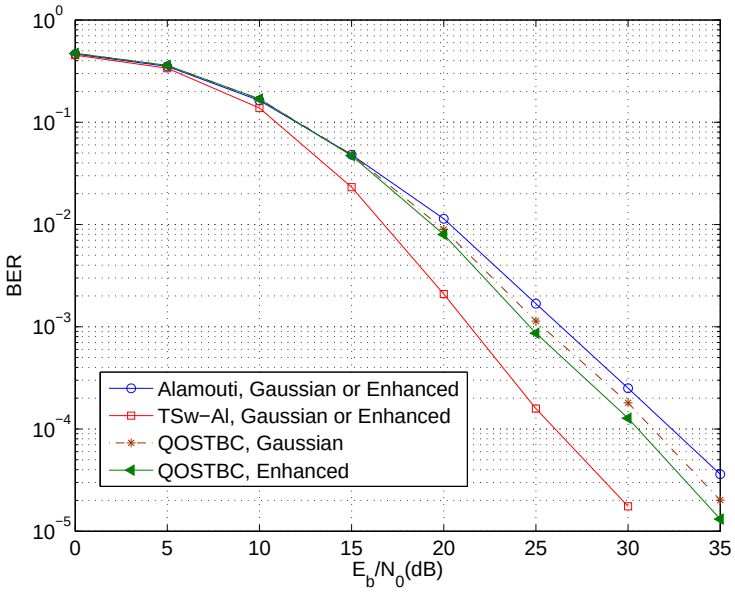

Figure 3.8 — Performance comparisons between Gaussian and enhanced Gaussian approximation, MMSE detection under perfect partial CSI, 16-QAM modulation and $(5,7)_8$ channel code.

tion.[2] In the sequel, we consider the simple Gaussian approximation for the receiver noise.

2. We will explain later in Chapter 5 that when IRI cancelation is performed in the case of QOSTBC, the enhanced Gaussian approximation becomes interesting.

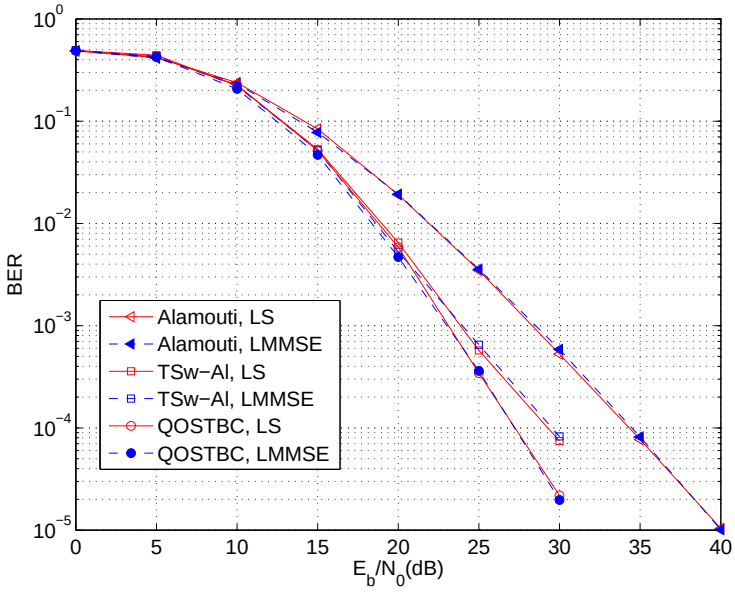

Figure 3.9 — Performance comparisons between LS and LMMSE, $N_p = 1$, QPSK modulation and $(5,7)_8$ channel code.

3.7.5 LS versus LMMSE channel estimation

We have compared the performances of LS and LMMSE estimation methods in Figure 3.9. We notice that the two estimation methods have almost the same performance. Therefore, we will consider hereafter the LS method which has a lower computational complexity.

3.7.6 LS estimation for different numbers of pilot blocks

Now, considering MMSE detection, Gaussian approximation for the received noise, and LS channel estimation, we compare the receiver performance for different numbers of pilot blocks. Results are shown in Figures 3.10 and 3.11 for the considered orthogonal and non-orthogonal DSTBCs, respectively. As reference, we have also presented the performance for the case of perfect partial CSI at the destination. Note that the number of channel-uses devoted to pilot transmission equals to $N_p T$. As we have fixed the total encoded bits per frame to $N_b = 128$, for the case of QPSK modulation, we have $N_s = 32$ and $N_s = 16$ blocks, for $R = 2$ and $R = 4$, respectively. Thus, for the two considered cases of $N_p = 1$ and 3, the percentage of the transmission rate devoted to pilots, i.e., N_p/N_s, equals 3.125% and 9.375%, respectively, for $R = 2$. This pilot overhead equals respectively 6.25% and 18.75% for $R = 4$. Assuming a target BER of 10^{-4}, for instance, from Figure 3.10 we notice that the improvement in E_b/N_0 by increasing N_p from 1 to 3, is about 2.3 dB and 2.7 dB for Alamouti and TSw-Al schemes, respectively. However, even with a considerable pilot overhead, we are still relatively far from the performance with perfect CSI. For the case of $R = 4$ with QOSTBC, the performance for $N_p = 3$ is closer to the perfect CSI case, compared to the TSw-Al scheme. This

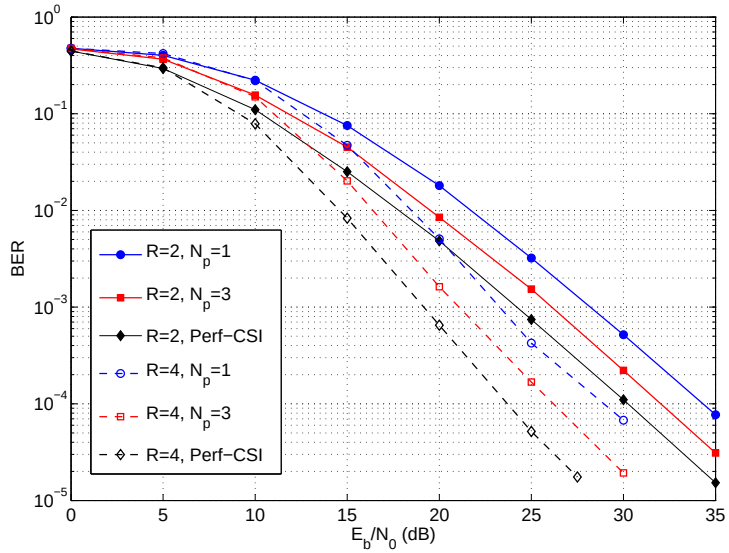

Figure 3.10 — LS pilot-only-based channel estimation with MMSE signal detection for orthogonal DSTBC. N_p is the number of pilot blocks per frame, QPSK modulation, $(5,7)_8$ channel code.

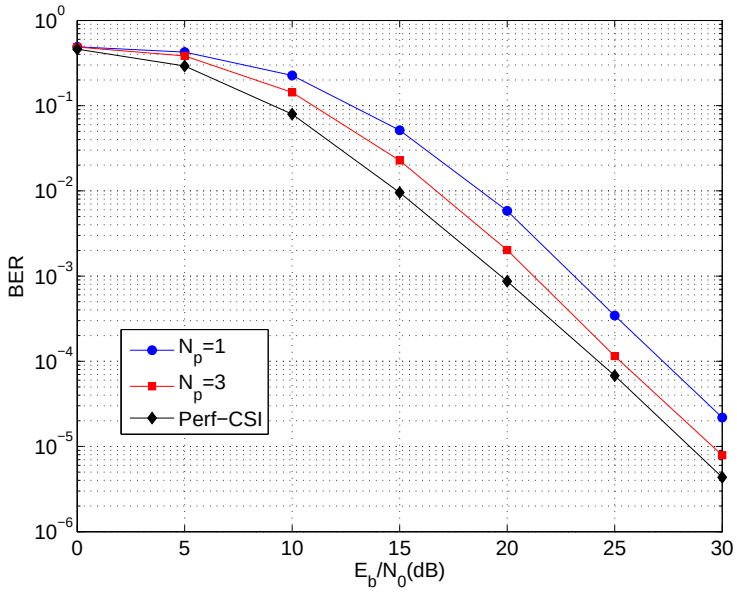

Figure 3.11 — LS pilot-only-based channel estimation with MMSE signal detection for QOSTBC. N_p is the number of pilot blocks per frame, QPSK modulation, $(5,7)_8$ channel code.

is due to the fact that QOSTBC benefits from more diversity gain than the latter scheme. Overall, we can deduce that increasing the number of pilot blocks is not an efficient solution to improve the performance, and moreover, this results in a larger data transmission rate loss. That is why we are going to consider semi-blind channel estimation in the next chapter.

3.8 Chapter conclusion

In this chapter, we considered the AF cooperative relay networks and specified the general assumptions and system model that we will use in the next chapters. Assuming equal available power at the all relay nodes and considering optimal power distribution over network nodes, we presented the data transmission formulation, related in particular to DSTBC at the relays. We explained that using the special DSTBC schemes that we presented, i.e., Alamouti [59], TSw-Al [58], and QOSTBC [61], we can perform signal detection at the destination based on partial CSI knowledge. This property, reduces considerably the network complexity and power consumption. We also compared the ML and MMSE detection methods, the two approximations concerning the received noise at the destination, and LS and LMMSE channel estimation based on pilot symbols, through some simulation results.

We explained that for the case of orthogonal DSTBCs at the relays, partial CSI knowledge is sufficient for optimal signal detection. Also, the statistics of the received noise do not affect the receiver performance. When a non-orthogonal DSTBC like the QOSTBC scheme is employed, however, full CSI knowledge takes its advantage over partial CSI. The performance degradation due to the use of partial CSI remains acceptable, given the increased network complexity to acquire full CSI. Moreover, the simple MMSE detection becomes suboptimal in this case, and also, the enhanced Gaussian approximation for the received noise appears to be a better solution. Regarding channel estimation, the LS method was shown to be a better approach, compared to LMMSE-based estimation.

Finally, we analyzed the performance improvement through increasing the number of pilots. This improvement is obviously obtained at the expense of increased energy consumption needed for pilot transmission, and also data rate reduction. We noticed that increasing the pilot overhead is not a suitable solution as it does not result in a considerable receiver performance improvement. For this reason, in the next chapter, we will consider semi-blind channel estimation, which is an efficient solution to improve the channel estimate quality while requiring a low pilot overhead.

CHAPTER 4

EM-Based Semi-Blind Channel Estimation

4.1 Introduction

In the previous chapter, we considered channel estimation based only on pilots. Obviously, the strategy of increasing the number of pilots to obtain a better CSI at the receiver is not justified in practice. In particular, as power consumption is a critical issue in sensor networks [71], [72], we should minimize the number of pilots in order to reduce power consumption at the source and the relays. We propose here to use semi-blind (SB) channel estimation based on the expectation-maximization (EM) algorithm. The interest of EM is that the estimate converges to the ML solution. Firstly, we present a simple formulation of this estimator implemented in an iterative receiver, and show that with this approach, we can considerably reduce the pilot overhead while obtaining a channel estimate of good quality. Afterwards, we propose a modification to the classical formulation of EM in order to further improve the quality of channel estimate. For this, we propose to combine appropriately the channel estimates obtained using pilots and data symbols separately in view of obtaining an unbiased channel estimate. As we will show, this approach is particularly interesting for modulations of relatively large constellation sizes.

We were inspired by a previous work on channel estimation for classical multiple-input multiple-output (MIMO) systems [73, 74]. Compared to [73], our contributions reside in adapting the formulation to the case of AF WRNs and considerations regarding the non-Gaussian noise at the destination, estimator formulation by taking DSTBC at the relays into account, and the extension to the general QAM modulations ([73] considers simple spatial multiplexing at the transmitter and QPSK modulation). SB estimation is obviously more computationally complex than the estimation based only on pilots. We suppose that, in contrary to the source and the relay nodes, we do not have stringent constraints on the energy, memory, and computational resources of the destination node. Notice that, in this chapter, we consider only the case of employing orthogonal DSTBC at the relays. EM-based channel estimation for the case of non-orthogonal DSTBC is left to the next chapter.

The reminder of this chapter is organized as follows. The formulation of the classical EM-based channel estimation is presented in Section 4.2. Then, we describe the idea behind the improved

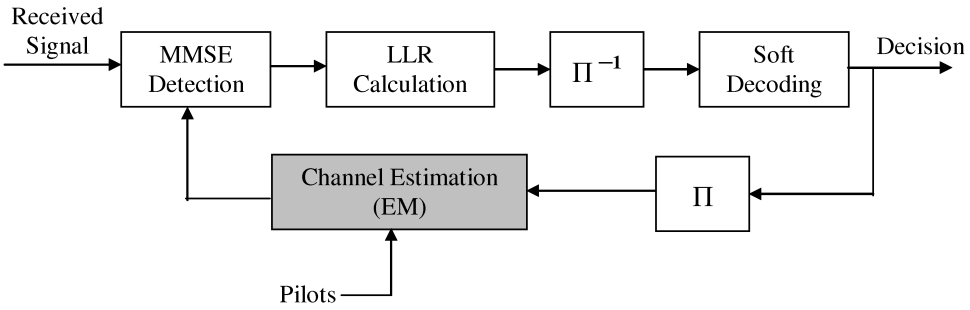

Figure 4.1 — Block diagram of the iterative channel estimator.

EM and its formulation in Section 4.3. Some simulation results are presented in Section 4.4 to compare the performances of different channel estimation methods. Finally, Section 4.5 concludes the chapter.

4.2 Classical EM-based channel estimation

In order to obtain a better channel estimate without suffering from a considerable loss in the transmission data rate by increasing the pilot overhead, SB (also called data-aided) channel estimation appears to be an appropriate solution. This way, we make use of the data symbols in addition to the pilots to improve the channel estimation quality. The scheme we propose here is based on the EM algorithm [75] and is implemented in an iterative receiver (at the destination). The block diagram of the receiver is shown in Figure 4.1. At the first iteration, for signal detection, we use a primary pilot-only (PO) channel estimation, e.g. $\hat{\boldsymbol{h}}_{\mathrm{LS}}^{p}$ from (3.38). After signal demodulation and channel decoding, we use the LLRs at the output of the channel decoder to modify the channel estimate based on EM. We should take into account the DSTBC processing at the relays in the estimator formulation.

The ML-based EM algorithm consists of two steps [76, 77] :

- Expectation : calculating the expected likelihood function of $(\boldsymbol{y},\boldsymbol{P})$ conditioned on the observation $\boldsymbol{y}$, that we denote by the function Q,
- Maximization : maximizing Q with respect to $\boldsymbol{h}$.

At the first iteration, PO estimation is used to initialize EM. After the i-th iteration, we have :

$$Q=\sum_{k=1}^{N_s}\sum_{u=1}^{|\chi|}\log\left[p\Big(\boldsymbol{y}(k)|\boldsymbol{h},\boldsymbol{P}(k)=\boldsymbol{P}_u\Big)\right]\;P\Big(\boldsymbol{P}(k)=\boldsymbol{P}_u\Big|\boldsymbol{y}(k),\hat{\boldsymbol{h}}^{\,i}\Big), \tag{4.1}$$

where k is the block time-reference, $\boldsymbol{P}_u$ and $\boldsymbol{P}(k)$ are respectively the u-th possible and the actual space-time precoded matrices from the relays corresponding to the block k, $\hat{\boldsymbol{h}}^{\,i}$ is the estimated channel at the i-th iteration, $p\Big(\boldsymbol{y}(k)|\boldsymbol{h},\boldsymbol{P}(k)=\boldsymbol{P}_u\Big)$ is the probability density function (PDF) of $\boldsymbol{y}(k)$ conditioned to $\boldsymbol{h}$ and $\boldsymbol{P}(k)=\boldsymbol{P}_u$, and the probability $P\big(\boldsymbol{P}(k)=\boldsymbol{P}_u|\,\boldsymbol{y}(k),\hat{\boldsymbol{h}}^{\,i}\big)$ is calculated using the *a posteriori* probabilities (APP) at the decoder output. Also, χ is the cardinality of $\boldsymbol{P}$ of size

$|\chi| = 2^{BT}$, that is, the set of all possible space-time precoded matrices from the relays, with B being the number of bits per symbol. Since there is a one-to-one correspondence between a vector of symbols $\boldsymbol{s}_u$ and its corresponding DSTBC-precoded matrix $\boldsymbol{P}_u$, we can denote this probability by $P\big(\boldsymbol{s}(k) = \boldsymbol{s}_u | \, \boldsymbol{y}(k), \hat{\boldsymbol{h}}^i\big)$. For notation simplicity, we further denote it by $\mathrm{APP}_k(\boldsymbol{s}_u | \, \hat{\boldsymbol{h}}^i)$.

To develop (4.1), we should take into account the distribution of $\boldsymbol{y}(k)$ given $\boldsymbol{P}_u$ (or $\boldsymbol{s}_u$) and $\boldsymbol{h}$, which reduces to the distribution of $\boldsymbol{z}$ from (3.10). However, as we consider only partial CSI at the destination, $\boldsymbol{z}$ is not Gaussian, and as a result, obtaining a closed form expression for the estimator is quite difficult. We propose to use again the simple Gaussian approximation for $\boldsymbol{z}$ (see Subsection 3.5.2), which results in :

$$Q = -\sum_{k=1}^{N_s} \sum_{u=1}^{|\chi|} \log \left[2\log(\sigma_{\hat{\boldsymbol{z}}}^2) + \frac{||\boldsymbol{y}(k) - c\sqrt{q_1}\boldsymbol{P}_u \boldsymbol{h}||^2}{2\sigma_{\hat{\boldsymbol{z}}}^2} + \kappa \right] \mathrm{APP}_k(\boldsymbol{s}_u | \hat{\boldsymbol{h}}^i), \tag{4.2}$$

where κ is a constant and $\sigma_{\hat{\boldsymbol{z}}}^2$ is calculated using (3.27). Now, to find the function that maximizes Q, we should differentiate it with respect to $\boldsymbol{h}$. We hence obtain the estimation update for the $(i+1)$th iteration :

$$\hat{\boldsymbol{h}}^{i+1} = \boldsymbol{R}_{Py} \boldsymbol{R}_P^{-1}, \tag{4.3}$$

where

$$\boldsymbol{R}_{Py} = c\sqrt{q_1} \sum_{k=1}^{N_s} \sum_{u=1}^{|\chi|} \boldsymbol{P}_u^\dagger \, \boldsymbol{y}(k) \, \mathrm{APP}_k(\boldsymbol{s}_u | \hat{\boldsymbol{h}}^i), \tag{4.4}$$

$$\boldsymbol{R}_P = c^2 q_1 \sum_{k=1}^{N_s} \sum_{u=1}^{|\chi|} \boldsymbol{P}_u^\dagger \boldsymbol{P}_u \mathrm{APP}_k(\boldsymbol{s}_u | \hat{\boldsymbol{h}}^i). \tag{4.5}$$

Note that for notation simplicity, we indicate the iteration number only for $\hat{\boldsymbol{h}}$. Similar to what is proposed in [73], we simplify these equations whose computational complexity grows exponentially with B and T. By this approach, using the decoder soft-outputs, we first calculate soft-estimates of the transmitted symbols, $\tilde{\boldsymbol{s}}(k)$:

$$\tilde{\boldsymbol{s}}(k) = \sum_{u=1}^{|\chi|} \boldsymbol{s}_u \mathrm{APP}_k(\boldsymbol{s}_u | \hat{\boldsymbol{h}}^i). \tag{4.6}$$

Then, we construct the estimated space-time-coded matrices $\widetilde{\boldsymbol{P}}(k)$, and rewrite (4.4) :

$$\boldsymbol{R}_{Py} = c\sqrt{q_1} \sum_{k=1}^{N_s} \widetilde{\boldsymbol{P}}^\dagger(k) \, \boldsymbol{y}(k). \tag{4.7}$$

Separating pilots and data symbols, we can also write $\boldsymbol{R}_{Py}$ in the following form :

$$\boldsymbol{R}_{Py} = c\sqrt{q_1} \left[\sum_{k=1}^{N_p} \boldsymbol{P}_0^\dagger \boldsymbol{y}_0(k) + \sum_{k=N_p+1}^{N_s} \widetilde{\boldsymbol{P}}^\dagger(k) \, \boldsymbol{y}(k) \right], \tag{4.8}$$

where we have used $\boldsymbol{P}_0(k) = \boldsymbol{P}_0$ since we use identical pilot blocks. Similarly, $\boldsymbol{R}_P$ from (4.5) can be written as follows.

$$\boldsymbol{R}_P = c^2 q_1 \left[\sum_{k=1}^{N_p} \boldsymbol{P}_0^\dagger \boldsymbol{P}_0 + \sum_{k=N_p+1}^{N_s} \sum_{u=1}^{|\chi|} \boldsymbol{P}_u^\dagger \boldsymbol{P}_u \mathrm{APP}_k(\boldsymbol{s}_u | \hat{\boldsymbol{h}}^i) \right] \tag{4.9}$$

The two terms in the brackets in (4.9) are diagonal matrices as we perform orthogonal DSTBC at the relays. Then, $\boldsymbol{R}_P$ can be simplified as :

$$\boldsymbol{R}_P = c^2 q_1 N_p T \boldsymbol{I}_R + \boldsymbol{R}_{P_d}, \tag{4.10}$$

and the diagonal matrix $\boldsymbol{R}_{P_d}$ is :

$$\boldsymbol{R}_{P_d} = \mathbf{diag}\big(\xi_1, ..., \xi_R\big) = c^2 q_1 \sum_{k=N_p+1}^{N_s} \widetilde{\boldsymbol{P}^2}(k). \tag{4.11}$$

$\widetilde{\boldsymbol{P}^2}(k)$ is a diagonal matrix specified below :

$$\widetilde{\boldsymbol{P}^2}(k) = \begin{cases} \Big(\sum_{i=1}^{R} \widetilde{s_i^2}(k)\Big)\boldsymbol{I}_R & : \quad \text{for } R = 2 \text{ with Alamouti} \\ 2 \cdot \mathbf{diag}\Big(\widetilde{s_1^2}(k) + \widetilde{s_2^2}(k)\,,\, \widetilde{s_3^2}(k) + \widetilde{s_4^2}(k)\Big) \otimes \boldsymbol{I}_2 & : \quad \text{for } R = 4 \text{ with TSw-Al} \end{cases} \tag{4.12}$$

Here, $\widetilde{s_i^2}(k)$ denotes the soft-estimate of $|s_i(k)|^2$ and $\otimes$ is the Kronecker matrix product. For the case of PSK modulations, we have $\widetilde{s_i^2}(k) = 1$, $\xi_i = c^2\, q_1\, N_d\, T$, and (4.10) simplifies to the following.

$$\boldsymbol{R}_P = c^2 q_1 N_s T \boldsymbol{I}_R \tag{4.13}$$

So, overall, we calculate in each iteration $\boldsymbol{R}_P$ from (4.10) and $\boldsymbol{R}_{Py}$ from (4.8), and update the channel estimate from (4.3). We will call this estimator CB-EM (CB standing for classical biased) because, as we explain in the following subsection, this classical EM formulation provides a biased estimate of the channel.

4.3 Improving the classical EM-based estimator

Let us focus on $\boldsymbol{R}_{Py}$ in (4.8) by replacing $\boldsymbol{y}$ and $\boldsymbol{y}_0$ from (3.10) and (3.36), respectively. We obtain (see Appendix A) :

$$\begin{aligned} \boldsymbol{R}_{Py} &= \underbrace{c^2 q_1 N_p\, T \boldsymbol{I}_R}_{\boldsymbol{R}_{P_0}} \boldsymbol{h} + \underbrace{c\sqrt{q_1} \sum_{k=1}^{N_p} \boldsymbol{P}_0^{\dagger} \boldsymbol{z}_0(k)}_{\boldsymbol{\eta}_0} + \underbrace{c^2 q_1 \left(\sum_{k=N_p+1}^{N_s} \widetilde{\boldsymbol{P}}^{\dagger}(k) \boldsymbol{P}(k) \right)}_{\boldsymbol{R}_P'} \boldsymbol{h} + \underbrace{c\sqrt{q_1} \sum_{k=N_p+1}^{N_s} \widetilde{\boldsymbol{P}}^{\dagger}(k)\, \boldsymbol{z}(k)}_{\boldsymbol{\eta}} \\ &= (\boldsymbol{R}_{P_0} + \boldsymbol{R}_P')\boldsymbol{h} + \boldsymbol{\eta}_0 + \boldsymbol{\eta}, \end{aligned} \tag{4.14}$$

where we have defined the matrices $\boldsymbol{R}_{P_0}$ and $\boldsymbol{R}_P'$ and the vectors $\boldsymbol{\eta}_0$ and $\boldsymbol{\eta}$. Comparing (4.14) with (4.10), we notice that $(\boldsymbol{R}_{P_0} + \boldsymbol{R}_P') \neq \boldsymbol{R}_P$, and hence, from (4.3), the obtained channel estimate by using CB-EM is biased. This bias that affects the data detection part, is due to the difference between $\widetilde{\boldsymbol{P}^2}$ and $\widetilde{\boldsymbol{P}}^{\dagger}\boldsymbol{P}$ (corresponding to data symbols), or in other words, due to the difference between $\widetilde{s_i^2}$ and $\tilde{s}_i^* s_i$, $i = 1, ..., R$. At very high SNR, however, we have $\tilde{s}_i \approx s_i$ and $\widetilde{s_i^2} \approx \tilde{s}_i^* s_i$, and the bias becomes negligible.

Our aim here is to propose a modified estimator in order to eliminate the bias and to improve the channel estimation quality. One simple solution is to remove the bias by multiplying $\hat{\boldsymbol{h}}$ by the

inverse of the matrix $\left[(\boldsymbol{R}_{P_0}+\boldsymbol{R}_P^{'})\boldsymbol{R}_P^{-1}\right]$. We propose here a more appropriate solution that results in a better receiver performance. Let us consider separately the channel estimates based on pilots and data symbols that we denote by $\hat{\boldsymbol{h}}^p$ and $\hat{\boldsymbol{h}}^d$, respectively. Note that $\hat{\boldsymbol{h}}^p$ is unbiased, in contrary to $\hat{\boldsymbol{h}}^d$. Then, we can write :

$$\hat{\boldsymbol{h}}^p = \boldsymbol{h}+\boldsymbol{\eta}_0' \quad , \quad \hat{\boldsymbol{h}}^d = \boldsymbol{\Lambda}\boldsymbol{h}+\boldsymbol{\eta}', \tag{4.15}$$

where the entries of the matrix $\boldsymbol{\Lambda}$ of dimension $(R\times R)$ are calculated as follows (see Appendix A).

$$\lambda_{ij} = \boldsymbol{\Lambda}(i,j) = \frac{1}{\xi_i}\boldsymbol{R}_P^{'}(i,j)\,, \quad i,j=1,...,R, \tag{4.16}$$

and ξ_i are defined in (4.11). Also, we have defined the estimation noise vectors $\boldsymbol{\eta}_0'$ and $\boldsymbol{\eta}'$. Using the definitions of $\boldsymbol{\eta}_0$ and $\boldsymbol{\eta}$ in (4.14), we have :

$$\boldsymbol{\eta}_0' = \frac{1}{c^2\,q_1\,N_p\,T}\,\boldsymbol{\eta}_0 \quad , \quad \boldsymbol{\eta}_i' = \frac{1}{\xi_i}\,\boldsymbol{\eta} \quad , \quad i=1,...,R. \tag{4.17}$$

Denoting the variance of the entries of $\boldsymbol{\eta}_0'$ by $\sigma^2_{\boldsymbol{\eta}_0'}$, and that of $\boldsymbol{\eta}_i'$ by $\sigma^2_{\boldsymbol{\eta}_i'}$, it can be shown that :

$$\sigma^2_{\boldsymbol{\eta}_0'} = \frac{\sigma^2_{\hat{\boldsymbol{z}}}}{c^2\,q_1\,N_p\,T} = \beta_0\,\sigma^2_{\hat{\boldsymbol{z}}} \quad , \quad \sigma^2_{\boldsymbol{\eta}_i'} = \frac{\boldsymbol{R}_P''(i,i)}{\xi_i^2}\,\sigma^2_{\hat{\boldsymbol{z}}} = \beta_i\,\sigma^2_{\hat{\boldsymbol{z}}}\,, \tag{4.18}$$

where we have defined the following two coefficients :

$$\beta_0 = \frac{1}{(c^2\,q_1\,N_p\,T)} \quad , \quad \beta_i = \frac{\boldsymbol{R}_P''(i,i)}{\xi_i^2}\,, \tag{4.19}$$

and also defined the matrix $\boldsymbol{R}_P''$ as follows.

$$\boldsymbol{R}_P'' = c^2 q_1 \sum_{k=N_p+1}^{N_s} \widetilde{\boldsymbol{P}}^{\dagger}(k)\widetilde{\boldsymbol{P}}(k) \tag{4.20}$$

On the other hand, given (4.16) and the definition of $\boldsymbol{R}_P'$ in (4.14), we notice that for the orthogonal DSTBC schemes, matrix $\boldsymbol{\Lambda}$ in (4.15) has the following property :

$$\boldsymbol{\Psi} = \boldsymbol{\Lambda}^{\dagger}\boldsymbol{\Lambda} = \mathbf{diag}\big(\psi_1,\psi_2,\cdots,\psi_R\big). \tag{4.21}$$

For instance, for $R=2$ with the Alamouti scheme, from (3.11), we have $\psi_1=\psi_2=|\lambda_{11}|^2+|\lambda_{12}|^2$. Also, for $R=4$ with TSw-Al, from (3.14), we have

$$\begin{cases} \psi_1=\psi_2=|\lambda_{11}|^2+|\lambda_{12}|^2 \\ \psi_3=\psi_4=|\lambda_{33}|^2+|\lambda_{34}|^2 \end{cases} \tag{4.22}$$

Now, to obtain an unbiased estimator, we propose to look for an appropriate combination of $\hat{\boldsymbol{h}}^p$ and $\hat{\boldsymbol{h}}^d$. As a simple and low complexity solution, we consider each entry of $\hat{\boldsymbol{h}}$ as a linear combination of the corresponding entries of $\hat{\boldsymbol{h}}^p$ and $\hat{\boldsymbol{h}}^d$. To write this in a vector form, we define two weight matrices $\boldsymbol{A}$ and $\boldsymbol{B}$. Then, the unbiased channel estimate is given by :

$$\hat{\boldsymbol{h}} = \boldsymbol{A}\,\hat{\boldsymbol{h}}^p + \boldsymbol{B}\,\hat{\boldsymbol{h}}^d\,. \tag{4.23}$$

We determine the matrices $\boldsymbol{A}$ and $\boldsymbol{B}$ so as to minimize the estimation error variance while satisfying the condition of unbiased estimation, that is [78],

$$\min_{\boldsymbol{A},\boldsymbol{B}} \mathrm{E}\left\{||\boldsymbol{A}\boldsymbol{\eta}_0' + \boldsymbol{B}\boldsymbol{\eta}'||^2\right\} \quad , \quad \text{satisfying } \boldsymbol{A} + \boldsymbol{B}\boldsymbol{\Lambda} = \boldsymbol{I}_R. \tag{4.24}$$

Notice that in [79], for the sake of simplicity and reducing the computational complexity of the estimator, we had approximated $\boldsymbol{R}_P'$ with a diagonal matrix, assuming large enough N_s. As a result, we had considered diagonal matrices for $\boldsymbol{A}$ and $\boldsymbol{B}$. Here, however, we make no special assumption on $\boldsymbol{R}_P'$ nor on $\boldsymbol{A}$ and $\boldsymbol{B}$. After some manipulations, we obtain the following optimized weight matrices for the proposed linear combination.

$$\boldsymbol{A} = \boldsymbol{I}_R - \boldsymbol{\Gamma}\boldsymbol{\Psi} \quad , \quad \boldsymbol{B} = \boldsymbol{\Gamma}\boldsymbol{\Lambda}^{\dagger}, \tag{4.25}$$

where $\boldsymbol{\Gamma}$ is an $(R \times R)$ diagonal matrix with the diagonal entries given below.

$$\gamma_{ii} = \boldsymbol{\Gamma}(i,i) = \frac{\beta_0}{\beta_i + \beta_0 \psi_i}, \quad i = 1, ..., R. \tag{4.26}$$

Remember that β_0 and β_i are obtained from (4.19) and ψ_i is defined in (4.21).

By further observation of (A.7) and (A.19) in Appendix A, we note that $\boldsymbol{R}_P'$ is not diagonal except when the detected symbols are exact (i.e., without any error). In order to further improve the performance, we should eliminate the interference from its off-diagonal entries. Therefore, it is rational that we directly set the off-diagonal entries to zero to simplify the estimator formulation.

We call the resulting estimation method "unbiased linearly-combined EM" and will denote it by UL-EM. This solution has almost the same computational complexity of what proposed by [79] but provides a better performance. The only remaining problem is to calculate λ_{ij} from (4.16). As, obviously, we do not know $\boldsymbol{P}$ at the destination, we cannot calculate $\boldsymbol{R}_P^{'}$ from (4.14). To calculate $\boldsymbol{R}_P^{'}$, we propose to simply construct $\boldsymbol{P}$ from the hard estimates of the transmitted symbols using the decoder soft outputs. Obviously, these hard estimates do not necessarily coincide with the true transmitted symbols, and as we will see in the next section, this limits the performance of the UL-EM method, especially for small constellations.

4.4 Performance comparison between CB-EM and UL-EM methods

We present in this section some numerical results to study the performance of the CB-EM and UL-EM estimation methods for the cases of two and four relays. Performance evaluation is done in terms of the average BER as a function of SNR.

4.4.1 Simulation parameters

At the transmitter, we consider pseudo-random interleaving and the rate 1/2 NRNSC code $(5,7)_8$ in the BICM scheme. Gray-mapped QPSK and 16-QAM modulations are considered. We

consider the quasi-static, flat, Rayleigh, IID-fading channel model. We assume that each frame of symbols corresponds to $N_s T = 64$ channel-uses. Also, to better illustrate the advantage of SB over PO channel estimation, we use the minimum number of pilot blocks per frame of symbols, i.e., we set $N_p = 1$. In the results that we present, we will indicate the number of processed iterations at the receiver by IT. When we do not indicate it on the figures, it means that only one iteration is processed.

4.4.2 Case of $R = 2$

We have compared the performances of different estimation methods in Figure 4.2 for the case of $R = 2$, where the Alamouti DSTBC is performed at the relays, and QPSK modulation. For SB es-

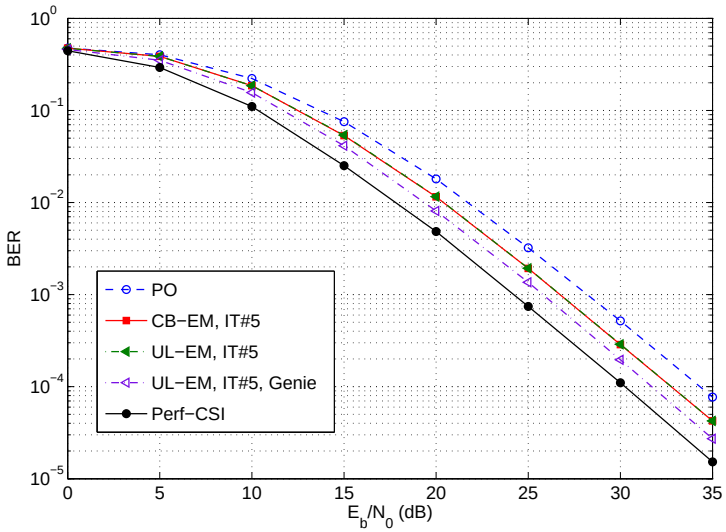

Figure 4.2 — Comparison of SB and PO channel estimation. $R = 2$ with Alamouti DSTBC, $N_s T = 64$, $N_p = 1$, QPSK modulation, $(5,7)_8$ channel code. IT denotes iteration number.

timation methods, five receiver iterations are necessary to attain almost full receiver convergence. The LS-based PO estimate is used at the first iteration to initialize the SB algorithms. We notice an interesting performance improvement in E_b/N_0 by SB estimation : it is about 1.5 dB at a target BER of 10^{-4}. The UL-EM does not offer any advantage over CB-EM in this case, however. Note that for increased frame size, the performance improvement by SB estimation methods becomes more significant (see [79]). Also, the UL-EM takes its advantage over CB-EM for increased N_s. For example, we have presented the receiver performance for $N_s T = 256$ in Figure 4.3 where we notice a slight improvement in BER by using the UL-EM method.

Let us now consider the case of the relatively large constellation of 16-QAM. Performance curves are shown in Figure 4.4. Here, for the cases of PO estimation and perfect CSI, we need to process only two iterations. We notice that at BER = 10^{-4}, CB-EM provides an improvement of about 1 dB in SNR compared with PO estimation. Moreover, the UL-EM approach allows 0.7 dB

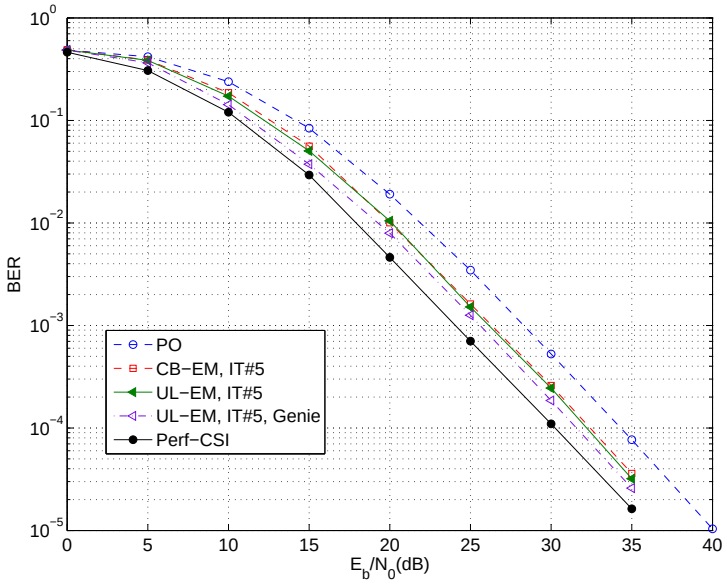

Figure 4.3 — Comparison of SB and PO channel estimation. $R = 2$ with Alamouti DSTBC, $N_s T = 256$, $N_p = 1$, QPSK modulation, $(5,7)_8$ channel code. IT denotes iteration number.

further improvement, compared to CB-EM.

To understand why the UL-EM method gives poor improvement for small constellations such as QPSK, we should come back to the calculation of $\boldsymbol{R}_P^{'}$ that is required to update $\hat{\boldsymbol{h}}$ by this method. The calculation of $\boldsymbol{R}_P^{'}$ was discussed at the last paragraph of Section 4.3, where we explained that we use the hard-estimates of the transmitted symbols obtained from the soft-decoder outputs to construct $\boldsymbol{P}$. As a matter of fact, the poor performance of UL-EM arises from the possible errors in these hard estimates. We have shown in the presented results the hypothetical BER curves that are obtained if we use the exact transmitted symbols (i.e., the exact $\boldsymbol{P}$) in the calculation of $\boldsymbol{R}_P^{'}$. We denote this case by "UL-EM, Genie" and notice that it provides an interesting improvement in the receiver performance. So, the limited performance improvement of UL-EM arises from this implementation constraint. For larger constellation sizes, the performance is less affected by the errors in this hard estimation, because it is done on a smaller "grid size" on the signal constellation plane.

4.4.3 Case of $R = 4$

Let us now consider the case of four relays. The corresponding performance results are shown in Figure 4.5 for the case of QPSK modulation. We notice that a substantial performance improvement can be obtained through using SB estimation. For instance, at a BER of 10^{-4}, we notice an SNR gain of about 2.5 dB. Similar to the case of $R = 2$, the UL-EM does not allow any improvement, compared to CB-EM. For the case of the 16-QAM modulation, results are shown in Figure 4.6, where we notice an improvement of 1.6 dB in E_b/N_0 at BER $= 10^{-4}$ by using the CB-EM method,

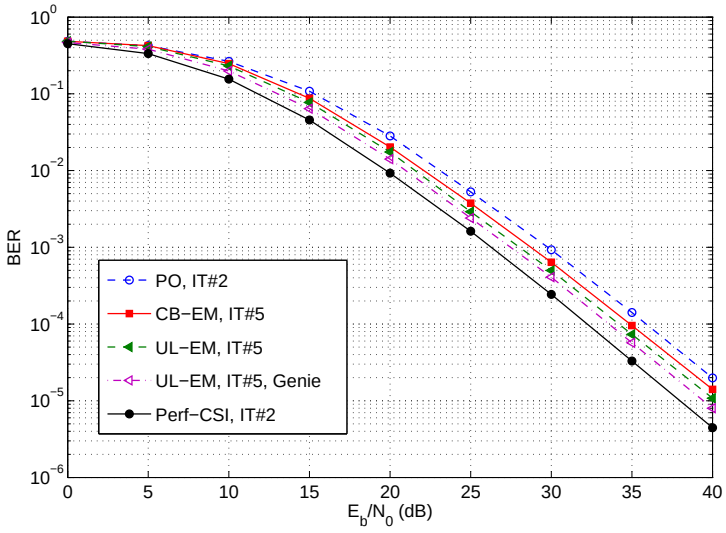

Figure 4.4 — Comparison of SB and PO channel estimation. $R = 2$ with Alamouti DSTBC, $N_s T = 64$, $N_p = 1$, 16-QAM modulation, $(5,7)_8$ channel code. IT denotes iteration number.

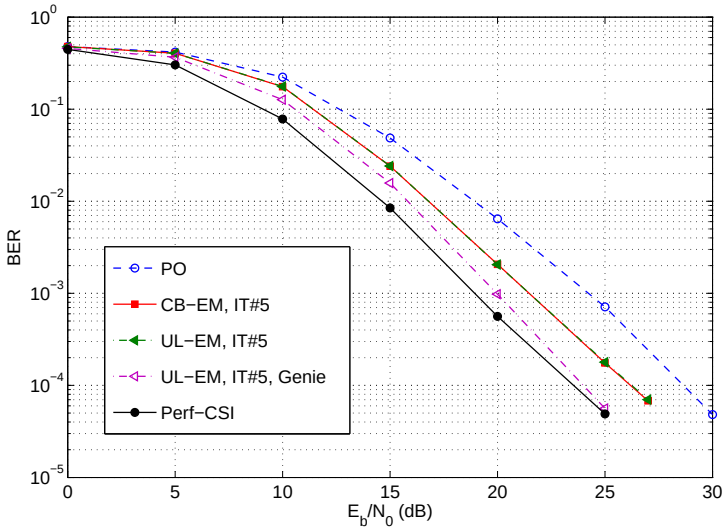

Figure 4.5 — Comparison of SB and PO channel estimation with TSw-Al. $R = 4$ with TSw-Al DSTBC, $N_s T = 64$, $N_p = 1$, QPSK modulation, $(5,7)_8$ channel code. IT denotes iteration number.

compared to PO. Also, the UL-EM method allows about 0.85 dB SNR improvement over CB-EM. Similar to the case of $R = 2$, we have shown the BER curves for the "UL-EM, Genie." We notice again that UL-EM suffers from the inaccuracy in the calculation of $\boldsymbol{R}'_p$.

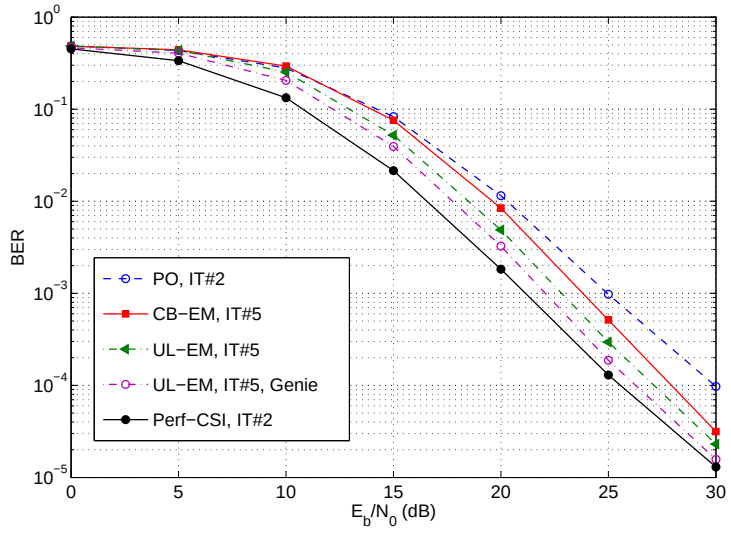

Figure 4.6 — Comparison of SB and PO channel estimation. $R = 4$ with TSw-Al DSTBC, $N_s T = 64$, $N_p = 1$, 16-QAM modulation, $(5,7)_8$ channel code. IT denotes iteration number.

4.4.4 Estimation error variance

It is quite useful to study the evolution of the variance of estimation errors for PO and SB methods. We have shown the curves of the mean square of estimation errors (MSE) versus E_b/N_0 for the case of $R = 4$ and 16-QAM modulation in Figure 4.7, for instance. As reference, we have also presented the MSE curve corresponding to the hypothetical case where the receiver has perfect knowledge of the transmitted data symbols. This curve is labeled LB (for Lower Bound) Figure 4.7 and can be used as a lower bound on the estimation MSE. We notice from this figure that the UL-EM method gives a lower MSE than CB-EM. Moreover, at the high SNR (larger than 25 dB), both the corresponding curves of CB-EM and UL-EM converge to the LB.

4.5 Chapter conclusion and discussions

We considered SB channel estimation for AF cooperative relay networks and orthogonal DSTBC, based on the EM algorithm. We firstly considered the classical EM-based channel estimation and provided the estimator formulation for the AF WRN system. We called this approach CB-EM. Considering the two case studies of two and four relay nodes, we demonstrated through simulations the interesting performance improvement that we obtain by SB estimation. This way, by devoting few channel-uses to pilot transmission, and hence, minimizing the nodes$'$ energy consumption and the pilot overhead, we can obtain a satisfying performance at the destination. Performance improvement with SB estimation is more significant for a larger number of relays. In fact, for a larger R, benefiting from more distributed diversity, we have a better detection performance, and the contribution of the detected data symbols to channel estimation becomes more

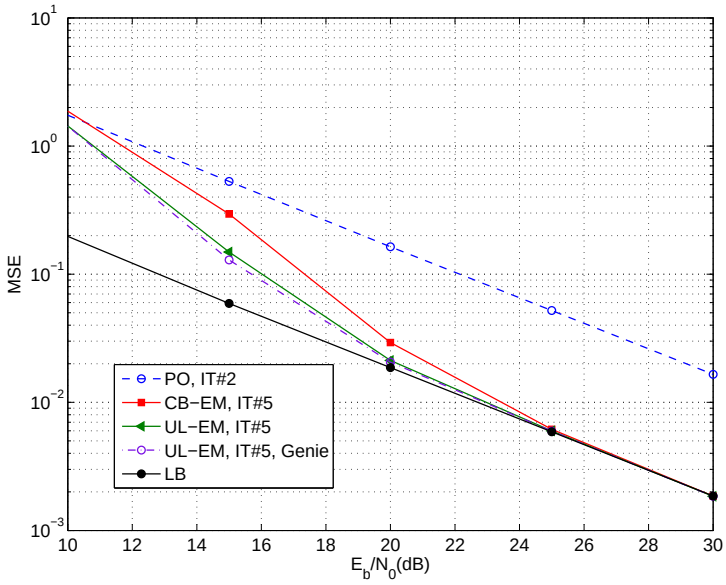

Figure 4.7 — Channel estimation MSE for SB and PO estimation methods. $R = 4$ with TSw-Al, $N_s T = 64$, $N_p = 1$, 16-QAM modulation, $(5,7)_8$ channel code.

beneficial. Also, more significant performance improvement is obtained for increased frame size.

We further showed that the CB-EM formulation provides a biased channel estimate and proposed a modification to it, in order to obtain an unbiased estimate. We called this approach UL-EM. Comparing the performances of CB-EM and UL-EM, we noticed that the latter is advantageous for relatively large signal constellations. The inherent bias in the CB-EM estimate appears to be penalizing in such cases. However, for the simple QPSK modulation case, we obtained negligible performance improvement that does not justify the computational complexity of UL-EM. We showed that this is due to the difference between the transmitted symbols and their hard estimates that we need in the implementation of UL-EM.

SB estimation is obviously more computationally complex than PO estimation. We assumed that there are less stringent constraints on the energy and computational resources of the destination node, compared to the source and the relay nodes. The increased computational complexity by SB estimation remains moderate and quite justified taking into account the significant achieved performance improvement.

CHAPTER 5

Iterative Data Detection and Channel Estimation for Non-Orthogonal DSTBC at Relays

5.1 Introduction

In the previous chapter, we considered the case of orthogonal DSTBC at the relays. The advantage of using orthogonal DSTBC is that the optimal decoder is of linear complexity. However, except the Alamouti scheme for $R = 2$, other orthogonal schemes suffer from low rate or low diversity gain, especially for the case of large number of relay nodes. For instance, the TSw-Al scheme that we considered previously for $R = 4$ is of full rate but has a diversity gain of 2 only.

In order to obtain a high spectral efficiency with orthogonal DSTBCs for $R > 2$, relatively high channel coding rates and/or large signal constellations should be used, which, in turn, increases the receiver computational complexity and also requires a higher SNR for signal detection at the receiver [58, 80, 81]. Non-orthogonal DSTBCs generally offer higher rates and diversity gains but suffer from high receiver complexity if optimal decoding is to be performed at the receiver. On the other hand, in such a case, suboptimal detectors like the MMSE detector suffer from inter-relay interference (IRI) due to the non-orthogonal structure of the DSTBC (see Subsection 3.7.2). Here, to circumvent this problem, we consider iterative soft parallel interference cancelation (PIC) at the receiver together with soft channel decoding.

This idea of iterative processing by making use of channel coding gain has been applied to several contexts in digital communications such as turbo decoding [82], channel equalization [83], channel estimation [68, 84], time synchronization [85], multiuser detection [86], and especially MIMO signal detection [58, 73, 74, 87, 88, 89, 90]. By this approach, as we will see in this chapter, we consider the use of soft and hard estimated symbols (using the decoder soft outputs) in channel estimation and soft-PIC signal detection.

In the rest of this chapter, we consider the case study of four relay nodes and the QOSTBC

scheme at the relays, introduced previously in Subsection 3.4.2. We also consider SB channel estimation based on the CB-EM formulation to improve the channel estimate through iterations. Moreover, we use the extrinsic information transfer (EXIT) charts to study the convergence of the different iterative schemes.

The reminder of this chapter is organized as follows. Firstly, we reformulate in Section 5.2 the data transmission link in order to provide general expressions for the PIC detector while taking into account the DSTBC at the relays. The iterative soft-PIC detector is then described in Section 5.3. Next, a brief introduction to EXIT chart tool is presented in Section 5.4. Some numerical results are provided in Section 5.5 to study the performance of the proposed detection schemes, and Section 5.6 concludes the chapter.

5.2 Reformulation of data transmission

In contrast to the formulation presented in Section 3.3, here, in order to obtain a general formulation for the received signal at the destination, we separate the real and imaginary parts of the parameters, like in [42]. By adopting this rule, (3.5) can equivalently be rewritten in the following form :

$$\boldsymbol{t}_i = c(\boldsymbol{A}_i\,\boldsymbol{r}_i + \boldsymbol{B}_i\,\boldsymbol{r}_i^*), \tag{5.1}$$

$\boldsymbol{A}_i$ and $\boldsymbol{B}_i$ are complex $(T \times T)$ DSTBC precoding matrices. We have :

$$\begin{bmatrix} \boldsymbol{t}_{i,\Re} \\ \boldsymbol{t}_{i,\Im} \end{bmatrix} = c \underbrace{\begin{bmatrix} \boldsymbol{A}_{i,\Re} + \boldsymbol{B}_{i,\Re} & -\boldsymbol{A}_{i,\Im} + \boldsymbol{B}_{i,\Im} \\ \boldsymbol{A}_{i,\Im} + \boldsymbol{B}_{i,\Im} & \boldsymbol{A}_{i,\Re} - \boldsymbol{B}_{i,\Re} \end{bmatrix}}_{\boldsymbol{D}_i} \begin{bmatrix} \boldsymbol{r}_{i,\Re} \\ \boldsymbol{r}_{i,\Im} \end{bmatrix}, \tag{5.2}$$

where, for instance, $\boldsymbol{A}_{i,\Re}$ and $\boldsymbol{A}_{i,\Im}$ denote the real and imaginary parts of $\boldsymbol{A}_i$, respectively. For notation simplicity, we also defined the matrix $\boldsymbol{D}_i$ in (5.2). At the destination, we rewrite the received vector :

$$\boldsymbol{y} = \sum_{i=1}^{R} g_i\ \boldsymbol{t}_i + \boldsymbol{n}_d. \tag{5.3}$$

We further separate the real and imaginary parts of the signals in $\boldsymbol{s}$ and $\boldsymbol{y}$, and define the vectors $\mathscr{S}$ and $\mathscr{Y}$ of dimension $(2T \times 1)$ as follows.

$$\mathscr{S} = \begin{bmatrix} \boldsymbol{s}_\Re \\ \boldsymbol{s}_\Im \end{bmatrix}, \quad \mathscr{Y} = \begin{bmatrix} \boldsymbol{y}_\Re \\ \boldsymbol{y}_\Im \end{bmatrix}. \tag{5.4}$$

where, for instance, $\boldsymbol{s}_\Re$ and $\boldsymbol{s}_\Im$ denote the real and imaginary parts of $\boldsymbol{s}$, respectively. Now, we can write $\mathscr{Y}$ as a function of $\mathscr{S}$ by considering an equivalent channel matrix $\mathscr{H}_{\text{eq}}$ of dimension $(2T \times 2T)$:

$$\mathscr{Y} = c\sqrt{q_1}\,\mathscr{H}_{\text{eq}}\,\mathscr{S} + \mathscr{Z}, \tag{5.5}$$

$$\mathscr{H}_{\text{eq}} = \sum_{i=1}^{R} \begin{bmatrix} g_{i,\Re}\,\boldsymbol{I}_T & -g_{i,\Im}\,\boldsymbol{I}_T \\ g_{i,\Im}\,\boldsymbol{I}_T & g_{i,\Re}\,\boldsymbol{I}_T \end{bmatrix} \boldsymbol{D}_i \begin{bmatrix} f_{i,\Re}\,\boldsymbol{I}_T & -f_{i,\Im}\,\boldsymbol{I}_T \\ f_{i,\Im}\,\boldsymbol{I}_T & f_{i,\Re}\,\boldsymbol{I}_T \end{bmatrix}, \tag{5.6}$$

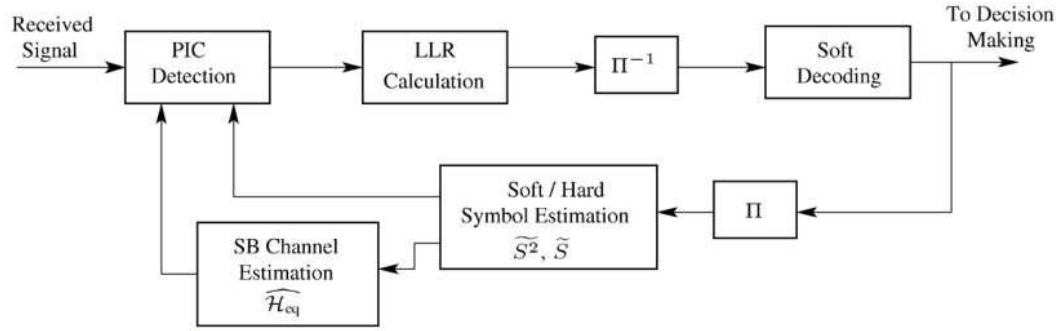

Figure 5.1 — Block diagram of the receiver performing iterative symbol detection and channel estimation. Blocks Π^{-1} and Π represent de-interleaving and interleaving, respectively.

where the vector $\mathscr{Z}$ is the total received noise at the destination :

$$\mathscr{Z} = \begin{bmatrix} \boldsymbol{n}_{d,\Re} \\ \boldsymbol{n}_{d,\Im} \end{bmatrix} + c \sum_{i=1}^{R} \begin{bmatrix} g_{i,\Re} \boldsymbol{I}_T & -g_{i,\Im} \boldsymbol{I}_T \\ g_{i,\Im} \boldsymbol{I}_T & g_{i,\Re} \boldsymbol{I}_T \end{bmatrix} \boldsymbol{D}_i \begin{bmatrix} \boldsymbol{n}_{ri,\Re} \\ \boldsymbol{n}_{ri,\Im} \end{bmatrix}. \tag{5.7}$$

In fact, $\mathscr{H}_{\text{eq}}$ is composed of the real and imaginary parts of $f_i^{(*)} g_i$. To study the performance of the proposed methods, we consider the case study of $R = 4$ with the QOSTBC scheme [61] at the relays, where the retransmitted signal matrix from the relays can be written as :

$$[\ \boldsymbol{t}_1\ \boldsymbol{t}_2\ \boldsymbol{t}_3\ \boldsymbol{t}_4\ ] = c \begin{bmatrix} r_{11} & -r_{22}^* & -r_{33}^* & r_{44} \\ r_{12} & r_{21}^* & -r_{34}^* & -r_{43} \\ r_{13} & -r_{24}^* & r_{31}^* & -r_{42} \\ r_{14} & r_{23}^* & r_{32}^* & r_{41} \end{bmatrix}. \tag{5.8}$$

Here, r_{ij} denotes the received signal at the i-th relay on the j-th time reference. Also, according to the (5.1), we can obtain the precoding matrices $\boldsymbol{A}_i$ and $\boldsymbol{B}_i$ as follows :

$$\boldsymbol{B}_1 = \boldsymbol{A}_2 = \boldsymbol{A}_3 = \boldsymbol{B}_4 = \boldsymbol{0}_{4\times 4}, \tag{5.9}$$

$$\boldsymbol{A}_1 = \boldsymbol{I}_4, \boldsymbol{B}_2 = \begin{bmatrix} 0 & -1 & 0 & 0 \\ 1 & 0 & 0 & 0 \\ 0 & 0 & 0 & -1 \\ 0 & 0 & 1 & 0 \end{bmatrix}, \boldsymbol{B}_3 = \begin{bmatrix} 0 & 0 & -1 & 0 \\ 0 & 0 & 0 & -1 \\ 1 & 0 & 0 & 0 \\ 0 & 1 & 0 & 0 \end{bmatrix}, \boldsymbol{A}_4 = \begin{bmatrix} 0 & 0 & 0 & 1 \\ 0 & 0 & -1 & 0 \\ 0 & -1 & 0 & 0 \\ 1 & 0 & 0 & 0 \end{bmatrix}, \tag{5.10}$$

and $\boldsymbol{0}_{4\times 4}$ denotes an all-zero matrix of size (4×4).

5.3 Signal detection and channel estimation at the destination

Now consider the general iterative receiver with PIC detection which is shown in Figure 5.1. We use the LLRs at the output of the channel decoder at the previous iteration to improve the channel estimate and data detection.

5.3.1 First iteration

For signal detection, we should firstly know the CSI at the destination before data transmission. In this chapter, we use the same scheme as the Section 4.2 for channel estimation. That means that, we can obtain the CSI through sending some pilot sequences. Then, the LS channel estimation is :

$$\hat{\boldsymbol{h}} = \frac{1}{c\sqrt{q_1}N_p}\left(\boldsymbol{P}_0^{\dagger}\boldsymbol{P}_0\right)^{-1}\sum_{k=1}^{N_p}\boldsymbol{P}_0^{\dagger}\boldsymbol{y}_0(k)\,. \tag{5.11}$$

Having $\hat{\boldsymbol{h}}$, we can obtain the estimate of the equivalent channel matrix $\hat{\mathscr{H}}_{\text{eq}}$. Next, we perform the classical MMSE signal demodulation followed by LLR calculation on bits, and then pass the LLRs to a Max-Log-MAP soft decoder (see [58] for details). Defining $\sigma^2_{\mathscr{Z}} = \mathrm{E}\{\mathscr{Z}^t\mathscr{Z}\}$, the detected symbols $\hat{\mathscr{S}}$ are :

$$\hat{\mathscr{S}} = c\sqrt{q_1}\widehat{\mathscr{H}_{\text{eq}}}^t\left(c^2 q_1\widehat{\mathscr{H}_{\text{eq}}}\widehat{\mathscr{H}_{\text{eq}}}^t + \sigma^2_{\mathscr{Z}}\boldsymbol{I}_{2T}\right)^{-1}\mathscr{Y} \tag{5.12}$$

As shown in Subsection 3.5.2, we can not directly calculate the $\sigma^2_{\mathscr{Z}}$ since we do not have full CSI available. As explained in this Subsection, we should use the Gaussian or the enhanced Gaussian approximation on $\mathscr{Z}$. We have noticed that for the case of $R = 4$ with QOSTBC, the enhanced Gaussian approximation provides a better performance of the iterative receiver than the simple Gaussian approximation (results are not presented for the sake of brevity). Therefore, we consider the former approximation and use the approximate variance $\sigma^2_{\tilde{\mathscr{Z}}}$ (given by (3.29)) in (5.12).

5.3.2 Succeeding iterations

5.3.2.1 Channel estimation

For the reason of computational complexity, here, we just take the SB estimator based on the CB-EM formulation into account. Remember from Section 4.2 that after obtaining the soft estimates of $\tilde{\boldsymbol{s}}$, the channel estimate can be calculated using (4.3), (4.8), and (4.10). As a second SB method, to reduce the receiver computational complexity, we propose here to use hard estimates of symbols in channel estimation. At relatively high SNR, these hard estimates likely correspond to the transmitted symbols and the resulting channel estimate would be of good accuracy. Concerning the estimator formulation, $\hat{\boldsymbol{h}}$ is still given by (4.3), but in (4.8) and (4.10), $\tilde{\boldsymbol{s}}$ and $\tilde{\boldsymbol{s}}^2$ will correspond to hard estimates.

5.3.2.2 PIC detection for non-orthogonal DSTBC

Since for iterative SB channel estimation we calculate soft or hard estimates of the transmitted data symbols, we propose to use them to reduce IRI and improve space-time decoding by performing PIC detection [58, 91]. Let $\hat{h}_p$ be the p-th column of $\widehat{\mathscr{H}_{\text{eq}}}$, and $\widehat{\mathscr{H}_{\text{eq}}}_p$ of dimension $(2T \times (2T-1))$ be $\widehat{\mathscr{H}_{\text{eq}}}$ with its p-th column removed. Also, let $\tilde{\mathscr{S}}$ denote the hard/soft estimate of $\mathscr{S}$, and $\tilde{\mathscr{S}}_p$ stand for $\tilde{\mathscr{S}}$ with its p-th entry removed. In order to obtain the detected signal $\hat{\mathscr{S}}_p$

(the p-th entry of $\hat{\mathscr{S}}$), we perform soft interference cancelation on $\mathscr{Y}$ by subtracting from $\mathscr{Y}$ the estimates of the $(2T-1)$ other transmitted signals :

$$\hat{\mathscr{Y}}_p = \mathscr{Y} - \widehat{\mathscr{H}_{\text{eq}}}_p \tilde{\mathscr{S}}_p; \quad p = 1, 2 \cdots 2T \tag{5.13}$$

Then, we apply an MMSE filter $\mathscr{W}_p$ to $\hat{\mathscr{Y}}_p$ and obtain [91] :

$$\hat{\mathscr{S}}_p = \mathscr{W}_p^t \hat{\mathscr{Y}}_p, \tag{5.14}$$

The filter coefficients $\mathscr{W}_p^t$ are given by :

$$\mathscr{W}_p^t = c\sqrt{q_1}\,\hat{h}_p^t \left(c^2 q_1 \hat{h}_p \hat{h}_p^t + \mathbf{\Omega} + \sigma_{\mathscr{Z}}^2 \boldsymbol{I}_{2T}\right)^{-1}, \tag{5.15}$$

where

$$\mathbf{\Omega} = \widehat{\mathscr{H}_{\text{eq}}}_p \left(\mathbf{\Theta}_p - \hat{\mathbf{\Theta}}_p\right) \widehat{\mathscr{H}_{\text{eq}}}_p^t. \tag{5.16}$$

The matrices $\mathbf{\Theta}_p$ and $\hat{\mathbf{\Theta}}_p$ are defined as follows :

$$\mathbf{\Theta}_p = \mathrm{E}\left\{\mathscr{S}_p \mathscr{S}_p^\dagger\right\} \approx \mathbf{diag}\left(\widetilde{s_1^2}, \cdots, \widetilde{s_{p-1}^2}, \widetilde{s_{p+1}^2}, \cdots, \widetilde{s_{2T}^2}\right), \tag{5.17}$$

$$\hat{\mathbf{\Theta}}_p = \mathrm{E}\left\{\hat{\mathscr{S}}_p \hat{\mathscr{S}}_p^{\,\dagger}\right\} \approx \mathbf{diag}\left(\widetilde{s_1}^2, \cdots, \widetilde{s_{p-1}}^2, \widetilde{s_{p+1}}^2, \cdots, \widetilde{s_{2T}}^2\right). \tag{5.18}$$

Notice that $\mathbf{\Theta}_p$ and $\hat{\mathbf{\Theta}}_p$ are not in fact diagonal [92]. However, we have approximated them in (5.17) and (5.18) by diagonal matrices to simplify the calculations. We have verified that using this approximation has a negligible influence on the system performance. For the case of PSK modulations, we have $\mathbf{\Theta}_p = \frac{1}{2}\boldsymbol{I}_{2T-1}$.

5.4 EXIT chart analysis

To study the convergence of the iterative receiver, we consider the extrinsic-information transfer (EXIT) charts which are a simple and efficient tool [93, 94]. They are based on the flow of the extrinsic information exchanged between the soft-input soft-output (SISO) blocks in an iterative scheme and give insight to the convergence behavior of the receiver. Here, we introduce briefly this tool and refer the reader to the provided references for more details.

In the EXIT chart analysis, the LLRs input to a SISO block are assumed to be uncorrelated and to follow a Gaussian distribution with its mean related to its variance [93]. Note that, these assumptions are not perfectly satisfied in practice. As a result, EXIT charts do not predict the convergence behavior of the receiver exactly. In our iterative receiver, *a posteriori* (and not extrinsic) LLRs are fed from the decoder to the soft-PIC detector. However, it is quite logical to consider the above-mentioned assumptions for the *a posteriori* LLRs too.

Let us use the subscripts $._{\text{A}}$ (for *a priori*) and $._{\text{E}}$ (for extrinsic) to denote the variables at the input and output of a SISO block, respectively. Note that for the soft-PIC detector, the subscript $._{\text{E}}$ corresponds to extrinsic LLRs, whereas for the decoder it corresponds to *a posteriori* LLRs. Also,

let us denote by I_{A} and I_{E}, the mutual information (MI) at the input and output of a SISO block, respectively. The EXIT chart is considered as the transfer function mapping the input information $I_{\mathrm{A}} \in [0,1]$ to the output information $I_{\mathrm{E}} \in [0,1]$. To obtain the EXIT curve, for each given I_{A}, we generate at the input of a SISO block, Gaussian distributed *a priori* LLRs with the appropriate variance. The mutual information I_{E} at the output of the module is then calculated by a histogram estimation. The behavior of the iterative detector is determined by associating $I_{\mathrm{E}}^{\mathrm{DET}} \Rightarrow I_{A}^{\mathrm{DEC}}$, and inversely, $I_{\mathrm{E}}^{\mathrm{DEC}} \Rightarrow I_{\mathrm{A}}^{\mathrm{DET}}$, where the superscripts $.^{\mathrm{DET}}$ and $.^{\mathrm{DEC}}$ refer to the soft-PIC detector and the channel decoder, respectively.

5.5 Simulation results

We present in this section some simulation results to study the performances of the proposed schemes. We use the rate 1/2 NRNSC code $(5,7)_8$, set the interleaver size to $N_b = 128$ bits, and consider the minimum number of pilot blocks, i.e., $N_p = 1$. Performance evaluation is done by considering the frame error rate (FER) versus E_b/N_0.

5.5.1 BER performance

Figure 5.2 contrasts the performances of different receivers when hard or soft estimates of symbols are used. Here, "Pilot-only, MMSE" denotes the classical approach, "Iter-Est, MMSE" iterative SB estimation with MMSE detection, "Iter-Est-Det" iterative estimation and PIC detection, and "Iter-Det, Perf-CSI" iterative PIC under perfect CSI. Convergence of the iterative schemes is attained after about 4 iterations. We notice firstly a significant improvement by SB estimation compared to the classical approach. If, in addition, interference cancelation is performed through iterations, we achieve a substantial SNR gain and the performance is quite close to the perfect CSI case. The interesting point is that, while having a lower computational complexity, the use of hard estimates of symbols gives satisfying performance results.

Consider now the case of 16-QAM modulation in Figure 5.3. Here, iterative channel estimation without interference cancelation brings a small improvement compared to the PO estimation and has practically no interest. Note that this is due to the poor performance of the MMSE detector in this case, which means that there is little to be gained by improved channel estimation. For the sake of comparison, we have also shown the FER curve corresponding to MMSE detection with perfect CSI, which is very close to the result with iterative estimation. In fact, when performing simple MMSE detection at the destination, the interference due to the non-orthogonal DSTBC affects more considerably the receiver performance for larger signal constellations like 16-QAM. Iterative SB estimation and PIC detection provides a significant improvement, however, while the soft-estimate-based method being a little more advantageous.

For the sake of completeness, we have also shown in Figure 5.4 the FER curves versus the number of iterations for the case of soft-estimate based method. We notice that the most part of the im-

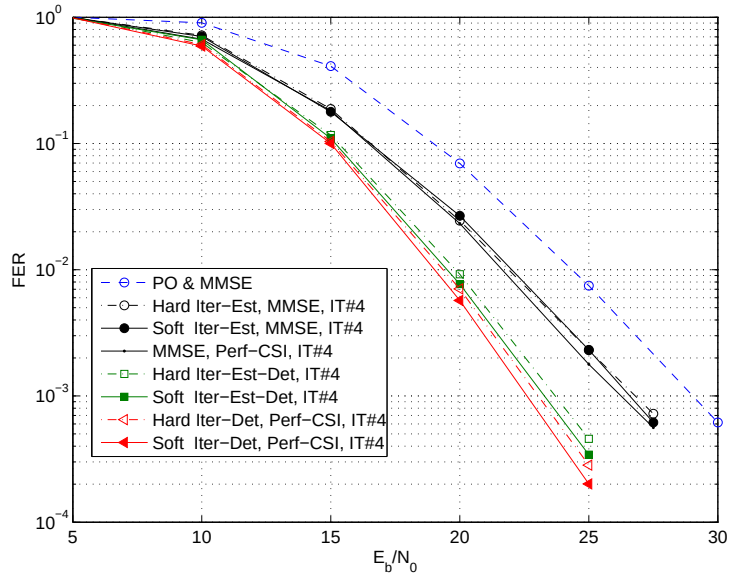

Figure 5.2 — Contrasting receiver performances for QPSK modulation, $(5,7)_8$ channel code, and $N_p = 1$. IT denotes iteration number.

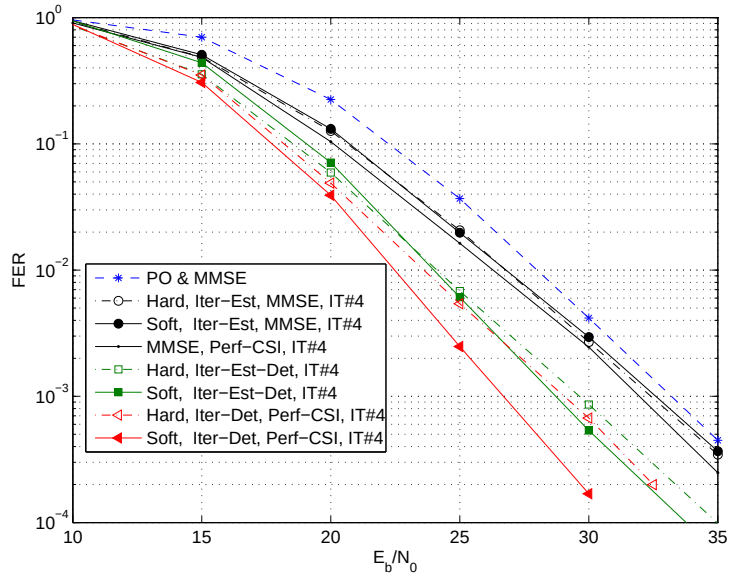

Figure 5.3 — Contrasting receiver performances for 16-QAM modulation, $(5,7)_8$ channel code, and $N_p = 1$. IT denotes iteration number.

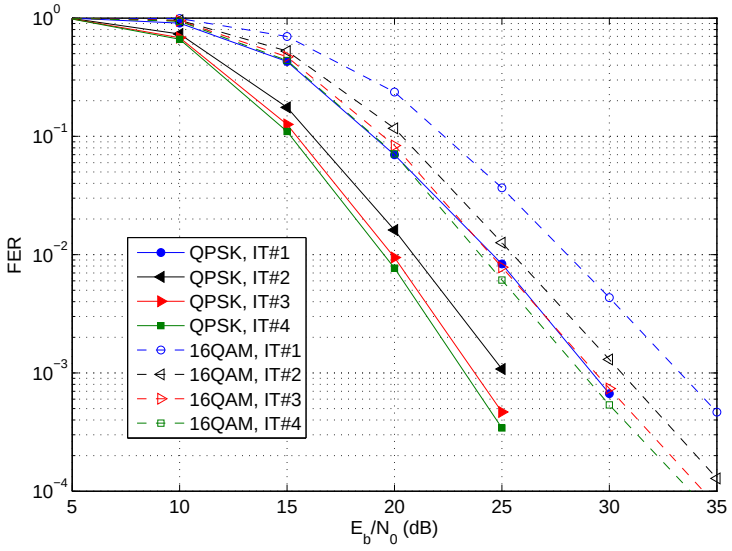

Figure 5.4 — Convergence of the receiver for QPSK and 16-QAM modulation cases. Soft-estimate based method. $(5,7)_8$ channel code, and $N_p = 1$.

provement is obtained at the second iteration. Similar results are obtained if the hard-estimates of symbols are used. That means that, for the reasons of complexity or latency, we may process only two iterations and still benefit from a significant improvement in the receiver performance.

5.5.2 EXIT Chart performance

An important point is to see the convergence behavior of the iterative receivers. This can be seen from Figure 5.5 where we have presented the EXIT charts of the detector and the channel decoder for the cases of QPSK, 16-QAM modulations with $E_b/N_0 = 17$dB, when soft or hard estimates of symbols are used. Note that the EXIT chart of the detector takes into account channel estimation and DSTBC decoding. We have presented the corresponding curves for "Iter-Est, MMSE" and "Iter-Est-Det" cases, as explained previously for Figures 5.2 and 5.3. At the first iteration, we start from the point corresponding to the MMSE detector. We notice that we have similar convergence behaviors when hard or soft estimates of symbols are used. Nevertheless, for perfect a priori information ($I_A^{DET} = 1$), the EXIT curve of the detector with soft estimates lays above that with hard estimates. Also, we notice that the performance of the receiver is affected more considerably for 16-QAM modulation when MMSE detection is performed without interference cancelation. This validates the results of Figure 5.3.

5.6 Chapter conclusion and discussions

For the case of non-orthogonal DSTBC at the relays, we proposed to perform iterative PIC detection and channel decoding at the receiver. The PIC detector was based on soft or hard esti-

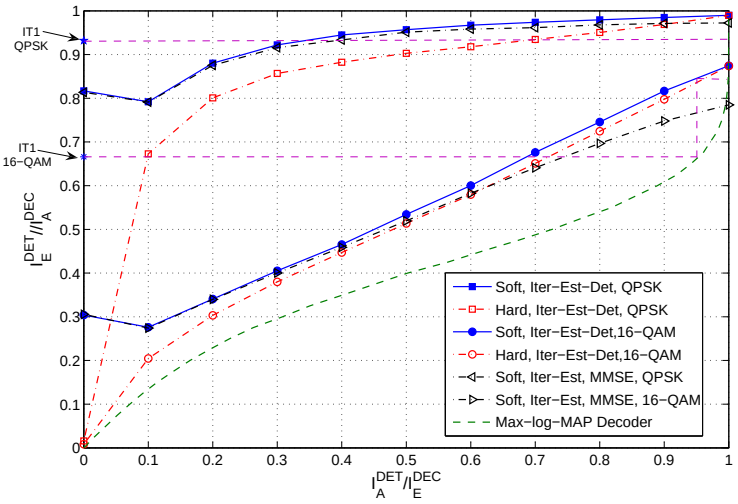

Figure 5.5 — Contrasting EXIT charts of the "PIC detector-SB estimator" for soft- and hard-estimate based methods. QPSK and 16-QAM modulations, $N_p = 1$. Convergence trajectories are shown for the soft-estimate-based receivers.

mates of the transmitted symbols, which are calculated using the channel decoder soft outputs. Also, CB-EM channel estimation was used in order to improve the channel estimate and data detection through iterations. We illustrated the performance improvement by the proposed method compared to the classical approach of PO channel estimation and MMSE detection. In particular, taking the receiver computational complexity into account, we noticed that, for large signal constellations, iterative estimation alone is not really interesting. The reason is that the IRI resulting from non-orthogonal DSTBC at the relays affects more considerably the receiver performance, compared to the simple case of QPSK. Iterative semi-blind channel estimation and PIC detection, however, was shown to be an efficient solution to deal with the IRI.

CHAPTER 6

Improved Detection for AF WRN with Imperfect Channel Estimation

6.1 Introduction

In the previous chapters, we illustrated the need to CSI at the destination in AF WRNs when coherent DSTBC is performed at the relays. As energy efficiency is an essential factor in WSNs [71], we should also minimize the energy consumption due to pilot transmission [72]. This means that we should minimize the number of pilots as well as their power, especially in relatively fast fading conditions. However, this obviously results in an increase of the variance of channel estimation errors and therefore in the performance degradation of the system. One solution is to perform SB channel estimation, as it was the subject of the two previous chapters, and to make use of data symbols in addition to pilots to improve the quality of the channel estimate. However, SB estimation methods could be regarded to suffer from relatively high computational complexity, compared to the simple PO channel estimation. This higher computational complexity of SB methods becomes problematic in relatively fast fading conditions, where the realtime implementation of the receiver may not be an easy task.

To deal with imperfect channel estimation, the suboptimal and classically-used approach consists in using the channel estimate in the detector in the same way as if it was a perfect estimate. This approach, known as "mismatched" detection, can highly degrade the detection performance when channel-estimation errors are important. Inspired by [68, 92, 95], we propose here an "improved" detector to be used at the destination node that allows to reduce the impact of imperfect channel estimation on the overall system performance. We use the improved detection method in an iterative receiver, which is an efficient technique when channel coding is employed. To illustrate the performance improvement by the proposed method, without loss of generality, we consider the special case of two relays and the conditions of fast fading. In other words, we assume that the channel coefficients (following IID Rayleigh statistics, as considered in the previous chapters) change to new independent values for each block of T symbols. Unfortunately, the idea of the improved detection, when applied to the MMSE detector provided only negligible

performance improvement. It provides, however, significant improvement in the case of MAP signal detection. That is why we consider the MAP detector in this chapter.

This chapter is organized as follows. In Section 6.2, we briefly recall the signal transmission formulation. MAP signal detection assuming available perfect CSI is presented in detail in Section 6.3. Next, in Section 6.4, we consider signal detection under imperfect channel estimation, where after introducing the classical mismatched detection, we describe our proposed improved detector and its formulation. Some numerical results are then provided in Section 6.5 in order to compare the performances of the mismatched and the improved detection approaches. Lastly, conclusions are given in Section 6.6.

6.2 Data transmission formulation

For the sake of simplicity of formulation, we consider the special case of $R = 2$ with the Alamouti DSTBC at the relays. The retransmitted signals from the relays are given by the following matrix :

$$[\, \boldsymbol{t}_1 \; \boldsymbol{t}_2 \,] = c \begin{bmatrix} r_{11} & -r_{22}^* \\ r_{12} & r_{21}^* \end{bmatrix}. \tag{6.1}$$

To elaborate a general formulation for the receiver, we resort to the special formulation presented in Section 5.2 in the previous chapter. Following (5.1), we have :

$$\boldsymbol{A}_1 = \boldsymbol{I}_2,\ \boldsymbol{B}_1 = \boldsymbol{0}_{2\times 2},\ \boldsymbol{A}_2 = \boldsymbol{0}_{2\times 2},\ \boldsymbol{B}_2 = \begin{bmatrix} 0 & -1 \\ 1 & 0 \end{bmatrix}. \tag{6.2}$$

Also,

$$\mathscr{H}_{\text{eq}} = \begin{bmatrix} \Re\{h_1\} & -\Re\{h_2\} & -\Im\{h_1\} & -\Im\{h_2\} \\ \Re\{h_2\} & \Re\{h_1\} & \Im\{h_2\} & -\Im\{h_1\} \\ \Im\{h_1\} & -\Im\{h_2\} & \Re\{h_1\} & \Re\{h_2\} \\ \Im\{h_2\} & \Im\{h_1\} & -\Re\{h_2\} & \Re\{h_1\} \end{bmatrix}, \tag{6.3}$$

where (see (3.7))

$$\boldsymbol{h} = \begin{bmatrix} h_1 \\ h_2 \end{bmatrix} = \begin{bmatrix} f_1\, g_1 \\ f_2^*\, g_2 \end{bmatrix}. \tag{6.4}$$

Consider now pilot-based channel estimation at the destination. In contrary to the data symbols that are considered power-normalized, pilot symbols will be considered of power E_p. We consider LS-based channel estimate given by (3.38) in Section 3.6. For the special case of $R = 2$ we define the matrix $\boldsymbol{\Lambda}_0$ as follows.

$$\boldsymbol{\Lambda}_0 \triangleq \boldsymbol{P}_0^{\dagger} \boldsymbol{P}_0 = \varrho\, \boldsymbol{I}_R \quad ; \quad \varrho \triangleq T\, N_p\, E_p \tag{6.5}$$

Here, ϱ represents the total power of the transmitted pilots per frame of N_s DSTBC blocks. Let us denote the vector of channel estimation error by $\mathscr{E}$:

$$\hat{\boldsymbol{h}} = \boldsymbol{h} + \mathscr{E}, \tag{6.6}$$

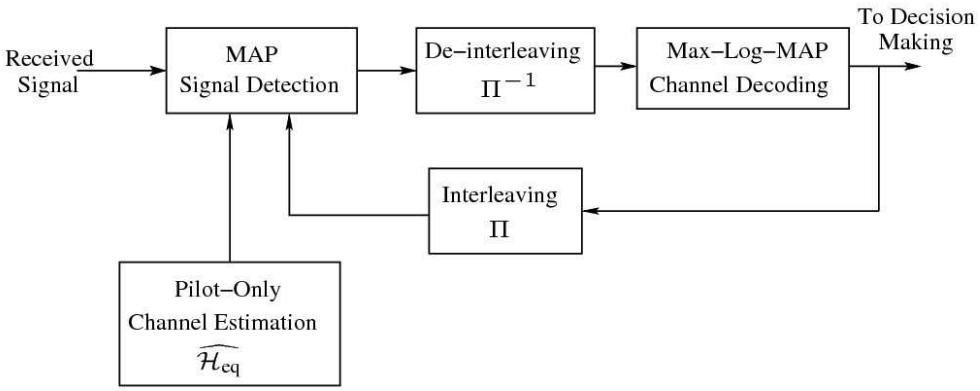

Figure 6.1 — Block diagram of the iterative receiver at the destination.

where

$$\mathscr{E} = \frac{1}{c\sqrt{q_1}\varrho}\boldsymbol{P}_0^{\dagger}\boldsymbol{z}_0. \tag{6.7}$$

The covariance matrix of $\mathscr{E}$ is given by :

$$\mathrm{E}\{\mathscr{E}^{\dagger}\mathscr{E}\} = \sigma_{\mathscr{E}}^2\boldsymbol{I}_R \quad \text{with} \quad \sigma_{\mathscr{E}}^2 = \frac{\sigma_{z_0}^2}{c^2 q_1 \varrho}. \tag{6.8}$$

6.3 Signal detection under perfect partial CSI

Let us first assume that the channel estimate is perfect. As it can be seen from the block diagram of Figure 6.1, at the destination, we perform iterative soft signal demodulation and channel decoding. We consider MAP demodulation and soft channel decoding based on the well-known Max-Log-MAP algorithm [63]. For MAP demodulation, we calculate the LLRs on the transmitted bits and then pass them to the soft-decoder after de-interleaving. We provide in the following details on the MAP demodulator formulation. Note that, as we will explain later in Section 6.5, iterative detection does not always bring a performance improvement (e.g. for Gray mapped QPSK modulation).

Remember the general formulation of (5.5) for the received signal $\mathscr{Y}$. Let b^m be the m-th ($m = 1,2,...,BT$) bit corresponding to the symbol vector $\mathscr{S}$, and $L(b^m)$ be the LLR on b^m at the output of the demodulator. Given $\mathscr{H}_{\mathrm{eq}}$ (under the condition of available perfect *partial* CSI), $L(b^m)$ is calculated as follows [92] :

$$L(b^m) = \log\frac{P(b^m = 1|\mathscr{Y},\mathscr{H}_{\mathrm{eq}})}{P(b^m = 0|\mathscr{Y},\mathscr{H}_{\mathrm{eq}})}, \tag{6.9}$$

where $P(b^m|\mathscr{Y},\mathscr{H}_{\mathrm{eq}})$ denotes the probability of transmission of b^m given $\mathscr{Y}$ and $\mathscr{H}_{\mathrm{eq}}$. To calculate these probabilities, we define $\boldsymbol{S}$ as the set of all possibly-transmitted symbol vectors $\mathscr{S}$. We partition $\boldsymbol{S}$ into two subsets of $\boldsymbol{S}_0^m$ and $\boldsymbol{S}_1^m$, for which b^m equals 0 or 1, respectively. We also take into account the *a priori* probabilities on each bit b^n in these subsets which come from the soft decoder (in the previous iteration), and denote them by $P_{\mathrm{dec}}^0(b^n)$ and $P_{\mathrm{dec}}^1(b^n)$. Note that, at the

first iteration, there is no *a priori* information on these bits and $P^0_{\text{dec}}(b^n)$ and $P^1_{\text{dec}}(b^n)$ are set to 1/2.

Denoting the likelihood function by $W(\mathscr{S},\mathscr{Y},\mathscr{H}_{\text{eq}})$, we can develop (6.9) as follows.

$$L(b^m) = \log \frac{\sum\limits_{\mathscr{S}\in \boldsymbol{S}_1^m} W(\mathscr{S},\mathscr{Y},\mathscr{H}_{\text{eq}}) \prod\limits_{\substack{n=1\\ n\neq m}}^{BT} P^1_{\text{dec}}\big(b^n\big)}{\sum\limits_{\mathscr{S}\in \boldsymbol{S}_0^m} W(\mathscr{S},\mathscr{Y},\mathscr{H}_{\text{eq}}) \prod\limits_{\substack{n=1\\ n\neq m}}^{BT} P^0_{\text{dec}}\big(b^n\big)} \tag{6.10}$$

We also define the ML metric $\mathscr{D}(\mathscr{S},\mathscr{Y},\mathscr{H}_{\text{eq}}) = -\log\big(W(\mathscr{S},\mathscr{Y},\mathscr{H}_{\text{eq}})\big)$. Considering Gaussian approximation for $\mathscr{Z}$, it can easily be shown that :

$$\mathscr{D}(\mathscr{S},\mathscr{Y},\mathscr{H}_{\text{eq}}) = T\log(\pi\sigma^2_{\mathscr{Z}}) + \frac{\big|\mathscr{Y}-\mathscr{H}_{\text{eq}}\mathscr{S}\big|^2}{\sigma^2_{\mathscr{Z}}}, \tag{6.11}$$

where $\sigma^2_{\mathscr{Z}}$ is approximated by $\sigma^2_{\hat{\mathscr{Z}}} = T(1+c^2R)\sigma^2$.

6.4 Signal detection under imperfect partial CSI

6.4.1 Mismatched signal detection

In practice, we can never have perfect CSI at the destination and some channel estimation errors are inevitable. The classical signal detection approach consists in using $\widehat{\mathscr{H}_{\text{eq}}}$ as if it was a perfect estimate. This is referred to as mismatched detection. This way, for signal demodulation, we replace $\mathscr{H}_{\text{eq}}$ in (6.10) by $\widehat{\mathscr{H}_{\text{eq}}}$. The resulting channel uncertainty degrades the system performance [96], and the degradation can be quite important especially when a small number of pilots is used or the pilot power is reduced in order to reduce the network power consumption.

6.4.2 Improved signal detection

In order to compensate partly the effect of channel estimation errors, we propose here an improved detection rule that takes the channel estimation errors into account. This is based on a Bayesian approach based on the *a posteriori* PDF of the perfect channel, conditioned on its estimate. Inspired by the idea of [68, 92], we consider a modified likelihood function $\widetilde{W}(\mathscr{S},\mathscr{Y},\mathscr{H}_{\text{eq}})$ such that :

$$\begin{aligned}\widetilde{W}(\mathscr{S},\mathscr{Y},\mathscr{H}_{\text{eq}}) = \quad &= \quad \mathrm{E}_{\mathscr{H}_{\text{eq}}|\widehat{\mathscr{H}_{\text{eq}}}}\Big\{W(\mathscr{Y},\mathscr{S},\mathscr{H}_{\text{eq}}) \mid \widehat{\mathscr{H}_{\text{eq}}}\Big\} \\ &= \int\limits_{\mathscr{H}_{\text{eq}}\in\mathbb{R}^{2T\times 2T}} W(\mathscr{Y},\mathscr{S},\mathscr{H}_{\text{eq}})\; p(\mathscr{H}_{\text{eq}}|\widehat{\mathscr{H}_{\text{eq}}})\; d\mathscr{H}_{\text{eq}},\end{aligned} \tag{6.12}$$

where $\mathbb{R}$ stands for the set of real numbers. In fact, the proposed modification consists in averaging the likelihood function W over all realizations of the unknown channel $\mathscr{H}_{\text{eq}}$ conditioned

to its available estimate $\widehat{\mathscr{H}_{\text{eq}}}$, by using the distribution $p(\mathscr{H}_{\text{eq}}|\widehat{\mathscr{H}_{\text{eq}}})$. Then, maximizing $\widetilde{W}$ will be equivalent to minimizing a new metric $\widetilde{\mathscr{D}}$ that we aim to calculate :

$$\widetilde{\mathscr{D}}(\mathscr{S},\mathscr{Y},\mathscr{H}_{\text{eq}}) = -\log\left(\widetilde{W}(\mathscr{S},\mathscr{Y},\mathscr{H}_{\text{eq}})\right). \tag{6.13}$$

Note that this is in contrast to the mismatched detector which tries to minimize the metric $\mathscr{D}$ in (6.11).

To calculate the new likelihood function $\widetilde{W}$, we need the posterior distribution of $\mathscr{H}_{\text{eq}}$ conditioned to $\widehat{\mathscr{H}_{\text{eq}}}$, i.e., $p(\mathscr{H}_{\text{eq}}|\widehat{\mathscr{H}_{\text{eq}}})$. To obtain this PDF, we have to consider some simplifying approximations. Let us denote the matrix of estimation errors of $\mathscr{H}_{\text{eq}}$ by $\boldsymbol{\varepsilon}$:

$$\widehat{\mathscr{H}_{\text{eq}}} = \mathscr{H}_{\text{eq}} + \boldsymbol{\varepsilon}. \tag{6.14}$$

In fact, $\boldsymbol{\varepsilon}$ is not Gaussian distributed because, as we saw previously in (5.5), $\mathscr{Z}$ is not Gaussian. Using (6.8) and taking the Gaussian approximation for $\mathscr{Z}$ into account from (3.27), we obtain the covariance matrix of $\boldsymbol{\varepsilon}$ as follows.

$$\Sigma_{\boldsymbol{\varepsilon}} = \text{E}\{\boldsymbol{\varepsilon}\boldsymbol{\varepsilon}^t\} = \frac{\sigma^2_{\hat{\mathscr{Z}}}}{c^2 q_1 \varrho}\boldsymbol{I}_{2T}. \tag{6.15}$$

As the second approximation, we assume that $\boldsymbol{\varepsilon}$ is Gaussian distributed. In other words, we approximate the PDF $p(\widehat{\mathscr{H}_{\text{eq}}}|\mathscr{H}_{\text{eq}})$ by a Gaussian [97] :

$$p(\widehat{\mathscr{H}_{\text{eq}}}|\mathscr{H}_{\text{eq}}) \approx \mathscr{N}\left(\mathscr{H}_{\text{eq}}, \Sigma_{\boldsymbol{\varepsilon}} \otimes \boldsymbol{I}_{2T}\right). \tag{6.16}$$

However, in (6.12) we need $p(\mathscr{H}_{\text{eq}}|\widehat{\mathscr{H}_{\text{eq}}})$. In [92], Appendix I-A, a lemma is presented that permits the derivation of $p(\mathscr{H}_{\text{eq}}|\widehat{\mathscr{H}_{\text{eq}}})$ for the case of Gaussian $\mathscr{H}_{\text{eq}}$ and $\widehat{\mathscr{H}_{\text{eq}}}$ (x_1 and x_2 in [92], respectively). In our case, none of these parameters is Gaussian. So, as the third approximation, we assume that $\mathscr{H}_{\text{eq}}$ is Gaussian distributed. Then, using the above-mentioned lemma and (6.16) we obtain :

$$p(\mathscr{H}_{\text{eq}}|\widehat{\mathscr{H}_{\text{eq}}}) \approx \mathscr{N}\left(\Sigma_\Delta\,\widehat{\mathscr{H}_{\text{eq}}}, \boldsymbol{I}_{2T} \otimes \Sigma_\Delta\,\Sigma_{\boldsymbol{\varepsilon}}\right), \tag{6.17}$$

where

$$\Sigma_\Delta = \Sigma_{\mathscr{H}_{\text{eq}}}(\Sigma_{\boldsymbol{\varepsilon}} + \Sigma_{\mathscr{H}_{\text{eq}}})^{-1} = \delta\,\boldsymbol{I}_{2T}, \tag{6.18}$$

and

$$\delta = \frac{R}{R + \dfrac{\sigma^2_{\hat{\mathscr{Z}}}}{c^2 q_1 \varrho}}. \tag{6.19}$$

Also,

$$\Sigma_{\mathscr{H}_{\text{eq}}} = \text{E}\{\mathscr{H}_{\text{eq}}\mathscr{H}^t_{\text{eq}}\} = R\,\boldsymbol{I}_{2T}. \tag{6.20}$$

We will later explain that these approximations have finally little impact on the receiver performance. Since $\Sigma_{\boldsymbol{\varepsilon}}$ and $\Sigma_{\mathscr{H}_{\text{eq}}}$ are diagonal, Σ_Δ is also a diagonal matrix. Hence, (6.17) can be simplified as follows.

$$p(\mathscr{H}_{\text{eq}}|\widehat{\mathscr{H}_{\text{eq}}}) \approx \mathscr{N}\left(\delta\,\widehat{\mathscr{H}_{\text{eq}}}, \delta\,\Sigma_{\boldsymbol{\varepsilon}} \otimes \boldsymbol{I}_{2T}\right), \tag{6.21}$$

Now, using (6.12), (6.13), and (6.21), it can be shown that the modified MAP decision metric for the improved detector is given by [97] :

$$\widetilde{\mathscr{D}}(\mathscr{S},\mathscr{Y},\widehat{\mathscr{H}_{\text{eq}}}) = T\log\pi(\sigma^2_{\hat{\mathscr{Z}}}+\delta\,\sigma^2_{\mathscr{E}}) + \frac{\left|\mathscr{Y}-\delta\widehat{\mathscr{H}_{\text{eq}}}\mathscr{S}\right|^2}{\sigma^2_{\hat{\mathscr{Z}}}+\delta\,\sigma^2_{\mathscr{E}}}. \tag{6.22}$$

Remember that $\sigma^2_{\mathscr{E}}$ is given by (6.8). We should now replace W in (6.10) by $\exp(-\widetilde{\mathscr{D}})$ for calculating the LLRs on the transmitted bits. Note that when we have almost perfect CSI at the destination (e.g. using a large number of pilots or increasing their power), δ is close to one, and the modified metric $\widetilde{\mathscr{D}}$ reduces to the mismatched one. For increased estimation error variance (e.g. due to reduced number of pilots or decreasing their power), however, the modified demodulator provides an improvement in the system performance, as we will show in the next section.

6.5 Numerical results

We present here some simulation results to study the performance of the proposed detector. The system performance is evaluated as the average BER versus the SNR. We use the rate 1/2 NRNSC code $(5,7)_8$ for channel coding and use the minimum number of pilot blocks for channel estimation, i.e., we set $N_p = 1$. Also, Rayleigh fast fading conditions are considered and the interleaver size is set to $N_b = 128$. Data and pilot symbols are taken from the same constellation and, unless otherwise mentioned, pilots and data symbols are considered of the same power, i.e., $E_p = 1$. Depending on the modulation and the bit/symbol mapping, a maximum of five iterations are processed at the destination to attain the receiver convergence.

6.5.1 BER performance

Let us first consider the case of QPSK modulation. For this case, iterative processing provides performance improvement only in the case of set-partition (SP) bit/symbol (also called anti-Gray) mapping [98]. Results of the mismatched and improved detection rules are shown in Figure 6.2. As reference, we have also presented the performance curve with perfect CSI. We notice that we have practically no improvement by using the modified detector. The improvement remains negligible even if we reduce the pilots power E_p. As a matter of fact, since in the modified metric, the absolute value of symbols intervenes, for a constant modulus modulation like QPSK, we have almost no improvement in the receiver performance.

Let us now consider a non-constant modulus modulation like 16-QAM. We have contrasted the performances of the two detectors in Figures 6.3 and 6.4 for the cases of Gray mapping and the SP mapping proposed in [99], respectively. We notice an interesting performance improvement : The SNR gain at BER= 10^{-5} is about 1.0 dB for both Gray and SP mappings. Note that the SNR gain becomes more significant at lower BERs as the curves corresponding to the mismatched and

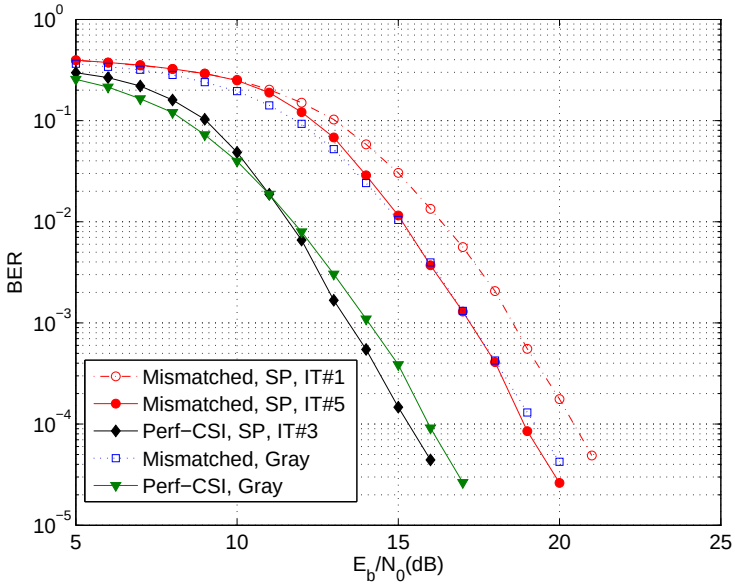

Figure 6.2 — BER performance of improved and mismatched detectors. $R = 2$ with Alamouti DSTBC, $N_p = 1$. QPSK modulation with SP and Gray mappings. IT denotes iteration number.

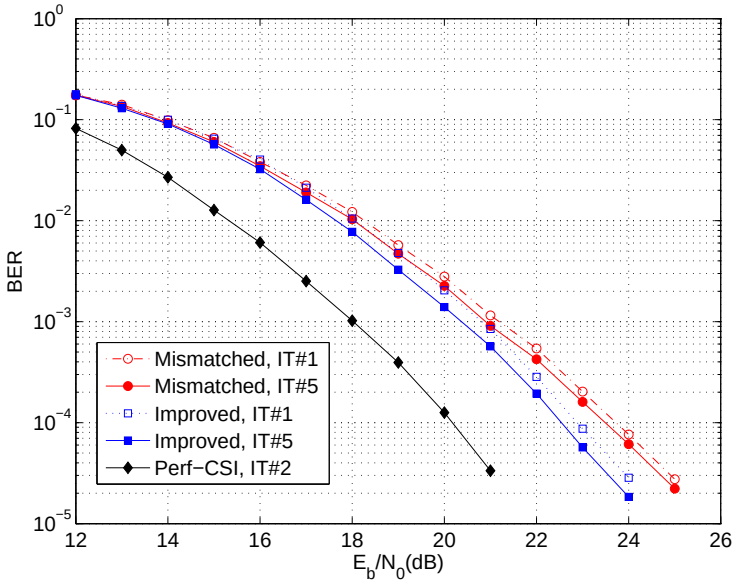

Figure 6.3 — BER performance of improved and mismatched detectors. $R = 2$ with Alamouti DSTBC, $N_p = 1$. 16-QAM modulation with Gray bit-symbol mapping. IT denotes iteration number.

improved detectors are diverging. However, we have limited the BER to 10^{-5} due to long Monte Carlo simulation time involved.

Consider now the case of SP-mapped 64-QAM. The BER performances of the mismatched and improved detectors are compared in Figure 6.5. The obtained gain is still more important in this

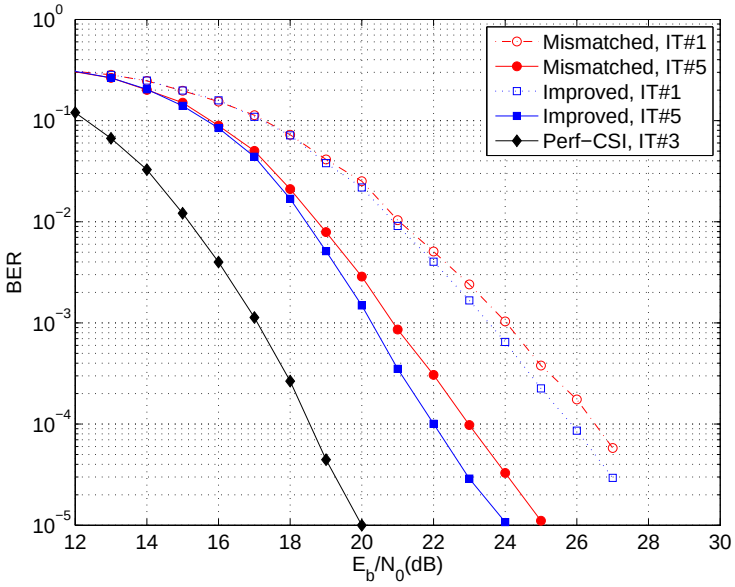

Figure 6.4 — BER performance of improved and mismatched detectors. $R = 2$ with Alamouti DSTBC, $N_p = 1$. 16-QAM modulation with SP bit-symbol mapping. IT denotes iteration number.

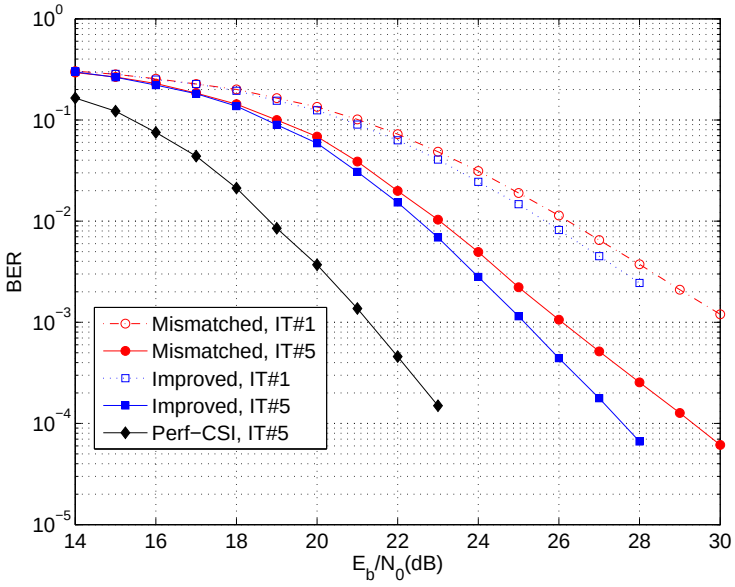

Figure 6.5 — BER performance of mismatched and improved detectors. $R = 2$ with Alamouti DSTBC, $N_p = 1$. 64-QAM modulation with SP mappings. IT denotes iteration number.

case ; we notice an SNR gain of about 2.0 dB at BER = 10^{-4}. For larger constellations, the estimation errors are more important, and result in a more considerable performance degradation of the mismatched detector. The improved detector, in turn, provides more performance improvement.

In the previous results, we had set $E_p = 1$. Since we are considering fast fading conditions,

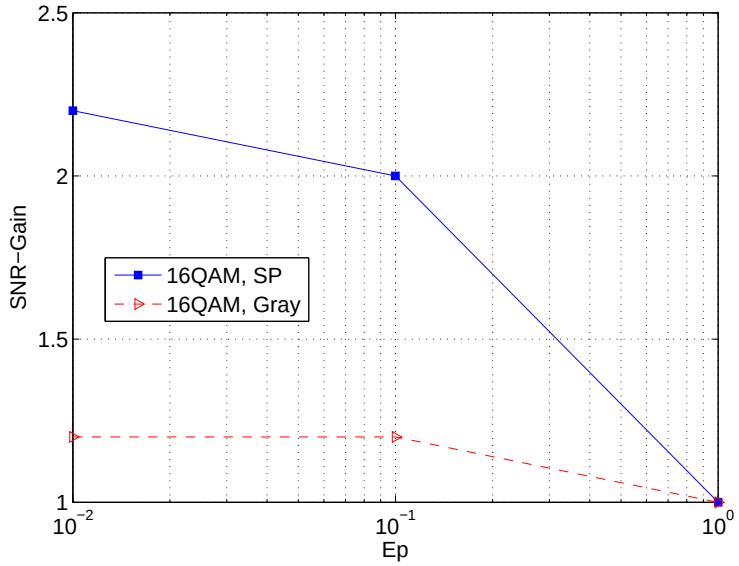

Figure 6.6 — Gain in E_b/N_0 as a function of pilots' power E_p by using the improved detector. $R = 2$ with Alamouti DSTBC, $N_p = 1$. 16-QAM modulation with Gray and SP mappings. BER $= 10^{-4}$. Results correspond to the fifth receiver iteration.

we send one pilot block for each block of data symbols. It is highly desirable to reduce the pilots' power E_p in such conditions in order to reduce the network's power consumption. In such situations, the estimation errors will be more important and the proposed improved detector provides more considerable performance gains. This can be seen from Figure 6.6, where we have presented the SNR gain obtained by the improved detector with respect to the mismatched detector, as a function of E_p, for the case of 16-QAM modulation and corresponding to BER $= 10^{-4}$.

Lastly, we have verified that if we consider the (hypothetical) case of Gaussian channel and Gaussian noise at the destination, we have the same order of improvement for the different modulations and mappings that we considered above. We can hence conclude that the simplifying assumptions that we made in developing the new detector formulation have little impact on the resulting performance.

6.5.2 Convergence analysis using EXIT charts

In order to better see the advantage of the proposed improved detection over mismatched detection, we have presented the EXIT charts of the detectors in Figure 6.7 for the case of 16-QAM modulation with SP bit/symbol mapping. We have considered two cases of power-normalized pilots, i.e., $E_p = 1$, and $E_p = 0.1$. Remember that $I_{\mathrm{A}}^{\mathrm{DET}}$ and $I_{\mathrm{E}}^{\mathrm{DET}}$ denote the *a priori* MI at the input of the detector and the extrinsic MI at its output, respectively. From Figure 6.7 we notice that the difference of the EXIT curves corresponding to $E_p = 1$ is rather small. Moreover, the improved detector takes its advantage only for $I_{\mathrm{A}}^{\mathrm{DET}}$ close to one. For $E_p = 0.1$, however, we notice the incontestable advantage of the improved detector over the mismatched one.

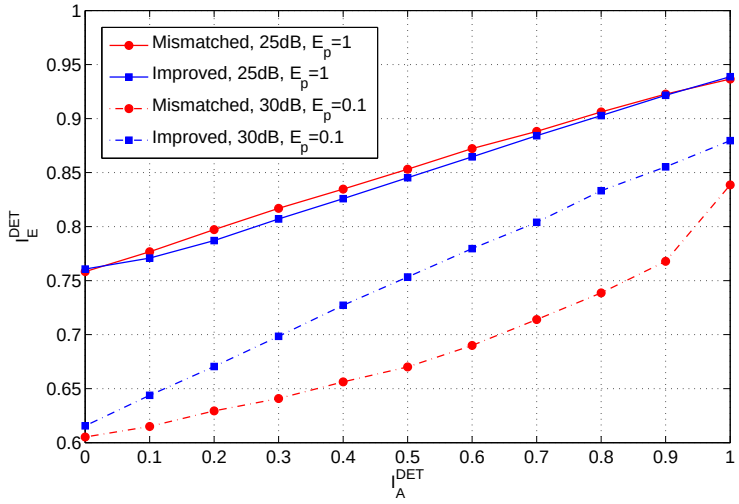

Figure 6.7 — Comparison of EXIT curves for the improved and mismatched detectors. 16-QAM modulation with SP bit/symbol mapping. with Alamouti DSTBC, $N_p = 1$, $E_b/N_0 = 25$ dB for $E_p = 1$ and $E_b/N_0 = 30$ dB for $E_p = 0.1$.

6.6 Chapter conclusion and discussions

In order to extend the lifetime of a sensor network, we should minimize the power consumption at its nodes. In relatively fast fading conditions, a considerable amount of network energy is spent for pilot transmission in order to estimate the channel state at the destination. Therefore, there is a high interest to reduce the number of pilots and their power as little as possible. At the same time, given the rapidly time-varying channel conditions considered here, realtime semi-blind channel estimation may be unfeasible in practice. We proposed in this chapter an improved detection rule that allows interesting performance improvement over the classically-used mismatched detection, while requiring acceptable computational complexity. We showed that the proposed detector is of special interest for relatively large signal constellations and for relatively low pilot powers.

CHAPTER 7

Conclusions and Perspective

7.1 Conclusions

There has been a huge amount of research on wireless sensor networks (WSNs) in the past few years. WSNs are a key technology of the future. However, there remain still many challenges ahead for them, especially concerning the implementation aspects of these networks. In particular, there are several practical limitations concerning the physical layer of wireless links. We were interested in this thesis in a special kind of cooperative WSNs, i.e., wireless relay networks (WRNs). Cooperative networks are an efficient solution to the problem of time-varying multipath fading that we encounter in most wireless networks. When the WRN works in the amplify-and-forward (AF) mode, we considered coherent signal detection at the destination and investigated deeply the channel estimation, which is an important aspect in practice.

Starting by a general state-of-the-art on WSNs including the main characteristics, limitations, and design challenges, in **Chapter 2**, we invoked the considerations relating to energy consumption in WSNs and the role of the physical layer. We also focused on the idea of cooperative communication and distributed space-time coding at the relay nodes in view of exploiting some distributed diversity.

In **Chapter 3**, we gave details on the special WRN that we consider in this thesis, and also specified our main assumptions regarding the transmission channel. We also presented the general signal transmission model and formulation in our WRN. Then, after a comparison of the detection techniques under full and partial channel state information (CSI), we considered channel estimation based on the transmission of some training symbols. Through some simulation results, we showed that for the case of non-orthogonal DSTBCs, we can suffer from a significant performance degradation if we resort to the simple MMSE detection without any inter-relay interference cancelation. Moreover, a somehow moderate performance degradation is noticed when we have only partial CSI available at the destination (compared to the case where full CSI is available). For orthogonal DSTBCs, however, by the simple MMSE detector and partial CSI we can attain optimal signal detection at the receiver. Furthermore, concerning partial CSI estimation based only on pilots, we compared the LS and LMMSE schemes and showed that the two methods have almost the same performance. We also studied the impact of the simplifying assumptions on the receiver

noise, i.e., the Gaussian and enhanced Gaussian approximations, on the system performance and noticed almost the same performance using both approximations. Finally, we showed the performance loss due to sending too few pilots, and hinted the reader on the importance of using an efficient channel estimation technique.

Assuming that we have loose constraints on the energy and computational resources at the destination, we proposed in **Chapter 4** to use a semi-blind (SB) channel estimation technique based on the EM algorithm. SB estimation allows to use a smaller number of pilot symbols for channel estimation. Focusing on orthogonal DSTBC schemes at the relays, we firstly considered the classical formulation of EM and called the resulting estimator CB-EM (for Classical Biased) and showed that it can provide substantial performance improvement, compared to the case where only pilots are used for channel estimation. We illustrated through simulation results that for a larger number of relays and larger frame sizes, we obtain a more interesting performance improvement. We then presented a more detailed analysis of CB-EM and showed that, albeit its relatively good performance, it provides a biased channel estimate. Then, a modified formulation of EM was developed that was called UL-EM (for Unbiased Linearly-combined EM). This new scheme outperforms CB-EM for relatively large signal constellations. The comparison of the MSE of estimation for the two SB schemes also showed the superiority of the UL-EM method. In the case of relatively small signal constellations, however, UL-EM does not seem to be of any practical interest.

Extending our results to the case of non-orthogonal DSTBCs in **Chapter 5**, we proposed to use soft parallel interference cancelation for signal detection together with SB channel estimation at the destination. This way, benefiting from the channel coding gain, we can reduce the inter-relay interference and improve the channel estimation through processing a few iterations. We illustrated the interest of this approach, especially for large signal constellations. Moreover, we presented a simple formulation of the iterative receiver based on the hard-estimates of the transmitted symbols, and showed that it makes a good compromise between complexity and performance.

Lastly, we generalized our study of channel estimation to the case of relatively fast fading channels in **Chapter 6**, where we explained that SB estimation may not be feasible for a real-time implementation due to its computational complexity. We proposed an alternative solution in order not to suffer from channel estimation errors as a result of reducing the number of pilots in such cases. Focusing on MAP signal detection, we proposed a modified detector formulation that takes into account the channel estimation errors while increasing slightly the receiver's computational complexity. This modified detection method was shown to provide an interesting performance improvement for relatively large signal constellations.

7.2 Perspectives

The objective of this thesis was to propose efficient channel estimation solutions for AF WRNs. Meanwhile, the work presented in this thesis tried to establish a connection between the theoretical aspects, concerning signal detection and channel estimation, and the implementation aspects of the proposed solutions. This research led to some theoretical results and opened the issue for further investigations. We propose here some research directions for a future extension of this work.

- Considering statistical modeling of channel fading, we limited our study to the case of IID Rayleigh model. This can be considered as the worst case for fading statistics, concerning its impact on the system performance. It is interesting to see the interest of the proposed channal estimation techniques in the case of correlated fading channel coefficients and/or for other fading models like Ricean fading. Also, we assumed through our study that the channel is frequency non-selective (flat). In most high data-rate communication systems, however, the channel cannot be considered as flat. The proposed estimation techniques should be adapted to such conditions. A particular case is when orthogonal frequency-division multiplexing (OFDM) is employed to simplify the channel equalization task at the receiver. In this view, an interesting method seems to be that based on the basis expansion model [100] that allows a reduction of the number of channel unknown parameters prior to channel estimation [101]. A practical example is the case of mobile ad hoc networks, and more particularly, the LTE (long-term evolution) standard [102]. In this fourth generation of mobile telephony, the multiple-access technique used is the OFDMA (orthogonal frequency-division multiple access). Note that applying the idea of WRNs to a cellular environment can be highly beneficial in the case of strong shadowing effects such as inside buildings and tunnels [103], or at the cell boundaries [104].
- The channel estimation techniques we proposed were well adapted to the AF signaling mode. A future research axis could investigate the adaptation of such techniques to other signaling modes. The extension of the network model to the case of multi-hop transmission [105] could also be a future research subject. The case of a larger number of relay nodes and the corresponding appropriate DSTBC schemes should also be investigated. Another promising approach is to use the estimated channel for sensor node selection processing for the purposes of energy saving and lifetime maximization [106].
- Apart from channel estimation, an important practical aspect is the time synchronization. We assumed through this manuscript that there is perfect time synchronization between the source, relay, and destination nodes. It is of crucial importance to consider this issue and to propose efficient synchronization methods adapted to the WRN context. One possible solution is to use a delay-locked loop or some newly proposed schemes such as internal model control [107].
- We considered in this work the use of cooperation diversity to mitigate the fading effect. No

other diversity technique was considered in our study. Exploiting other possible diversity techniques together with cooperative diversity appears to be an interesting idea. For instance, we can resort to polarization diversity techniques [62, 108, 109] combined with the spatial diversity offered by node cooperation. Another potential solution is to equip all the sensor nodes with multiple antennas. Coupling MIMO technology with a WRN can provide additional degrees of freedom and can significantly improve the spectral and power efficiencies [110, 111, 112, 113, 114, 115]. Especially, by employing MIMO relay nodes, we can benefit from an intra-node diversity and array gain at each relay [104]. The ideas of this thesis can be applied to this context.

– Finally, the channel estimation solutions proposed in this thesis can also be promising for the case of optical sensor networks in indoor or free-space applications [116, 117]. In particular, free-space optical communication systems suffer from channel turbulence in practice. User cooperation diversity can employed as a new form of spatial diversity when, due to practical reasons, neither multiple lenses nor multiple laser beams can be used [118, 119]. In such systems, channel estimation is required for most modulation schemes when optimal signal detection is to be done at the receiver. Applying the proposed ideas in this thesis to this context seems to be potentially interesting.

ANNEXE

A Details on the formulation of UL-EM channel estimation

According to the analysis of CB channel estimation, we note that the estimation is biased. In order to obtain an unbiased channel estimation, we proposed the UL scheme in Chapter 5. In the following, we consider the cases of two (and four) relays with Alamouti (and TSw-Al) DSTBC, and we present the details on how to obtain the UL channel estimation.

A.1 Case of $R = 2$ with Alamouti DSTBC

According to (3.10) and (3.36), we can calculate $\boldsymbol{R}_{Py}$ as follows :

$$\begin{aligned}\boldsymbol{R}_{Py} &= c\sqrt{q_1}\left[\sum_{k=1}^{N_p}\boldsymbol{P}_0^{\dagger}\boldsymbol{y}_0(k)+\sum_{k=N_p+1}^{N_s}\widetilde{\boldsymbol{P}}^{\dagger}(k)\boldsymbol{y}(k)\right]\\ &= c\sqrt{q_1}\left[\sum_{k=1}^{N_p}\boldsymbol{P}_0^{\dagger}\big(c\sqrt{q_1}\boldsymbol{P}_0\boldsymbol{h}+\boldsymbol{z}_0(k)\big)+\sum_{k=N_p+1}^{N_s}\widetilde{\boldsymbol{P}}(k)^{\dagger}\boldsymbol{h}+\boldsymbol{z}(k)\right].\end{aligned} \tag{A.1}$$

So, we obtain (4.14) which is rewritten below :

$$\begin{aligned}\boldsymbol{R}_{Py} &= \underbrace{c^2 q_1 N_p T \boldsymbol{I}_R}_{\boldsymbol{R}_{P_0}}\boldsymbol{h}+\underbrace{c\sqrt{q_1}\sum_{k=1}^{N_p}\boldsymbol{P}_0^{\dagger}\boldsymbol{z}_0(k)}_{\boldsymbol{\eta}_0}+\underbrace{c^2 q_1\left(\sum_{k=N_p+1}^{N_s}\widetilde{\boldsymbol{P}}^{\dagger}(k)\boldsymbol{P}(k)\right)}_{\boldsymbol{R}_P^{'}}\boldsymbol{h}+\underbrace{c\sqrt{q_1}\sum_{k=N_p+1}^{N_s}\widetilde{\boldsymbol{P}}^{\dagger}(k)\boldsymbol{z}(k)}_{\boldsymbol{\eta}}\\ &= (\boldsymbol{R}_{P_0}+\boldsymbol{R}_P^{'})\boldsymbol{h}+\boldsymbol{\eta}_0+\boldsymbol{\eta}.\end{aligned} \tag{A.2}$$

We consider separately the channel estimates based on pilots and data symbols that we denote by $\hat{\boldsymbol{h}}^p$ and $\hat{\boldsymbol{h}}^d$, respectively. Then, we can write :

$$\hat{\boldsymbol{h}}^p = \boldsymbol{h}+\boldsymbol{\eta}_0' \quad , \quad \hat{\boldsymbol{h}}^d = \boldsymbol{\Lambda}\boldsymbol{h}+\boldsymbol{\eta}', \tag{A.3}$$

where

$$\boldsymbol{\eta}_0' = \frac{\boldsymbol{\eta}_0}{\boldsymbol{R}_{P_0}} \quad , \quad \boldsymbol{R}_{P_0} = c^2 q_1 N_p T \boldsymbol{I}_R, \tag{A.4}$$

$$\boldsymbol{\eta}' = \frac{\boldsymbol{\eta}}{\boldsymbol{R}_{P_d}} \quad , \quad \boldsymbol{\Lambda} = \frac{\boldsymbol{R}_P^{'}}{\boldsymbol{R}_{P_d}}, \tag{A.5}$$

$$\boldsymbol{R}_{P_d} = c^2 q_1 \sum_{k=N_p+1}^{N_s} \begin{bmatrix} \sum_{i=1}^{R} \widetilde{s_i^2}(k) & 0 \\ 0 & \sum_{i=1}^{R} \widetilde{s_i^2}(k) \end{bmatrix} = \xi \boldsymbol{I}_2 . \tag{A.6}$$

Based on the property of the Alamouti DSTBC, $\boldsymbol{R}_P^{'}$ can be shown to be :

$$\begin{aligned} \boldsymbol{R}_p^{'} &= c^2 q_1 \sum_{k=N_p+1}^{N_s} \begin{bmatrix} \widetilde{s_1^*}(k) & \widetilde{s_2^*}(k) \\ -\widetilde{s_2}(k) & \widetilde{s_1}(k) \end{bmatrix} \begin{bmatrix} s_1(k) & -s_2^*(k) \\ s_2(k) & s_1^*(k) \end{bmatrix} \\ &= c^2 q_1 \sum_{k=N_p+1}^{N_s} \begin{bmatrix} \widetilde{s_1^*}(k)s_1(k) + \widetilde{s_2^*}(k)s_2(k) & -\widetilde{s_1^*}(k)s_2^*(k) + \widetilde{s_2^*}(k)s_1^*(k) \\ -\widetilde{s_2^*}(k)s_1(k) + \widetilde{s_1}(k)s_2(k) & \widetilde{s_2}(k)s_2^*(k) + \widetilde{s_1}(k)s_1^*(k) \end{bmatrix} \\ &= c^2 q_1 \sum_{k=N_p+1}^{N_s} \begin{bmatrix} \lambda_{11}(k) & -\lambda_{21}^*(k) \\ \lambda_{21}(k) & \lambda_{11}^*(k) \end{bmatrix}, \end{aligned} \tag{A.7}$$

So, using (A.5) and (A.7), we can write $\boldsymbol{\Lambda}$ as :

$$\boldsymbol{\Lambda} = \begin{bmatrix} \lambda_{11} & \lambda_{12} \\ \lambda_{21} & \lambda_{22} \end{bmatrix} = \frac{c^2 q_1}{\xi} \sum_{k=N_p+1}^{N_s} \begin{bmatrix} \lambda_{11}(k) & -\lambda_{21}^*(k) \\ \lambda_{21}(k) & \lambda_{11}^*(k) \end{bmatrix}. \tag{A.8}$$

We note that :

$$\lambda_{11} = \lambda_{22}^*, \quad \lambda_{21} = -\lambda_{12}^*. \tag{A.9}$$

To obtain an unbiased channel estimate, we should combine appropriately $\hat{\boldsymbol{h}}_p$ and $\hat{\boldsymbol{h}}_d$. For this purpose, we define two weight matrices $\boldsymbol{A}$ and $\boldsymbol{B}$:

$$\hat{\boldsymbol{h}} = \boldsymbol{A}\hat{\boldsymbol{h}}^p + \boldsymbol{B}\hat{\boldsymbol{h}}^d . \tag{A.10}$$

We determine the matrices $\boldsymbol{A}$ and $\boldsymbol{B}$ so as to minimize the channel estimation error variance and, at the same time, to satisfy the condition of unbiased estimation. Let,

$$\boldsymbol{A} = \begin{bmatrix} a_1 & a_2 \\ a_3 & a_4 \end{bmatrix}, \boldsymbol{B} = \begin{bmatrix} b_1 & b_2 \\ b_3 & b_4 \end{bmatrix}. \tag{A.11}$$

Optimizing channel estimation in (A.11) in the sense of minimum mean-square of estimation errors gives :

$$\min \mathrm{E}\left\{ ||\boldsymbol{A}\boldsymbol{\eta}_0' + \boldsymbol{B}\boldsymbol{\eta}'||^2 \right\} \quad , \quad \text{satisfying } \boldsymbol{A} + \boldsymbol{B}\boldsymbol{\Lambda} = \boldsymbol{I}_R. \tag{A.12}$$

In other words, $\boldsymbol{A}$ and $\boldsymbol{B}$ should satisfy :

$$\begin{cases} a_1^* \lambda_{11}^* + a_2^* \lambda_{21}^* + b_1^* = 1 \\ a_2^* \lambda_{11} - a_1^* \lambda_{21} + b_2^* = 0 \\ a_3^* \lambda_{11}^* + a_4^* \lambda_{21}^* + b_3^* = 0 \\ a_4^* \lambda_{11} + a_3^* \lambda_{21} + b_4^* = 1 \end{cases}, \tag{A.13}$$

and

$$\mathrm{E}\left\{||\boldsymbol{A}\boldsymbol{\eta}_0' + \boldsymbol{B}\boldsymbol{\eta}'||^2\right\} = \mathrm{E}\left\{\boldsymbol{\eta}'^{\dagger}\boldsymbol{A}^{\dagger}\boldsymbol{A}\boldsymbol{\eta}' + \boldsymbol{\eta}_0'^{\dagger}\boldsymbol{B}^{\dagger}\boldsymbol{B}\boldsymbol{\eta}_0'\right\} \tag{A.14}$$

Based on the definitions of β_0 and β_i of (4.19), we consider separately the two parts in the brackets in (A.14) :

$$\mathrm{E}\left\{\boldsymbol{\eta}'^{\dagger}\boldsymbol{A}^{\dagger}\boldsymbol{A}\boldsymbol{\eta}'\right\} = \beta_i\sigma_{\boldsymbol{z}}^2\sum_{j=1}^{4}|a_j|^2, \qquad i = 1 \text{ or } 2, \tag{A.15}$$

and

$$\begin{aligned}
\mathrm{E}\left\{\boldsymbol{\eta}_0'^{\dagger}\boldsymbol{B}^{\dagger}\boldsymbol{B}\boldsymbol{\eta}_0'\right\} &= \beta_0\sigma_{\boldsymbol{z}}^2\sum_{j=1}^{4}|b_j|^2 \qquad (A.16)\\
&= \beta_0\Big[|a_1|^2|\lambda_{21}|^2 + |a_2|^2|\lambda_{11}|^2 + a_1a_2^*\lambda_{11}\lambda_{21}^* - a_1^*a_2\lambda_{11}^*\lambda_{21}\\
&+ |a_3|^2|\lambda_{11}|^2 + |a_4|^2|\lambda_{21}|^2 + a_3a_4^*\lambda_{11}\lambda_{21}^* + a_3^*a_4\lambda_{11}^*\lambda_{21}\\
&+ 1 + |a_1|^2|\lambda_{11}|^2 + |a_2|^2|\lambda_{21}|^2 + a_1^*\lambda 11^*(a_2\lambda_{21} - 1) + a_2^*\lambda_{21}^*(a_1\lambda_{11} - 1) - a_1\lambda_{11} - a_2\lambda_{21}\\
&+ 1 + |a_3|^2|\lambda_{21}|^2 + |a_4|^2|\lambda_{11}|^2 + a_3^*\lambda_{21}(1 - a_4\lambda_{11}^*) + a_3\lambda_{21}^*(1 - a_4^*\lambda_{11}) - a_4^*\lambda_{11} - a_4\lambda_{11}^*\Big]\sigma_{\boldsymbol{z}}^2
\end{aligned}$$

From (A.14), we calculate the derivative of $\mathrm{E}\left\{||\boldsymbol{A}\boldsymbol{\eta}_0' + \boldsymbol{B}\boldsymbol{\eta}'||^2\right\}$ with respect to a_i^* :

$$\begin{cases}
\frac{\partial \mathrm{E}\left\{||\boldsymbol{A}\boldsymbol{\eta}_0' + \boldsymbol{B}\boldsymbol{\eta}'||^2\right\}}{\partial a_1^*} = \beta_i a_1 + \beta_0\left[a_1\left(|\lambda_{11}|^2 + |\lambda_{21}|^2\right) - \lambda_{11}^*\right] = 0\\
\frac{\partial \mathrm{E}\left\{||\boldsymbol{A}\boldsymbol{\eta}_0' + \boldsymbol{B}\boldsymbol{\eta}'||^2\right\}}{\partial a_2^*} = \beta_i a_2 + \beta_0\left[a_2\left(|\lambda_{11}|^2 + |\lambda_{21}|^2\right) - \lambda_{21}^*\right] = 0\\
\frac{\partial \mathrm{E}\left\{||\boldsymbol{A}\boldsymbol{\eta}_0' + \boldsymbol{B}\boldsymbol{\eta}'||^2\right\}}{\partial a_3^*} = \beta_i a_3 + \beta_0\left[a_3\left(|\lambda_{11}|^2 + |\lambda_{21}|^2\right) + \lambda_{21}\right] = 0\\
\frac{\partial \mathrm{E}\left\{||\boldsymbol{A}\boldsymbol{\eta}_0' + \boldsymbol{B}\boldsymbol{\eta}'||^2\right\}}{\partial a_4^*} = \beta_i a_4 + \beta_0\left[a_4\left(|\lambda_{11}|^2 + |\lambda_{21}|^2\right) - \lambda_{11}\right] = 0
\end{cases} \tag{A.17}$$

Then based on (4.21) and (4.26), we can easily calculate the optimal weight matrices $\boldsymbol{A}$ and $\boldsymbol{B}$ as given by (4.25).

A.2 Case of $R = 4$ with TSw-Al DSTBC

In the case of four relays with TSw-Al, we use the similar idea for calculating $\boldsymbol{A}$ and $\boldsymbol{B}$. Firstly, we get $\boldsymbol{R}_{P_0}$ as (A.4) and $\boldsymbol{R}_{P_d}$ as follows :

$$\begin{aligned}
\boldsymbol{R}_{P_d} &= 2c^2q_1\sum_{k=N_p+1}^{N_s}\mathbf{diag}\left(\widetilde{s_1^2}(k) + \widetilde{s_2^2}(k), \widetilde{s_3^2}(k) + \widetilde{s_4^2}(k)\right)\otimes\boldsymbol{I}_2 \qquad (A.18)\\
&= \mathbf{diag}(\xi_1, \xi_2, \xi_3, \xi_4)
\end{aligned}$$

In (A.18), we note that $\xi_1 = \xi_2$ and $\xi_3 = \xi_4$. Additionally, the $\boldsymbol{R}'_P$ is :

$$\boldsymbol{R}'_P = 2c^2 q_1 \sum_{k=N_p+1}^{N_s} \begin{bmatrix} \lambda_{11}(k) & \lambda_{12}(k) & 0 & 0 \\ \lambda_{21}(k) & \lambda_{22}(k) & 0 & 0 \\ 0 & 0 & \lambda_{33}(k) & \lambda_{34}(k) \\ 0 & 0 & \lambda_{43}(k) & \lambda_{44}(k) \end{bmatrix}. \tag{A.19}$$

Based on (A.18) and (A.19), matrix $\boldsymbol{\Lambda}$ can be written as :

$$\boldsymbol{\Lambda} = \begin{bmatrix} \lambda_{11} & \lambda_{12} & 0 & 0 \\ \lambda_{21} & \lambda_{22} & 0 & 0 \\ 0 & 0 & \lambda_{33} & \lambda_{34} \\ 0 & 0 & \lambda_{43} & \lambda_{44} \end{bmatrix}, \tag{A.20}$$

where

$$\begin{cases} \lambda_{11} = \frac{2c^2 q_1}{\xi_1} \sum_{k=N_p+1}^{N_s} \left[\widetilde{s_1^*}(k) s_1(k) + \widetilde{s_2^*}(k) s_2(k) \right] \\ \lambda_{21} = \frac{2c^2 q_1}{\xi_1} \sum_{k=N_p+1}^{N_s} \left[-\widetilde{s_2}(k) s_1(k) + \widetilde{s_1}(k) s_2(k) \right] \\ \lambda_{33} = \frac{2c^2 q_1}{\xi_3} \sum_{k=N_p+1}^{N_s} \left[\widetilde{s_3^*}(k) s_3(k) + \widetilde{s_4^*}(k) s_4(k) \right] \\ \lambda_{43} = \frac{2c^2 q_1}{\xi_3} \sum_{k=N_p+1}^{N_s} \left[-\widetilde{s_4}(k) s_3(k) + \widetilde{s_3}(k) s_4(k) \right] \end{cases} \tag{A.21}$$

and

$$\begin{cases} \lambda_{11} = \lambda_{22}^*, \quad \lambda_{21} = -\lambda_{12}^* \\ \lambda_{33} = \lambda_{44}^*, \quad \lambda_{43} = -\lambda_{34}^* \end{cases} \tag{A.22}$$

To impose unbiased channel estimation, we consider the following weight matrices $\boldsymbol{A}$ and $\boldsymbol{B}$:

$$\boldsymbol{A} = \begin{bmatrix} a_1 & a_2 & 0 & 0 \\ a_3 & a_4 & 0 & 0 \\ 0 & 0 & a_5 & a_6 \\ 0 & 0 & a_7 & a_8 \end{bmatrix}, \ \boldsymbol{B} = \begin{bmatrix} b_1 & b_2 & 0 & 0 \\ b_3 & b_4 & 0 & 0 \\ 0 & 0 & b_5 & b_6 \\ 0 & 0 & b_7 & b_8 \end{bmatrix} \tag{A.23}$$

Then, similar to the case of $R = 2$, the optimal weight functions can be calculated, resulting in (4.25).

References

[1] I. F. Akyildiz, W. Su, Y. Sankarasubramaniam, and E. Cayirci, "A survey on sensor networks," *IEEE Communications Magazine*, vol. 40, no. 8, pp. 102–114, Aug. 2002.

[2] Y. Yuan, Z. He, and M. Chen, "Virtual MIMO-based cross-layer design for wireless sensor networks," *IEEE Transactions on Vehicular Technology*, vol. 55, no. 3, pp. 856–864, May 2006.

[3] A. Swami, Q. Zhao, Y. W. Hong, and L. Tong, *Wireless Sensor Networks : Signal Processing and Communication Perspectives*, Wiley, 2007.

[4] C. Y. Chong and S. P. Kumar, "Sensor networks : Evolution, opportunities and chanllenges," *Proceedings of IEEE*, vol. 91, no. 8, pp. 1247–1256, Aug. 2003.

[5] J. L. Hill, *System Architecture for Wireless Sensor Networks*, Ph.D. thesis, University of California, Berkeley, CA, 2003.

[6] T. Q. S. Quek, D. Dardari, and M. Z. Win, "Energy efficiency of dense wireless sensor networks : To cooperate or not to cooperate," *IEEE Journal on Selected Areas in Communications*, vol. 25, no. 2, pp. 459–470, Feb. 2007.

[7] X. Y. Li, *Wireless Ad Hoc and Sensor Networks : Theory and Applications*, Cambrige University Press, 2008.

[8] I. F. Akyildiz, W. Su, Y. Sankarasubramaniam, and E. Cayirci, "Wireless sensor networks : a survey," *Computer Networks*, vol. 38, no. 4, pp. 393–422, Mar. 2002.

[9] J. Guevara, F. Barrero, E. Vargas, J. Becerra, and S. Toral, "Environmental wireless sensor network for road traffic applications," *IET Intelligent Transport Systems*, vol. 6, no. 2, pp. 177–186, June 2012.

[10] Y. S. Li, M. T. Thai, and W. L. Wu, *Wireless Sensor Networks and Applications*, Springer, 2008.

[11] J. Yick, B. Mukherjee, and D. Ghosal, "Wireless sensor network survey," *Computer Networks*, vol. 52, no. 12, pp. 2292–2330, Aug. 2008.

[12] I. F. Akyildiz and E. P. Stuntebeck, "Wireless underground sensor networks : research challenges," *Ad-Hoc Networks*, vol. 4, pp. 669–686, July 2006.

[13] M. Li and Y. Liu, "Underground structure monitoring with wireless sensor networks," *International Symposium on Information Processing in Sensor Networks (ISPN)*, pp. 69–78, Apr. 2007, Cambridge, Massachusetts.

[14] R. C. Shah and J. M. Rabaey, "Energy aware routing for low energy ad hoc sensor networks," *IEEE International Conference on Wireless Communications and Networking*, vol. 1, pp. 350–355, Mar. 2002, Orlando, FL.

[15] K. Sohrabi and G. J. Pottie, "Performance of a novel self-organization protocol for wireless ad-hoc sensor networks," *IEEE Conference on Vehicular Technology*, vol. 2, pp. 1222–1226, Sept. 1999, Amsterdam.

[16] Y. Chen and Q. Zhao, "On the lifetime of wireless sensor networks," *IEEE Communications Letters*, vol. 9, no. 11, pp. 976–978, Nov. 2005.

[17] A. Lapidoth and S. M. Moser, "Capacity bounds via duality with applications to multiple-antenna systems on flat-fading channels," *IEEE Transactions on Information Theory*, vol. 49, no. 10, pp. 2426–2467, Oct. 2003.

[18] W. Yu, W. Rhee, and J. M. Cioffi, "Optimal power control in multiple access fading channels with multiple antennas," *IEEE International Conference on Communications (ICC)*, vol. 2, pp. 575–579, June 2001, Helsinki, Finland.

[19] A. Nosratinia, T. E. Hunter, and A. Hedayat, "Cooperative communication in wireless networks," *IEEE Communications Magazine*, vol. 42, no. 10, pp. 74–80, Oct. 2004.

[20] A. Sendonaris, E. Erkip, and B. Aazhang, "User cooperation diversity - Part I : system description," *IEEE Transactions on Communications*, vol. 51, no. 11, pp. 1927–1938, Nov. 2003.

[21] A. Sendonaris, E. Erkip, and B. Aazhang, "User cooperation diversity - Part II : implementation aspects and performance analysis," *IEEE Transactions on Communications*, vol. 51, no. 11, pp. 1939–1948, Nov. 2003.

[22] J. N. Laneman, D. N. C. Tse, and G. W. Wornell, "Cooperative diversity in wireless networks : Efficient protocols and outage behavior," *IEEE Transactions on Information Theory*, vol. 50, no. 12, pp. 3062–3080, Dec. 2004.

[23] J. N. Laneman, G. W. Wornell, and D. N. C. Tse, "An efficient protocol for realizing cooperative diversity in wireless network," *IEEE International Symposium on Information Theory*, June 2001, Washington, DC.

[24] T. E. Hunter and A. Nosratinia, "Diversity through coded cooperation," *IEEE Transactions on Wireless Communications*, vol. 5, no. 2, pp. 283–289, Feb. 2006.

[25] M. Gastpar and M. Vetterli, "On the capacity of large Gaussian relay networks," *IEEE Transactions on Information Theory*, vol. 51, no. 3, pp. 765–779, Mar. 2005.

[26] S. Borade, L. Zheng, and R. Gallager, "Amplify-and-forward in wireless relay networks : Rate, diversity, and network size," *IEEE Transactions on Information Theory*, vol. 53, no. 10, pp. 3302–3318, Oct. 2007.

[27] Y. Jing and H. Jafarkhani, "Distributed differential space-time coding for wireless relay networks," *IEEE Transactions on Communications*, vol. 56, no. 7, pp. 1092–1100, July 2008.

[28] M. Kobayashi and X. Mestre, "Impact of CSI on distributed space-time coding in wireless relay networks," *IEEE Transactions on Wireless Communications*, vol. 8, no. 5, pp. 2580–2591, May 2009.

[29] C. T. K. Ng and A. J. Goldsmith, "The impact of CSI and power allocation on relay channel capacity and cooperation strategies," *IEEE Transactions on Wireless Communications*, vol. 7, no. 12, pp. 5380–5389, Dec. 2008.

[30] A. Chowdhery and R. K. Mallik, "Linear detection for the nonorthogonal amplify and forward protocol," *IEEE Transactions on Wireless Communications*, vol. 8, no. 2, pp. 826–835, Feb. 2009.

[31] G. M. Kraidy, N. Gresset, and J. J. Boutros, "Coding for the non-orthogonal amplify-and-forward cooperative channel," *IEEE Information Theory Workshop*, pp. 626–631, Sept. 2007, Lake Tahoe, NV.

[32] G. Farhadi and N. C. Beaulieu, "A low complexity receiver for noncoherent amplify-and-forward cooperative systems," *IEEE Transactions on Communications*, vol. 58, no. 9, pp. 2499–2504, Sept. 2010.

[33] Q. Liu, W. Zhang, and X. Ma, "Practical and general amplify-and-forward designs for cooperative networks," *IEEE INFOCOM Conference*, pp. 1–9, Mar. 2010, San Diego, CA.

[34] A. F. Dana and B. Hassibi, "On the power-efficiency of sensory and ad hoc wireless networks," *IEEE Transactions on Information Theory*, vol. 52, no. 7, pp. 2890–2914, July 2006.

[35] K. Azarian, H. E. Gamal, and P. Schniter, "On the achievable diversity-multiplexing tradeoff in half-duplex cooperative channels," *IEEE Transactions on Information Theory*, vol. 51, no. 12, pp. 4152–4172, Dec. 2005.

[36] Y. Gong, C. Luo, and Z. Chen, "Two-path succussive relaying with hybrid demodulated and forward," *IEEE Transactions on Vehicular Technology*, vol. 61, no. 5, pp. 2044–2053, June 2012.

[37] R. Annavajjala, A. Maaref, and J. Zhang, "Demodulate-and-forward relaying with higher order modulations : impact of channel state uncertainty," *IEEE International Conference on Communications (ICC)*, pp. 1–5, May 2010, Cape Town, South Africa.

[38] Y. Li, "Distributed coding for cooperative wireless networks : An overview and recent advances," *IEEE Communications Magazine*, vol. 47, no. 8, pp. 71–77, Aug. 2009.

[39] J. Boyer, D. D. Falconer, and H. Yanikomeroglu, "Multihop diversity in wireless relaying channels," *IEEE Transactions on Communications*, vol. 52, no. 10, pp. 1820–1830, Oct. 2004.

[40] C. S. Patel and G. L. Stuber, "Channel estimation for amplify and forward relay based cooperation diversity systems," *IEEE Transactions on Wireless Communications*, vol. 6, no. 6, pp. 2348–2356, June 2007.

[41] D. Chen and J. N. Laneman, "Modulation and demodulation for cooperative diversity in wireless systems," *IEEE Transactions on Wireless Communications*, vol. 5, no. 7, pp. 1785–1794, July 2006.

[42] Y. Jing and B. Hassibi, "Distributed space-time coding in wireless relay networks," *IEEE Transactions on Wireless Communications*, vol. 5, no. 12, pp. 3524–3536, Dec. 2006.

[43] J. N. Laneman and G. W. Wornell, "Distributed space-time-coded protocols for exploiting cooperative diversity in wireless networks," *IEEE Transactions on Information Theory*, vol. 49, no. 10, pp. 2415–2425, Oct. 2003.

[44] Y. Jing and H. Jafarkhani, "Using orthogonal and quasi-orthogonal designs in wireless relay networks," *IEEE Transactions on Information Theory*, vol. 53, no. 11, pp. 4106–4118, Nov. 2007.

[45] Y. Jing and B. Hassibi, "Cooperative diversity in wireless relay networks with multiple-antenna nodes," *IEEE International Symposium on Information Theory*, pp. 815–819, Sept. 2005, Adelaide, Australia.

[46] T. L. Marzetta and B. M. Hochwald, "Capacity of a mobile multiple-antenna communication link in rayleigh flat fading," *IEEE Transactions on Information Theory*, vol. 45, no. 1, pp. 139–157, Jan. 1999.

[47] H. E. Gamal, D. Aktas, and M. O. Damen, "Noncoherent space-time coding : An algebraic perspetives," *IEEE Transactions on Information Theory*, vol. 51, no. 7, pp. 2380–2390, July 2005.

[48] G. S. Rajan and B. S. Rajan, "Leveraging coherent distributed space-time codes for noncoherent communication in relay networks via training," *IEEE Transactions on Wireless Communications*, vol. 8, no. 2, pp. 683–688, Feb. 2009.

[49] P. Dayal, M. Brehler, and M. K. Varanasi, "Leveraging coherent space-time codes for noncoherent communication via training," *IEEE Transactions on Information Theory*, vol. 50, no. 9, pp. 2058–2080, Sept. 2004.

[50] T. Kiran and B. S. Rajan, "Distributed space-time codes with reduced decoding complexity," *IEEE International Symposium on Information Theory*, pp. 542–546, July 2006, Seattle, WA.

[51] T. Kiran and B. S. Rajan, "Partially-coherent distributed space-time codes with differential encoder and decoder," *IEEE Journal on Selected Areas in Communications*, vol. 25, no. 2, pp. 426–433, Feb. 2007.

[52] V. Tarokh and H. Jafarkhani, "A differential detection scheme for transmit diversity," *IEEE Journal on Selected Areas in Communications*, vol. 18, no. 7, pp. 1169–1174, July 2000.

[53] G. S. Rajan and B. S. Rajan, "Algebraic distributed differential space-time codes with low decoding complexity," *IEEE Transactions on Wireless Communications*, vol. 7, no. 10, pp. 3962–3971, Oct. 2008.

[54] T. Wang, A. Cano, G. B. Giannakis, and J. N. Laneman, "High-performance cooperative demodulation with decode-and-forward relays," *IEEE Transactions on Communications*, vol. 55, no. 7, pp. 1427–1438, July 2007.

[55] G. Caire, G. Taricco, and E. Biglieri, "Bit-interleaved coded modulation," *IEEE Transactions on Information Theory*, vol. 44, no. 3, pp. 927–946, May 1998.

[56] F. Gao, T. Cui, and A. Nallanathan, "On channel estimation and optimal training design for amplify and forward relay networks," *IEEE Transaction on Wireless Communications*, vol. 7, no. 5, pp. 1907–1916, May 2008.

[57] B. Hassibi and B. M. Hochwald, "High-rate codes that are linear in space and time," *IEEE Transactions on Information Theory*, vol. 48, no. 7, pp. 1804–1824, July 2002.

[58] M. A. Khalighi, J.-F. Hélard, S. M. S. Sadough, and S. Bourennane, "Suitable combination of channel coding and space-time schemes for moderate-to-high spectral efficiency MIMO systems," *AEÜE International Journal of Electronics and Communications*, vol. 64, no. 7, pp. 595–606, July 2010.

[59] S. M. Alamouti, "A simple transmit diversity technique for wireless communications," *IEEE Journal on Selected Areas in Communications*, vol. 16, no. 8, pp. 1451–1458, Oct. 1998.

[60] J. G. Proakis and M. Salehi, *Digital Communications*, McGraw-Hill, 5th edition, 2008.

[61] H. Jafarkhani, "A quasi-orthogonal space-time block code," *IEEE Transactions on Communications*, vol. 49, no. 1, pp. 1–4, Jan. 2001.

[62] K. Raoof, M. A. Khalighi, and N. Prayongpun, *Adaptive Signal Processing For Wireless Communications*, chapter MIMO Systems : Principles, Iterative Techniques and Advance Polarization, CRC Press, Aug. 2008.

[63] P. Robertson, P. Hoeher, and E. Villebrun, "Optimal and sub-optimal maximum a posteriori algorithms suitable for turbo decoding," *European Transactions on Telecommunications*, vol. 8, no. 2, pp. 119–125, Mar. 1997.

[64] S. M. Kay, *Fundamentals of Statistical Signal Processing : Estimation Theory*, Prentice Hall, 1993.

[65] R. Zhao, Y. Lin, and D. Yang, "A kind of quasi-orthogonal space-time block codes and its decoding methods," *The Journal of China University of Posts and Telecommunication*, vol. 13, no. 1, pp. 10–13, Mar. 2006.

[66] M. Malkawi and I. M. Kim, "Hard/soft detection with limited CSI for multi-hop systems," *IEEE Transactions on Wireless Communications*, vol. 8, no. 7, pp. 3435–3441, July 2009.

[67] P. Liu and I. M. Kim, "Optimum/sub-optimum detectors for multi-branch dual-hop amplify-and-forward cooperative diversity networks with limited CSI," *IEEE Transactions on Wireless Communications*, vol. 9, no. 1, pp. 78–85, Jan. 2010.

[68] S. M. S. Sadough and P. Duhamel, "Improved iterative detection and achieved throughputs of OFDM systems under imperfect channel estimation," *IEEE Transactions on Wireless Communications*, vol. 7, no. 12, pp. 5039–5050, Dec. 2008.

[69] B. Gedik, O. Amin, and M. Uysal, "Power allocation for cooperative systems with training-aided channel estimation," *IEEE Transactions on Wireless Communications*, vol. 8, no. 9, pp. 4773–4783, Sept. 2009.

[70] J. Balakrishnan, M. Rupp, and H. Viswanathan, *Multiaccess, Mobility and Teletraffic for Wireless Communications*, vol. 5, Springer, 2000.

[71] S. Cui, A. J. Goldsmith, and A. Bahai, "Energy-efficiency of MIMO and cooperative MIMO techniques in sensor networks," *IEEE Journal on Selected Areas in Communications*, vol. 22, no. 6, pp. 1089–1098, Aug. 2004.

[72] S. K. Jayaweera, "Virtual MIMO-based cooperative communication for energy-constrained wireless sensor networks," *IEEE Transactions on Wireless Communications*, vol. 5, no. 5, pp. 984–989, May 2006.

[73] M. A. Khalighi and J. J. Boutros, "Semi-blind channel estimation using EM algorithm in iterative MIMO APP detectors," *IEEE Transactions on Wireless Communications*, vol. 5, no. 11, pp. 3165–3173, Nov. 2006.

[74] S. M. S. Sadough and M. A. Khalighi, *Radio Communications*, chapter Recent Developments in Channel Estimation and Detection for MIMO Systems, IN-TECH Press, Apr. 2010.

[75] A. P. Dempster, N. M. Laird, and D. B. Rubin, "Maximum-likelihood from incomplete data via the EM algorithm," *Journal of the Royal Statistical Society*, vol. 39, no. 1, pp. 1–38, Dec. 1976.

[76] T. K. Moon, "The expectation-maximization algorithm," *IEEE Signal Processing Magazine*, vol. 13, no. 6, pp. 47–60, Nov. 1996.

[77] C. Lamy, *Communications à Grande Efficacité Spectrale sur le Canal à Évanouissements*, Ph.D. thesis, École Nationale Supérieure des Télécommunications (Télécom Paris-Tech), Paris, France, Apr. 2000.

[78] Yi Zhang, M. A. Khalighi, and S. Bourennane, "EM-based semi-blind channel estimation for amplify-and-forward cooperative relay networks," *EURASIP Signal Processing*, under revision.

[79] Yi Zhang, M. A. Khalighi, and S. Bourennane, "EM-based channel estimation for cooperative relay networks," *IEEE International Conference on Telecommunications (ConTEL)*, pp. 279–286, June 2011, Graz, Austria.

[80] M. A. Khalighi, J.-F. Hélard, and S. Bourennane, "Choice of appropriate space-time coding scheme for MIMO systems employing channel coding under BICM," *IEEE International Workshop on Signal Processing Advances for Wireless Communications (SPAWC)*, July 2006, Cannes, France.

[81] M. A. Khalighi, J.-F. Hélard, and S. Bourennane, "Contrasting orthogonal and non-orthogonal space-time schemes for perfectly-known and estimated MIMO channels," *International Conference on Communication Systems (ICCS)*, Oct.-Nov. 2006, Singapore.

[82] C. Berrou and A. Glavieux, "Near optimum error correcting coding and decoding : turbo-codes," *IEEE Transactions on Communications*, vol. 44, no. 10, pp. 1261–1271, Oct. 1996.

[83] C. Douillard, M. Jézéquel, C. Berrou, A. Picart, P. Didier, and A. Glavieux, "Iterative correction of intersymbol interference : Turbo-equalization," *European Transactions on Telecommunications*, vol. 6, no. 5, pp. 507–511, Sept.-Oct. 1995.

[84] M. Kobayashi, J. Boutros, and G. Caire, "Successive interference cancellation with SISO decoding and EM channel estimation," *IEEE Journal on Selected Areas in Communications*, vol. 19, no. 8, pp. 1450–1460, Aug. 2001.

[85] N. Noels, C. Herzet, A. Dejonghe, V. Lottici, H. Steendam, M. Moeneclaey, M. Luise, and L. Vandendorpe, "Turbo synchronization : An EM algorithm interpretation," *IEEE International Conference on Communications (ICC)*, vol. 4, pp. 2933–2937, May 2003, Anchorage, AK.

[86] H. El Gamal and E. Geraniotis, "Iterative multiuser detection for coded CDMA signals in AWGN and fading channels," *IEEE Journal on Selected Areas in Communications*, vol. 18, no. 1, pp. 30–41, Jan. 2000.

[87] G. J. Foschini, G. D. Golden, R. A. Valenzuela, and P. W. Wolniansky, "Simplified processing for wireless communication at high spectral efficiency wireless communication employing multi-element arrays," *IEEE Journal on Selected Areas in Communications*, vol. 17, no. 11, pp. 1841–1852, Nov. 1999.

[88] M. Sellathurai and S. Haykin, "Turbo-BLAST for wireless communications : theory and experiments," *IEEE Transactions on Signal Processing*, vol. 50, no. 10, pp. 2538– 2546, Oct. 2002.

[89] H. Lee, B. Lee, and I. Lee, "Iterative detection and decoding with improved V-BLAST for MIMO-OFDM systems," *IEEE Journal on Selected Areas in Communications*, vol. 24, no. 3, pp. 504–513, Mar. 2006.

[90] M. A. Khalighi, J. J. Boutros, and J.-F. Hélard, "Data-aided channel estimation for turbo-PIC MIMO detectors," *IEEE Communications Letters*, vol. 10, no. 5, pp. 350–352, May 2006.

[91] Yi Zhang, M. A. Khalighi, and S. Bourennane, "Iterative channel estimation and data detection for amplify-and-forward relay networks," *IEEE Communications Letters*, vol. 16, no. 5, pp. 710–713, May 2012.

[92] S. M. S. Sadough, M. A. Khalighi, and P. Duhamel, "Improved iterative MIMO signal detection accounting for channel estimation errors," *IEEE Transactions on Vehicular Technology*, vol. 58, no. 7, pp. 3154–3167, Sept. 2009.

[93] S. ten Brink, "Convergence behavior of iteratively decoded parallel concatenated codes," *IEEE Transactions on Communications*, vol. 49, no. 10, pp. 1727–1737, Oct. 2001.

[94] M. Tüchler, R. Koetter, and A. C. Singer, "Turbo equalization : principles and new results," *IEEE Transactions on Communications*, vol. 50, no. 5, pp. 754–767, May 2002.

[95] G. Taricco and E. Biglieri, "Space-time decoding with imperfect channel estimation," *IEEE Transactions on Wireless Communications*, vol. 4, no. 4, pp. 1874–1888, July 2005.

[96] V. Tarokh, A. Naguib, N. Seshadri, and A. R. Calderbank, "Space-time codes for high data rate wireless communication : Performance criteria in the presence of channel estimation errors, mobility, and multiple paths," *IEEE Transactions on Communications*, vol. 47, no. 2, pp. 199–207, Feb. 1999.

[97] Yi Zhang, M. A. Khalighi, M. S. Sadough, and S. Bourennane, "Signal detection for amplify-and-forward relay networks with imperfect channel estimation," *IEEE International Symposium on Communication Systems, Networks and Digital Signal Processing (CSNDSP)*, pp. 1–5, July 2012, Poznań, Poland.

[98] S. ten Brink, "Designing iterative decoding schemes with the extrinsic information transfer charts," *AEÜE International Journal of Electronics and Communications*, vol. 54, no. 6, pp. 389–398, Nov. 2000.

[99] Y. Huang and J. A. Ritcey, "Optimal constellation labeling for iteratively decoded bit-interleaved space-time coded modulation," *IEEE Transactions on Information Theory*, vol. 51, no. 5, pp. 1865–1871, May 2005.

[100] G. B. Giannakis and C. Tepedelenlioglu, "Basis expansion models and diversity techniques for blind identification and equalization of time-varying channels," *Proceedings of the IEEE*, vol. 86, no. 10, pp. 1969–1986, Oct. 1998.

[101] H. Zhang, H. Cui, D. Pan, and Y. Wang, "Time-varying channel estimation for MIMO/OFDM systems using superimposed training and basis expansion models," *Wireless Communications and Mobile Computing*, 2012, online library.

[102] E. Dahlman, S. Parkvall, and J. Skold, *4G : LTE/LTE-Advanced for Mobile Broadband*, Elsevier, Academic Press, 2011.

[103] X. Tang and Y. Hua, "Optimal design of non-regenerative MIMO wireless relays," *IEEE Transactions on Wireless Communication*, vol. 6, no. 4, pp. 1398–1407, Apr. 2007.

[104] H. Shi, T. Abe, T. Asai, and H. Yoshino, "Relaying schemes using matrix triangularization for MIMO wireless networks," *IEEE Transactions on Communications*, vol. 55, no. 9, pp. 1683–1688, Sept. 2007.

[105] S. S. Ikki and S. Aissa, "Multihop wireless relaying systems in the presence of cochannel interferences : Performance analysis and design optimization," *IEEE Transactions on Vehicular Technology*, vol. 61, no. 2, pp. 566–573, Feb. 2012.

[106] M. Ben Zid, K. Raoof, and A. Bouallegue, "Sensor nodes selection in wireless sensor networks over a rich scattering environment," *International Conference on Communications, Computing and Control Applications (CCCA)*, pp. 1–5, Mar. 2011, Hammamet, Tunisia.

[107] R. Alhakim, E. Simeu, and K. Raoof, "Internal model control for a self-tuning delay-locked loop in UWB communication systems," *IEEE International On-Line Testing Symposium (IOLTS)*, pp. 121–126, July 2011, Athens, Greece.

[108] N. Prayongpun and K. Raoof, "MIMO channel capacity with polarization diversity and power allocation technique," *IEEE International Conference on Signal Processing and Communications (ICSPC)*, pp. 185 – 188, Nov. 2007, Dubai, United Arab Emirates.

[109] M. Ben Zid, K. Raoof, and A. Bouallegue, "Dual polarized versus single polarized MIMO : A study over NLOS propagation with polarization discrimination and spatial correlation effects," *European Conference on Antennas and Propagation (EUCAP)*, pp. 1979 – 1983, 2012, Prague, Czech Republic.

[110] H. Bölcskei, R.U. Nabar, O. Oyman, and A. J. Paulraj, "Capacity scaling laws in MIMO relay networks," *IEEE Transactions on Wireless Communications*, vol. 5, no. 6, pp. 1433–1444, June 2006.

[111] O. Oyman and A. J. Paulraj, "Design and analysis of linear distributed MIMO relaying algorithms," *IEE Proceedings-Communications*, vol. 153, no. 4, pp. 565–572, Aug. 2006.

[112] A. S. Behbahani, R. Merched, and A. M. Eltawil, "Optimizations of a MIMO relay network," *IEEE Transactions on Signal Processing*, vol. 56, no. 10, pp. 5062–5073, Oct. 2008.

[113] S. Berger, M. Kuhn, A. Wittneben, T. Unger, and A. Klein, "Recent advances in amplify-and-forward two-hop relaying," *IEEE Communications Magazine*, vol. 47, no. 7, pp. 50–56, July 2009.

[114] Y. Fu, L. Yang, and W. Zhu, "A nearly optimal amplify-and-forward relaying scheme for two-hop MIMO multi-relay networks," *IEEE Communications Letters*, vol. 14, no. 3, pp. 229–231, Mar. 2010.

[115] Y. Fu, L. Yang, W.-P. Zhu, and C. Liu, "Optimum linear design of two-hop MIMO relay networks with QoS requirements," *IEEE Transactions on Signal Processing*, vol. 59, no. 5, pp. 2257–2269, May 2011.

[116] Z. Ghassemlooy and W. O. Popoola, *Mobile and Wireless Communications Network Layer and Circuit Level Design*, chapter Terrestrial Free-Space Optical Communications, IN-TECH Press, Jan. 2010.

[117] Z. Ghassemlooy, W. Popoola, and S. Rajbhandari, *Optical Wireless Communications : System and Channel Modelling with MATLAB*, CRC Press, 2012.

[118] M. Karimi and M. Nasiri-Kenari, "BER analysis of cooperative systems in free-space optical networks," *Journal of Lightwave Technology*, vol. 27, no. 24, pp. 5639–5647, Dec. 2009.

[119] M. Safari, M. M. Rad, and M. Uysal, "Multi-hop relaying over the atmospheric poisson channel : Outage analysis and optimization," *IEEE Transactions on Communications*, vol. 60, no. 3, pp. 817–829, Mar. 2012.